

Design, Synthesis, and Properties of Inorganic and Hybrid Thin Films Having Periodically Organized Nanoporosity[†]

Clément Sanchez,* Cédric Boissière, David Grosso, Christel Laberty, and Lionel Nicole

Laboratoire de Chimie de la Matière Condensée de Paris, Université Pierre et Marie Curie-Paris6 and CNRS, 4, place Jussieu, 75252 Paris, France

Received July 30, 2007. Revised Manuscript Received October 10, 2007

This review presents an extensive discussion on the major advances in the field of periodically organized mesoporous thin films (POMTFs) obtained via surfactant templated growth of inorganic or hybrid polymers. A large variety of templating agents can be coupled with inorganic polymerization reactions for the design of periodically organized nanostructured hybrid phases that yield POMTFs. The tuning of the interface between the template and the polymerizing phase and the control over chemical and processing conditions are the key parameters in producing tailor-made POMTFs with a high degree of reproducibility. This dynamic coupling between chemical and processing conditions dictates extensive use of complementary *ex situ* measurements with *in situ* characterization techniques that follow, in real time, film formation from the molecular precursor solutions to the final stabilized POMTF. Among modern analytical tools, 2D-GISAXS, ellipsoporosimetry, HRTEM, X-ray reflectometry, WAXS, time-resolved infrared spectroscopy, SAW, and optically polarized xenon NMR have proved to be highly relevant for this purpose. POMTFs combine the intrinsic physical and chemical properties of the inorganic or hybrid matrices with a highly defined nanoporous network having a tunable pore size and connectivity, high surface area and accessibility, and a specific orientation with respect to the substrate. As such, POMTFs are a promising family of advanced materials for a host of future applications including micro-optics and photonic devices, microelectronics, nanoionics and energy, environment, functional and protective coatings, biomaterials, environmentally responsive materials, and biomicrofluidics, among others.

1. Introduction

The synergetic coupling between soft matter physical chemistry^{1,2} and inorganic or hybrid sol–gel chemistry^{3–6} has opened new avenues for advanced materials research. Indeed, the ability to create “organized matter” at the micro-, meso-, and nano-scales¹⁰ has been a significant breakthrough^{7,9,13,14} since the discovery that micellar and lyotropic liquid-crystal phases can act as templates for the designed synthesis of periodically organized mesoporous materials (POMMs).^{7–15} POMMs constitute a challenging domain in materials chemistry that is experiencing explosive growth. In the past few years, an increasing quantity of mesostructured and mesoporous materials with very diverse chemical compositions (oxides, metals, carbons, chalcogenides, semiconductors, etc.) shaped as powders, monoliths, thin films, membranes, or fibers have appeared.¹⁶ The so-called M41S,^{9,17} MSU,^{14,18} HMS,¹⁹ and SBA^{13,20,21} families were discovered through innovative combinations of templates or texturing agents (ionic and nonionic surfactants, amphiphilic block copolymers, biopolymers, ionic liquids, dendrimers, etc.), starting from mineral precursors (salts, alkoxides, organosilanes, nanobuilding blocks: clusters, nanoparticles, etc.) and sol–gel reaction media (solvents, water content, pH, complexing agents, aging conditions, etc.). These novel materials offer a high degree of versatility in terms of structure, texture,

and functionality.¹⁶ This first generation of mesoporous powders, mainly based on silica and alumino-silicates, were obtained through precipitation or gelation.^{13,14,17,19} Other mesoporous compositions, such as transition metal oxide based POMMs or periodically organized mesoporous carbon metals, appeared at the end of the 1990s.^{15,22–25}

POMMs are processed using several approaches, among them *true*²⁶ or evaporation induced^{27–29} liquid crystal templating and nanocasting,^{30–32} or through the use of sacrificial mesoporous silica as a nanostructured scaffolds.^{33,34} An exhaustive description of all the periodically organized mesoporous materials is beyond of the scope of this article, and the reader is referred to some excellent reviews.^{10,16,35–44} To summarize, two main mechanisms have been proposed to explain nano-organization of inorganic or hybrid structures in the presence of nanosegregating surfactants as templating agents. The first mechanism is the liquid crystal templating (LCT) mechanism in which the inorganic phase condenses around a stable surfactant mesophase.^{17,26,35} The second mechanism is cooperative self-assembly, in which surfactant molecules and inorganic species combine in a first step to form hybrid intermediate entities that behave as independent composite hybrid species. These hybrid species are composed of oligomeric building blocks that associate with the amphiphilic component.^{45–47}

However, it is most likely that depending on the critical chemical and processing parameters, a combined effect of both mechanisms governs the construction of such meso-

[†] Part of the “Templated Materials Special Issue”.

* Corresponding author. E-mail: clems@ccr.jussieu.fr.

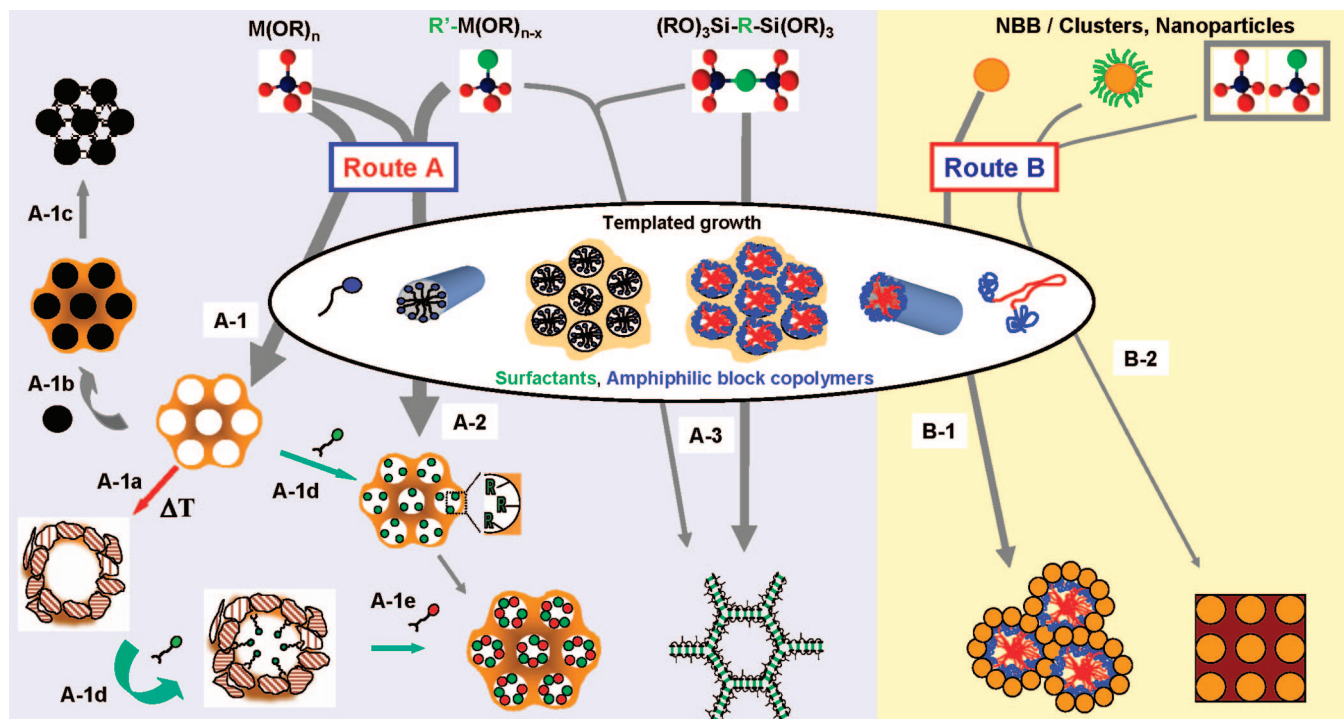


Figure 1. Chemical strategies for the synthesis of inorganic and hybrid POMMs.

structured hybrid phases. These make understanding the mechanisms of construction very difficult. The different chemical strategies for the synthesis of POMMs are shown in Figure 1.

(i) Chemical paths that follow route A correspond to the coupling of molecular precursors of sol–gel chemistry with amphiphilic block copolymer templating. The resulting mesostructured hybrid networks are obtained through the surfactant directed assembling of hydrolyzed precursors. The most extensively used precursors are metal alkoxides, metal chloro-alkoxides, metallic salts, and complexed metal alkoxides. The use of inorganic precursors allows for high temperature and/or UV treatment and/or solvent extraction to achieve complete template removal (A1), the consolidation of the inorganic backbone, and under some conditions, inorganic crystallization into nanosized particles (path A-1a). Stabilized inorganic POMMs can also be used as exotemplates to grow inorganic (metals, carbon, oxides, chalcogenides, etc.) or organic nano-objects (path A-1b). The POMM based scaffolds either can keep their integrity to allow the formation of new nanocomposites^{41,48,49} (path A-1b) or can be used as molds which, after chemically assisted dissolution, yield replicas with tunable shapes and compositions (CMK,³³ g C₃N₄,^{50,51} etc.; path A-1c). The hybridization of POMMs can be accomplished directly (one pot synthesis^{52–54}) using organically modified alkoxysilanes or alkoxy stannanes ($R'_n\text{Si}(\text{OR})_{4-n}$, $R'_n\text{Sn}(\text{X})_{4-n}$) as precursors (path A-2) or in a subsequent post-grafting step (path A-1d). In this latter case the porous inorganic surface is organically functionalized through chemical grafting of organoalkoxysilanes or complexing organic molecules or macromolecules. The nature of the grafting group and of the property carrier function must be selected to match the chemical composition of the inorganic wall and the targeted application, respectively.^{43,55–60} Another strategy that can be very

convenient to functionalize POMMs with fragile, less common, or expansive organic or bio-functionalities consists of the hybrid POMMs (path A-1d or A-2) containing reactive organic function (amino, thiol, isocyanate, acid, etc.) as a template. In a second step a high yield coupling organic reaction can be performed (amide, imine, ureido, etc.)⁶¹ allowing the POMMs with the targeted new functionality to be tailored (A-1e).

Bridged precursors of silsesquioxanes $\text{X}_3\text{Si}-\text{R}'-\text{SiX}_3$ or more recently bridged stananes $\text{X}_3\text{Sn}-\text{R}'-\text{SnX}_3$ (R' is an organic spacer, $\text{X} = \text{Cl}, \text{Br}, -\text{OR}$) have opened a plethora of new possibilities for the controlled design of hybrid POMMs (path A-3).^{44,62–71} Indeed, under surfactant directed assembly conditions, their condensation (path A-3) or co-condensation with metal alkoxides or organically modified alkoxysilanes (path A-3 with association of molecular precursors of path A-1 or A-2) allows the selective placement of different organic functionalities inside the pores, walls, or both via a convenient one pot synthesis.

The strategies under the rubric of route A are simple: potentially low cost and yield of mesostructured inorganic hybrid materials with tunable functionality.

(ii) Strategies that combine surfactant directed assembling of presynthesized well-defined nanobuilding blocks (NBBs) are also under development (route B).^{72–80} This approach uses precursors based on perfectly calibrated, preformed objects that preserve their integrity in the mesostructured templated hybrid phase. The size of the NBBs should be at least four times smaller than the micelles to be able to adopt the curvature of the organic (2–30 nm in size)–domain interface. The large variety of nanobuilding blocks (nature, structure, and functionality) and possible surface modifications with organic functions or organic connectors allows the creation of a vast range of different architectures. Indeed, such NBBs can be clusters (metallic oxoclusters, zindtl phase,

etc.), inorganic nanoparticles (metallic oxides, metals, chalcogenides, etc.), and nanocore–shells (path B-1).

The use of NBBs presents several advantages: (1) It is an ideal method for precisely defining the inorganic component and in potentially minimizing collapse problems that may be associated with template removal and crystallization. (2) Precondensed species exhibit a lower hydrolytic reactivity than molecular precursors so that the chemistry, self-assembly, and processing parameters are more decoupled. (3) The nanobuilding components are nanometric and monodispersed, with perfectly defined structures, which can be crystalline, that facilitate the characterization of mesostructured hybrid phases. (4) The step-by-step preparation of the mesostructured materials can allow for a high control over their semilocal structure.

(iii) Alternative approaches based on the combination of path A and path B (path B-2) may be conceived to achieve further control in terms of the local and semilocal structure and function of POMMs.^{81–85} This corresponds to surfactant directed assembling of hydrolyzed precursors in the presence of NBBs. The success of this strategy results from the ability of materials chemists to control and tune the hybrid interfaces. An example is the use of nano-objects capped with organic molecules to tune their affinities for different components of the surfactant and for the growing polymeric phase. In principle this strategy should permit tailor-made nanocomposites with directed positioning of NBBs inside the mesopores or inside the walls as ordered dispersions of nanobricks cemented by a polycondensed inorganic phase.

Beyond the relevant chemical and self-assembly phenomena, the processing and shaping of POMMs is also extremely important in targeted, real-world applications. The majority of research studies to date concerns periodically organized mesoporous materials shaped as powders or monoliths because these morphologies are especially suited for catalysis and adsorption applications.^{37,86–88} Periodically organized mesoporous thin films (POMTFs) are net shaped and present advantages in both facilitating the integration of matter and in the miniaturization of materials and devices. The first POMTFs were processed by Anderson et al.,⁸⁹ Ogawa,^{90,91} Ozin et al.,^{92,93} and Brinker et al.^{27,29,94,95} and consist of mesoporous layers of amorphous silica or organosilicas. The field of nonsilicate, transition metal oxide, rare earth, multimetallic oxide based POMTFs has exploded very recently.^{56,58,96–127} Today, these POMTFs can be designed with amorphous or nanocrystalline walls^{104,113,128} opening new opportunities for the development of many applications arising from the active properties (optic, electronic, dielectric, magnetic, etc.) created by metallic centers having *d* or *f* orbitals. The wide variety of different POMTFs will be detailed in part 4 for the pure inorganic matrixes and in part 6 for the hybrid organic–inorganic materials.

The various processing approaches used for the synthesis of POMTFs will be described in part 2. Among these methods, the chemical solution deposition methods are the most employed.^{27,94,129} In this approach, the meso-ordering occurs through the evaporation induced self-assembly (EISA) mechanism. Other less known processes have been also used. Film growth by electrochemical techniques,^{124,130–132} at

air–solution or substrate–solution interfaces (ASI or SSI respectively),^{92,133–135} or even by impregnation in vapor phase or in solution^{136,137} will be discussed. Pulsed laser deposition (PLD) techniques, involving laser volatilization followed by deposition onto a substrate of fragments coming from a target constituted of periodically organized mesoporous inorganic powder, have also been reported.¹³⁸

The tuning of the hybrid organic–inorganic interface between the template and the polymerizing phase, the control of the chemistry of the reaction media, and the template removal are of course key parameters during the elaboration of both POMTFs and POMMs. However, as thoroughly reported, the elaboration of POMTFs with a high degree of reproducibility requires a more comprehensive control of the highly coupled chemical and processing conditions.¹²⁹

Consequently, in the past seven years a strong emphasis has been given to the study of the mechanisms of formation of POMTFs through in situ characterization techniques (2D-GISAXS, WAXS, X-ray reflectometry, time-resolved infrared spectroscopy). For example, the use of high flux synchrotron beam lines allows the study of the film formation all the way from the molecular precursor solutions to the final mesoporous films,^{139,140} including consolidation, template removal, stabilization, and in some cases, crystallization to be followed in real time.^{113,141}

Full characterization of POMTFs does also require *ex situ* investigations that include conventional and unconventional advanced characterization techniques. The second category of techniques is required since thin films are anisotropic samples which have one dimension that is submicronic and which is often supported on a solid substrate. The very low quantity of material and contribution of the much greater quantity of the support make a complete characterization a challenge. Structural characteristics are obtained through TEM, SEM, and XRD but need to be completed by more adapted techniques such as GI-SAXS,^{113,139–141} X-ray reflectometry,^{142–146} ellipsometry porosimetry,^{147–150} or optically polarized xenon NMR.^{151–153} These techniques operate directly in thin films and then allow a complete characterization of the porous materials such as texture, connectivity, and so forth.

Today, POMTFs have reached a level of maturity where the intrinsic physical and chemical properties of the inorganic or hybrid matrixes, either amorphous or nanocrystalline, can be combined efficiently with a highly defined porous network having tunable pore size and connectivity, high surface area, and accessibility. The control of pore dimension and arrangement with respect to both the substrate and the atmosphere interfaces leads to direct or indirect accessibility to the substrate surface. This area is still new. However, promising results emanating from confinement effects, surface modification, and mesophase alignment via external fields demonstrate that new advances on oriented POMTFs can be expected.

Indeed, they already found applications in a wide range of domains (e.g., separation techniques, sensors, catalysis, modified nanoelectrodes, nanopatterning of composites, fuel cells, batteries, photovoltaic cells, micro-optics and photonic devices, microelectronics (low *k*), nanoionics, cells, func-

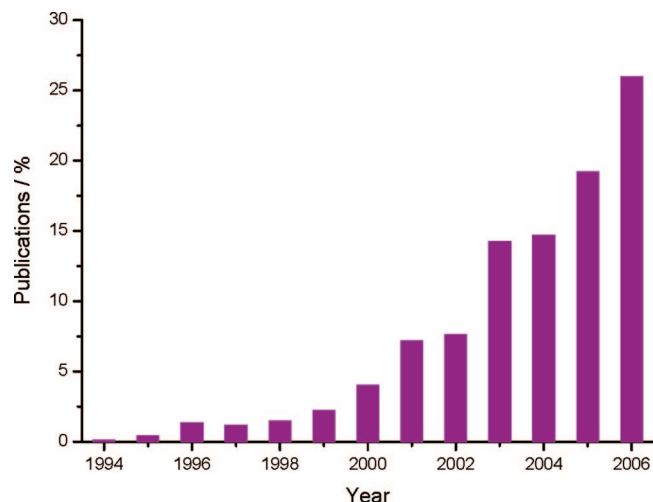


Figure 2. Published scientific articles on the field of POMTFs.

tional, protective coatings, biomaterials, biomicrofluidics, etc.) that will be presented in part 7.

The mushrooming of this field is illustrated in the Figure 2 which shows the evolution of the number of published scientific articles on the field of POMTFs obtained through surfactant templated growth since 1994.

As concluded in the several articles reviewing more specifically the different chemical, physical, and processing aspects associated with mesoporous films formation and properties,^{55,60,94,129,133,154} there is no question that the development of POMTFs will continue in the years to come as the scientific and technological aspects associated with the chemical, physical, and processing of POMTF formation and properties continue to be elucidated.

This article is focused on mesoporous “thin films” having micronic or submicronic thickness (typically between 5 nm and 1 μm). This distinction is made because, for thicker films and membranes, such as those prepared by casting, the boundary between a film and a monolith is fairly subjective.^{135,155} Moreover, for thicker films generally obtained through casting by evaporation of precursor sols or via gelation, the homogeneity is more difficult to control over the film thickness, resulting in the formation of chemical and structural gradients.¹⁵⁵ The present article reviews and discusses the major advances in the field of periodically organized mesoporous thin films (POMTFs) obtained through templated growth in the presence of molecular polymeric surfactants.

The second part of this article is focused on the different techniques used for the synthesis of POMTF. The third part is dedicated to the detailed presentation of characterization techniques that are specifically dedicated, and more or less routinely used, for the characterization of the mesostructure and mechanical properties of thin films. Then, an overview of inorganic and hybrid POMTFs that have been developed to date together with their corresponding properties is reported. The fifth part of the article concerns the mechanism of the hybrid surfactant-mesostructured phase and the associated chemical, optical, and thermal treatments used for the stabilization of the final POMTF. Then, the synthesis and the formation of hybrid P.O. mesoporous films are

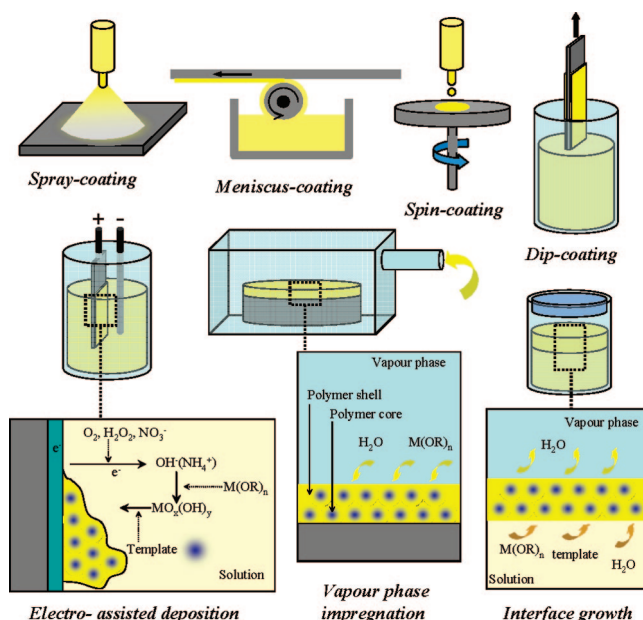


Figure 3. Various processing methods used to prepare POMTFs.

reported. Before the final outlook and concluding remarks, the most striking examples of the properties and applications of POMTFs will be presented.

2. Processing of POMTFs

Thin solid films can be prepared through a great number of different techniques that can be classified in three main categories, which are chemical, physicochemical, and physical.

While physical deposition techniques are preferred when dense thin films are to be prepared, chemical deposition approaches are much more appropriated to the preparation of porous layers. Preparing POMTFs using the template approach has thus mainly been achieved through chemical routes for which films are formed through the polycondensation of the inorganic precursors around organic supramolecular micellar assemblies at the substrate interface vicinity. The various non-exhaustive methods that can be applied to prepare such systems are illustrated in Figure 3.

The following part aims at briefly describing these methods in terms of process, involved mechanisms, achievement, critical parameters, advantages, and drawbacks. Most of the reported POMTFs were prepared by the evaporation-induced self-assembly (EISA) approach, where both templating agents and inorganic precursors are cooperatively self-assembled at the surface of the substrate through the evaporation of the solvent, within which these were previously dispersed. EISA is compatible with chemical solution deposition (CSD) techniques such as dip, spin, meniscus, and spray coatings.

These are widely employed for four main reasons: (1) they are easy to make use of, (2) they are already commonly used in industries, (3) one has a fairly good control on the chemical state of both volatile and nonvolatile parts in the solution before self-assembly, and (4) it is cheap and does not require expensive equipment. Even if preparing an ordered silica thin film is easy and does not require chemical and processing conditions to be controlled too drastically, understanding the whole sequence of phenomena involved

in the formation mechanism is necessary to be able to perfectly control the final mesostructure (pore size, density, morphology, order, and interconnection) and the associated stability. Because numerous efforts have been specifically dedicated to point out the critical parameters associated to EISA and to understand their effect on the self-assembly, these specific points will not be detailed here but in the upcoming part 5. Other approaches such as polymer layer casting, growth at solution/air interfaces, or electrochemical deposition have been attempted with more or less success. These methods do not ensure good reproducibility and mesostructured control as well as EISA can.

2.1. Chemical Solution Deposition Techniques, Compatible with EISA. In CSD the solution is cast over the surface of the substrate and is allowed to evaporate in a specific environment so as to control the evaporation rate of each volatile constituent. These conditions are also adjusted to prevent dewetting of the solution, usually observed with high surface tension solvents such as water, which would lead to nonhomogeneous covering and thickness. A good interaction between the substrate interface and the dry film is then required. The self-assembly is thus triggered during progressive concentration in template and inorganic precursors up to when a quasi equilibrium state is reached. This latter state, also called the tunable steady state (see part 5), is attained when the film composition is in equilibrium with its environment. Consolidation of the inorganic network around the micelles and anchoring of the film at the substrate surface are completed by further polycondensation. The initial solution casting is achieved through withdrawing the substrate from the solution at a constant rate for the dip-coating technique. In spray coating, the solution is pulverized onto the surface of the substrate using an aerosol generator or an atomizer. Spin coating is slightly different from the latter three other techniques in the way that a few milliliters of solution is dropped at the center of the spinning substrate and is spread by the centrifugal force. The film is thus formed at the same time of being submitted to a shearing force, applying between both interfaces of the drying solution layer. All these techniques are illustrated in Figure 3.

2.2. Impregnation of Copolymer Layers. This alternative method consists in preparing a first layer of pure template, (e.g., block copolymers, latex beads, etc.) and placing this layer into a saturated vapor phase of the inorganic precursor in the presence of the appropriate catalyst. The volatile inorganic precursor is first adsorbed on the template layer and diffuses into the layer to eventually undergo hydrolysis/condensation.^{156,157} Polycondensation thus takes place around the templates that have to be eliminated to liberate porosity. In this method a solution of the templating surfactant (CTAB) in ethanol/water is deposited onto a silicon substrate by spin coating. The substrate was placed vertically in a closed vessel and exposed to TEOS or TMOS vapor and a catalyst (ammonia or HCl vapor).¹³⁶ The vessel was heated at 90–180 °C for 0–12 h. Similar approaches can be used to infiltrate predeposited block copolymer films from an inorganic precursor solution.^{158,159} However, one must make sure

that the polymer layer must be stable toward dissolution in such media.

2.3. Growth at Interfaces. This method is used to prepare self-standing films and self-supporting films. It consists of using interfaces, such as atmosphere/solution or aqueous solution/organic solution, to concentrate the various reactive precursors and templating agents.^{160,161} Processing times are generally longer than the ones for EISA but provide free-standing and self-supporting films, both very useful for the understanding of the formation mechanisms of surfactant templated growth.¹³⁵ Advantages of this technique are that thicker mesoporous films can be grown without cracks at liquid/liquid or liquid/air interfaces. A typical synthetic procedure is as follows: Films were grown on substrates in acidic solution containing tetraethoxysilane (TEOS), water, HCl, and hexadecyltrimethyl ammonium chloride (C16TAC). The substrates were held upside down in the solution to prevent bulk precipitate from sticking to the film surface. Films were grown at room temperature or at 80 °C under hydrothermal conditions. Free-standing films formed by the nucleation at the air–water interface^{93,161–164} while CTAB templated silica films were grown at oil/water interfaces.^{165,166} Exotic methods are also proposed: less than 100 nm mesoporous silica films were prepared by convective self-assembly (capillarity raise of the solution between two substrates followed by EISA),¹⁶⁷ but infinitely thin films can more easily be performed by conventional liquid deposition techniques. SAM (self-assembled monolayer) macropatterns were also obtained by such an approach.¹⁶⁸

2.4. Electrodeposition. Electrodeposition is usually well suited for the preparation of mesostructured metal layers on electrode surfaces.^{15,26,130,169,170} Mesoporous Co, Ni, and Bi (semimetal) films have been formed by reduction into a lyotropic liquid crystalline solution of PEO-based surfactant.¹³¹ Mesoporous thin ceramic films have been prepared on electrode surfaces using electroassisted deposition. This latter method involves the precipitation of MOn at such interfaces where exchange of electrons takes place. In general, the oxidation state of a soluble cation M^{n+} , which is the inorganic precursor, is modified through oxidoreduction so as to form insoluble species locally at the electrode. Precipitation under hydroxide or oxyhydroxide phase takes place. If this occurs in a liquid crystalline mesophase, there is a great chance for the precipitate to build up around micellar templates. The hybrid wet layer must thus undergo the classical network condensation and template elimination treatments to obtain the mesoporous solid film.¹³² An alternative route consists in precipitating inorganic precursor through electrochemically induced local pH change. Typically, OH^- species are generated at the electrode when NO_3^- , O_2 , or H_2O_2 are reduced at the cathode. Species that are only soluble in acidic conditions can be precipitated on the cathode upon pH raise.¹³⁰ Recently, the double-gyroid nanoporous-film-coated electrodes are used to fabricate inverse double-gyroid platinum nanostructures by electrodeposition, followed by etching to remove the silica.¹⁷¹

2.5. Physical Techniques. The pulsed laser deposition (PLD) technique has been used to prepare nanoporous silica thin films on solid substrates.¹³⁸ A subsequent hydrothermal

treatment of the ablated films led to nanoporous silica films with the pores oriented perpendicular to the substrate.

2.6. Control of Thickness. Thickness is the primary characteristic of a thin layer. Usually, thicknesses are comprised between several nanometers to several micrometers, depending on the application, and one must be careful in choosing the adapted method of deposition since some are more appropriated to ultra-thin film preparation (spin-coating, dip-coating), while others (spray, electrodeposition) allow thick film elaboration. Parameters controlling the thickness vary with techniques and one can easily understand that these are the density of exchanged electrons for electrochemical assisted deposition, the time for diffusion limited methods (interface growth), or the quantity and the concentration of the deposited solution in chemical solution deposition methods. For these latter CSDs, it is sometimes difficult to predict the thickness, and some specific studies were carried out especially for dip- and spin-coatings. The thickness of SBA15-type silica films was related to the solution density and viscosity (concentration) in addition to the dip-coating withdrawal rate of the substrate.¹⁷² They confirmed that the presence of the templating agent does not dramatically affect the formal rules established by Brinker and Sherrer^{6,173} for pure silica sol–gel solutions, as long as the proper viscosity is used in the equation.

3. Characterization Techniques of POMTFs

Mesoporous thin films are made of a very small amount of matter (usually between 10 and 500 $\mu\text{g}/\text{cm}^2$ of film) spread onto a substrate. Their characterization, more difficult than for bulk materials, is thus limited to spectroscopic investigations and very sensitive techniques. Different levels of analysis are found in the literature. At microscopic level, the chemical composition is determined by Fourier transform infrared spectroscopy (FTIR), Rutherford back scattering (RBS), energy dispersive X-ray analysis (EDX), and X-ray photoelectron spectroscopy (XPS). The microstructure is obtained by Raman scattering (RS) and wide angle X-ray diffraction (XRD). The mesostructure is probed by electron microscopies (SEM and (HR)TEM) and diffusion and reflectometry techniques (SANS, SAXS, XRR, neutron reflectometry). The porous texture (often required for applications) can be described by gas adsorption, monitored by gas consumption (Krypton adsorption), spectroscopic ellipsometry (ellipsometric porosimetry, EP), X-ray reflectometry, surface acoustic wave (SAW) or hyperpolarized ^{129}Xe NMR. Although it was reported only for nonperiodically organized porous dielectrics, positron annihilation lifetime spectroscopy (PALS) in principle can also be used.^{174,175} For porous or hybrid nonporous films, the texture can be investigated by following the diffusion of a chemical probe through the porous (organic) mesoscopic network by electrochemical characterization or spectroscopy. Because of its high sensitivity, fluorescence spectroscopy is also used for characterizing locally the environment of a probe, collecting information on the organic domains of a hybrid film, on the organic/inorganic interface (detailed further in section 6), or on the symmetry and chemistry of an emitting inorganic center of the inorganic matrix. Finally, the me-

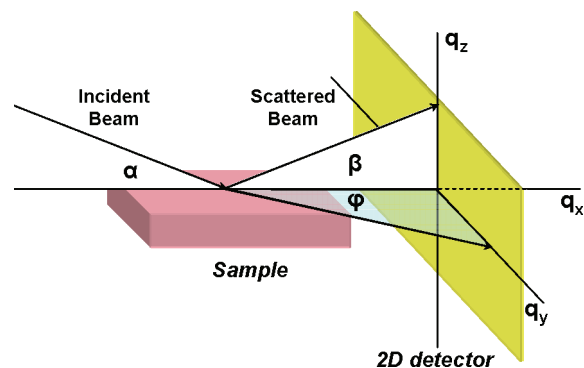


Figure 4. GI-SAXS experimental setup for thick substrate.

chanical properties of the thin films can be obtained by nano-indentation (NI), ellipsometric porosimetry, or acoustic waves analyses (SAW, Brillouin light Scattering).

This part is dedicated to the detailed presentation of techniques that are specifically dedicated to, and more or less routinely used for, the characterization of the mesostructure and mechanical properties of thin films. The coupling of some of them will be detailed further in the section 5.

3.1. Structural characterizations. Until recently, most of the works reported in the literature were using conventional 1D XRD techniques (Bragg–Brentano geometry) to assess the mesostructure of the POMTFs. Yet, it was demonstrated that this simple technique is, in most cases, insufficient to correctly define the structure as a result of the mono-orientation of the ordered domains with respect to the substrate interface. Indeed, a straightforward and nonambiguous characterization of the structural periodic organization of the mesoporous network can only be visualized by 2D-SAXS.¹⁷⁶ Even if the very few number of laboratory SAXS equipments available and the difficulties to access synchrotron SAXS lines make such investigations difficult to perform, it remains the absolute tool. When access to GI-SAXS is possible, one of the most common way of assessing the proper structure is to combine 2D diffraction patterns and TEM images,^{98,176–182} which provides a direct observation of the mesoporous network and the measurement of its periodicity, space group, and potential network contraction. Figure 5 illustrates the high complementarity of both techniques. Occasionally, AFM investigations complete the structural analyses.

3.1.1. GI-SAXS (Grazing Incidence Small Angle X-ray Scattering). GI-SAXS is based on angular distribution of X-ray coherent scattering intensity, and is well suited to the characterization of thin mesoporous films since it allows probing the entire thickness and informs on the periodicity, the orientation, and the space group of the ordered domains. Diffusion scattering (and potentially diffraction) is observed at low angles when electron density inhomogeneities exist in the nanometer range. The experimental setup is usually a film irradiated by a narrow X-ray beam at very low angle (α angle $< 1^\circ$). The angular distribution of the scattered X-rays is collected onto a 2D detector as shown in Figure 4.

For POMTFs, the obtained diffraction diagrams exhibit diffraction spots characteristic of the periodical mesostructure of the film (some examples are given in Figure 5).

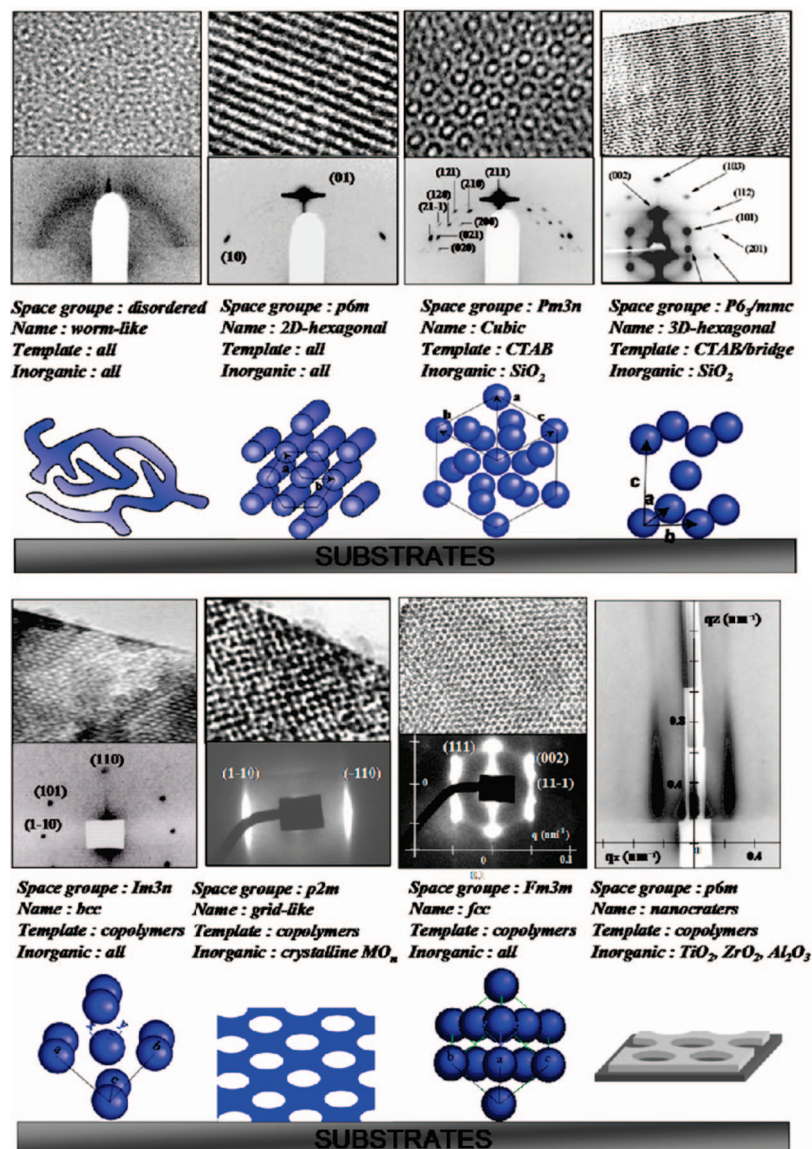


Figure 5. 2D SAXS patterns corresponding to the various types of mesostructures obtained. Lattice models of similar symmetry group and typical TEM images representing various cutting directions. Adapted with permission from ref 129. Copyright 2004 Wiley–VCH.

The z -axis information is not sufficient to discriminate between a hexagonal, a lamellar, or a cubic phase of the same z axis periodicity. From the complete 2D diffraction pattern, one can identify the packing geometry of the mesophase. The structure attribution should be made with much care by coupling 2D diagrams with TEM. One meets too often in literature some errors in mesostructure determination when only comparisons with known 2D-diffraction diagrams are made. To discard some artifact, the experimental data are generally fitted with different software such as FIT2D¹⁸³ and A.P. Hammersley/ESRF¹⁸⁴ and compared to diagrams simulated by the CMR¹⁸⁵ or the NANOCELL¹⁸⁶ codes.

However, some of these software packages (FIT2D and CMR) do not account for dynamic effects which are important to include as they cause the appearance of additional spots and the shifting of spots away from the position predicted implementation of the Born approximation. The only code that accounts for all spots and accurately simulated the spot position and the full intensities is the NANOCELL^{186,187} codes. This NANOCELL software can

also be used to calculate diffraction patterns in 2D SAXS geometry for arbitrary angles of incidence, that is, nongrazing incidence conditions. However, the influence of the disorder and the orientation of the films with respect to the substrates are not taken into account on 2D SAXS data using these softwares. Recently, Ruland and Smarsly reported the possible disorder effects on 2D SAXS data for cubic mesostructures, for arbitrary angles of incidence of the X-ray beam.¹⁸⁸ Depending on the intensity of the X-ray source, GI-SAXS is used only for structural determination of a stabilized film (laboratory SAXS)^{189,190} or for time-resolved analysis (Synchrotron sources).¹²⁹ The latter configuration is a very powerful tool for the understanding of mesostructure formation mechanisms and rapid mesophase transformation (uniaxial contraction and/or crystallization of inorganic walls).^{103–105,113,129,139,191,192}

GI-SAXS allows the determination of the mesostructure, the anisotropy of a mesostructure (needed for accurate pore size determination by other techniques described hereafter), and the coexistence of several mesophases (either due to a lack of

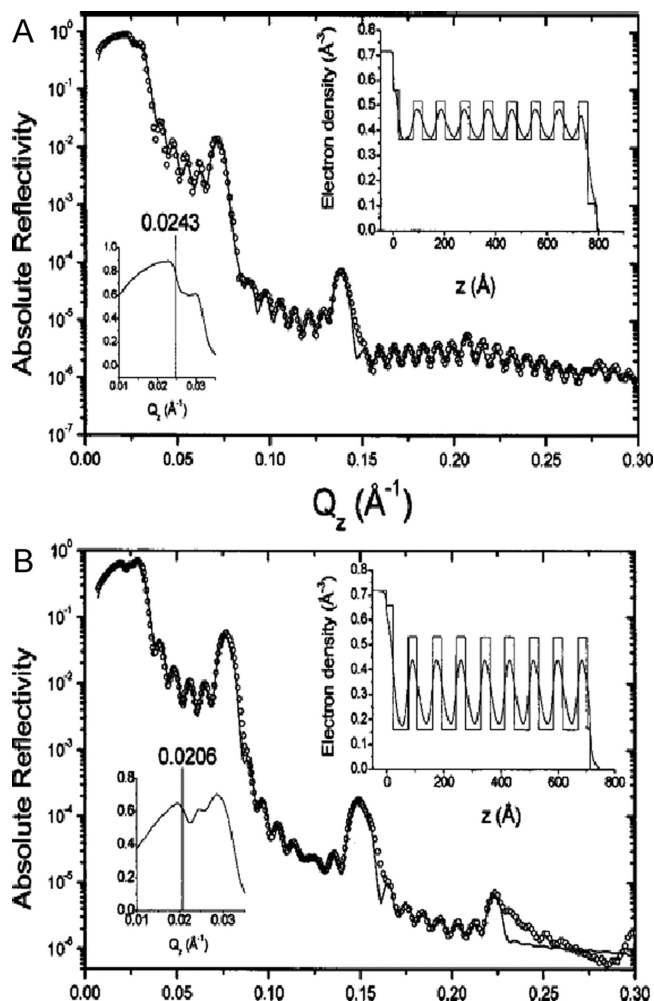


Figure 6. Absolute reflectometry diagram of (A) as made and (B) washed periodically organized (P.O.) silica film. The top inset gives the electron density profile obtained after a fit via the matrix technique. The bottom inset shows the critical angle region. Reprinted with permission from ref 142. Copyright 2005 American Institute of Physics.

homogeneity of the film or by stacking of different mesostructured layers).¹⁹³ No film thickness limitation is met in GI-SAXS.

3.1.2. X-ray Reflectometry (XRR). XRR is a scattering technique allowing the nondestructive determination of the electronic density, the thickness, and the interfacial rugosity of a thin film. The experimental setup is usually the same as described in Figure 4: a film irradiated by a narrow X-ray beam at low incidence angle ($<1.5^\circ$). However, in this case, the incident and detecting angle are similar ($\alpha = \beta$), $\varphi = 0$, and the detector is punctual. For such configuration, one can only observe electronic density variations along the (z) axis. The complete acquisition time varies from 5 min to 24 h, depending on the thickness of the film and the quality of the obtained data. The resulting reflectometric diagram is produced by the interferences of the beam reflected at the surface of the film and the beam reflected by the other interfaces of the system (the film–substrate interface and the “high electronic density”–“low electronic density” interfaces of the mesostructure). At low wave vector (bottom inset in Figure 6), one measures the critical angle of penetration of the beam into a homogeneous film from which the refractive index of the film is determined according to the Snell–Descartes law (eq 1).

$$\cos \theta_C = n_{\text{FILM}} \quad (1)$$

For angles $\theta > \theta_C$, interference fringes appear: these fluctuations can be described by the extended Bragg law. In addition POMTFs exhibit diffraction peaks characteristic of the meso-ordered phase of the film that overlap the interference diagram. A complete fitting of these contributions is usually needed and allows the determination of structural information such as refractive index of the film, film thickness, electronic and (if the chemical composition is known) mass densities, and electronic density profile of the film along the (z) axis. For porous films, one can estimate also with a good accuracy the mesostructure wall density¹⁴² and the pore volume. The knowledge of the mesostructure symmetry allows sometimes a deeper analysis of reflectometry data by taking into account the average micellar radius and its variance, the average lattice parameter of the mesostructure, and the finite number of layers of organic (porous) domains constituting the film.^{194,195}

A good example of such an approach is given in the following reference from Smarsly et al.¹⁹⁶ in which the pores size of a silica POMTF with 2D-hexagonal structure could be measured along the (z) axis. This approach assumes that pores are cylinders with a perfect round section. XRR pattern fitting can be performed with a total film thickness varying from a few nanometers to 450 nanometers. The fitting equation can be also solved for multilayer systems (limited at three layers). XRR and GI-SAXS are very complementary techniques.

3.2. Textural characterizations. 3.2.1. Gas Physisorption Porosimetry. Although the determination of the mesostructural parameters of a POMTF is a first necessity for materials scientists, many applications involving porous films are crucially depending on the accurate knowledge of the pore size distribution (PSD), pore connectivity of the network, and the ability to determine matter exchange and matter adsorption capacities of the porous network and the film environment. Adsorption porosimetry is considered as the reference analytical approach for the description of micro- and mesoporous parameters. By analyzing the multilayer physisorption and capillary condensation of a gas within the pores, a plot of the adsorbed volume of gas versus the partial pressure P/P_0 of gas is obtained. The mono- and multilayer physisorption of the gas observed at low P/P_0 can be plotted by the Brunauer–Emmett–Teller (BET) equation eq 2 and allows the determination of the surface area, with n_m being the number of molecules needed to cover the accessible surface with a monolayer of molecules, n , the number of molecules adsorbed at the partial pressure P/P_0 , and C , a parameter characteristic of the net heat of adsorption of the molecule at the surface.^{197,198}

$$\frac{P}{n(P_0 - P)} = \frac{1}{n_m C} + \frac{C - 1}{n_m C} \frac{P}{P_0} \quad (2)$$

The gas uptake observed at higher P/P_0 values, characteristic capillary condensation, is used for the determination of the PSD between 2 and 50 nm via the Kelvin equation (eq 3) that describes the condition of appearance of the capillary condensation at a given value of P/P_0 , with γ , the condensed liquid surface tension, V_L the molar volume of

the liquid adsorbate, r_p the radius of the pore, and G , a geometrical factor characteristic of the liquid–air meniscus curvature (BJH model).¹⁹⁹ More sophisticated models taking into account the internal curvature of the liquid–solid interfaces^{200–202} and the thickness of adsorbed gas layer before capillary condensation (modified Kelvin equation²⁰²) or taking a nonporous material of similar surface properties as the reference (t -plot or α -plots^{197,198}) are advantageously employed.

$$RT \ln\left(\frac{P}{P_0}\right) = -\gamma V_L \frac{G}{r_p} \quad (3)$$

The micropores characterization is obtained by plotting the adsorption curve at very low partial pressure ($P/P_0 < 0.1$). Originally developed by Dubinin and Radushkevitch,^{197,198} the micropore size distribution determination is now being efficiently supplanted by the DFT approaches whenever a realistic description of the surface can be given.^{203–206}

The physisorption can be monitored by measuring various physical parameters (adsorbed gas volume pressure, electronic density, refractive index, weight of gas adsorbed, spectroscopic absorbance of the adsorbed gas, etc.). Depending on the physical parameters, various theories are used to obtain the experimental plot of the adsorbed volume versus the external gas partial pressure.

3.2.2. Nitrogen and Krypton Physisorption. The sample is heat-outgased several hours in a vacuum chamber for removing any adsorbed molecule from its surface. A controlled partial pressure of nitrogen at 77 K is then applied over the sample, and the adsorbed volume of gas is directly measured. The DFT approach previously described can be used to characterize the porous network. However, other approaches such as BdB and BJH where the condensed N_2 density is approximated to the bulk liquid N_2 density have been also developed. Yet, easily used for bulk materials, this technique is difficult to apply to thin films attending the very limited amount of porous matter available on one film deposited onto a substrate of several square centimeters surface. Only a few examples of nitrogen adsorption onto POMTFs have been reported. In these cases, the authors have used several tens of films to collect the minimum amount of porous matter needed.²⁰⁷ This fastidious work pushed scientists to develop alternative porosimetry techniques implying only one film.

Replacing N_2 by Kr (sublimation pressure at 77 K is ~ 1.7 torr) reduces drastically the amount of unadsorbed molecules in the dead volume. The adsorbed amount of gas is then monitored with an improved accuracy (about ten times less matter is needed in this case to obtain adsorption–desorption isotherms as shown in Figure 7). However, unless special conditions are applied, mesopores larger than approximately 6 nm cannot be studied for fundamental reasons at 77 K using Kr, because for these pore size Kr does not condense to a liquid.²⁰⁸

3.2.3. Spectroscopic Ellipsometry Porosimetry (EP). The ellipsometry is a nondestructive optical technique based on the analysis of the change of polarization state of a polarized light beam after reflection onto a surface. The ellipsometric parameters (Ψ and Δ), obtained from the Fresnel coefficients

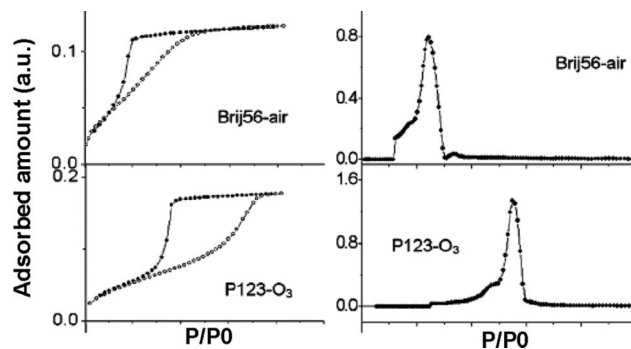


Figure 7. Kr physisorption isotherms of periodically organized silica films prepared with different structuring agent. The PSD is determined with the BdB model. Reprinted with permission from ref 209. Copyright 2006 Elsevier.

of the reflected beam, are very sensitive to the presence of a superficial layer of optical properties different from those of the substrate. This technique is routinely used to assess the film physical thickness and its optical density. It can be applied to multilayer systems. By knowing the number of layers constituting the film analyzed and the measuring Fresnel coefficients, one can simulate the optical system by the matrix method initiated by Abeles²¹⁰ or can use iterations with a dispersion law to determine the optical properties and thicknesses of the different layers of the system for each wavelength of the incident light beam. Spectroscopic ellipsometers give thus more reliable data than single wavelength ellipsometers.

For the porosimetry measurements, two types of apparatus exist. The first one (ellipsometric porosimetry) is a spectroscopic ellipsometer on which a vacuum chamber is fixed. A partial pressure of gas is applied over the film for a controlled physisorption, in the same way of usual N_2 porosimetry.²¹¹ The second type of apparatus was developed more recently in our laboratory.¹⁴⁸ In this case the analysis is performed at atmospheric pressure (environmental ellipsometric porosimetry, Figure 8) by applying onto the film a dynamic flux of air containing a controlled relative pressure of gas (usually water or alcohol). This last setup allows the analysis time to be decreased by a factor ten (1 h is needed to obtain a complete adsorption–desorption isotherm) and is very advantageous for the simulation of environmental adsorption of gas.

The physisorption of a gas into the porous network of a POMTF gives several types of very interesting data. First, the isotherm of the variation of the refractive index of the film can be plotted versus the relative pressure of gas (cf. Figure 8). By using classical Lorentz–Lorentz or Bruggeman effective medium approximation models, this isotherm allows the determination the porous volume of the film (optical properties of the skeleton are needed) and the determination of the adsorbed volume of gas at each relative pressure (the optical properties of the adsorbant in liquid state are needed). The classical analysis of this isotherm produces a first approximation of the porous structure parameters. However, this analysis can be improved by taking into account the specificity of the adsorbate–surface interactions (wetting angle) and the specific geometry of the pores that are never spherical nor cylindrical for POMTFs prepared by the

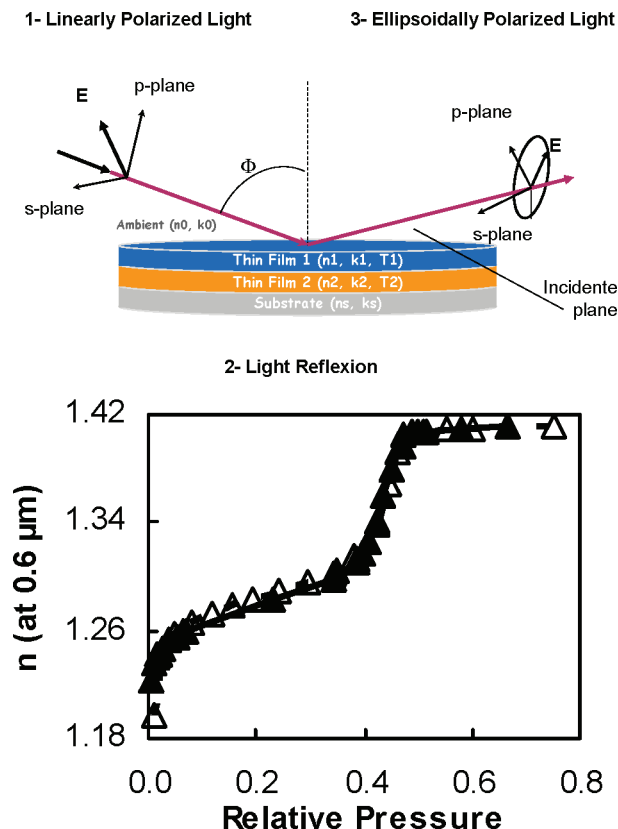


Figure 8. (top) Scheme of the reflection of a linearly polarized light beam onto a substrate coated with two layers of matter of real and imaginary parts of the refractive index of n_i and k_i and of thickness T_i ; (bottom) example of adsorption-desorption of ethanol into a P.O. mesoporous silica film. Reprinted with permission from ref 149. Copyright 2004 Elsevier.

sol-gel route.¹⁴⁸ Finally, only one analysis is needed for the complete characterization of a multilayer periodically organized system such as those described by Soler-Illia and co-workers.^{193,212,213}

In a second time, EP and EEP analysis allow the determination of variation of film thickness versus the adsorbate partial (relative) pressure. The observed swelling and contraction of the POMTFs (impossible to obtain with the standard N_2 or Kr physisorption) are very informative on the adsorption mechanisms taking place. A low pressure swelling is characteristic of micropores with molecular adsorption mechanism. On the other hand, the contraction observed whenever mesopores are analyzed is due to capillary forces (a collective effect of the adsorbed molecules forming a liquid meniscus, Figure 9). From this contraction isotherm, the transverse Young's modulus E of the film can be easily determined at pressure higher than the capillary condensation with the general eq 4 in which T_0 is the film thickness, V_L is the molar volume of the liquid adsorbate, $\cos \theta$ is the adsorbate-film wetting angle at high partial (relative) pressure of adsorbate, and k is the variation of film thickness versus the logarithm of the partial (relative pressure) during the relaxation of capillary stress.^{148,214-216}

$$E = \frac{T_0 RT}{V_L \cos \theta} \frac{1}{k} \quad (4)$$

XRR measuring both film thickness and refractive index and its adaptation with a controlled pressure chamber allows

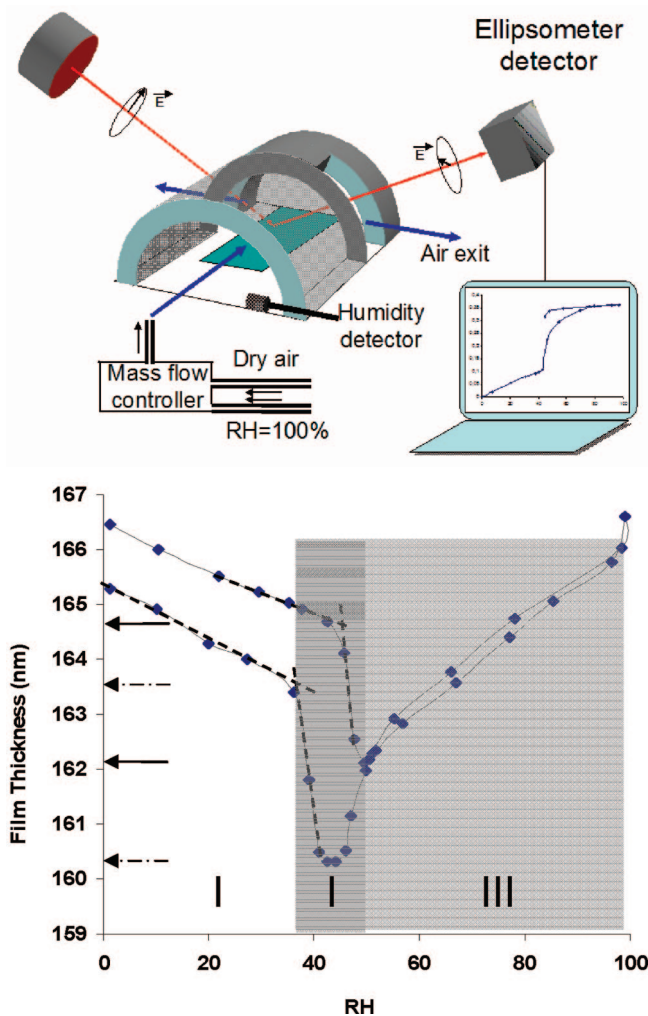


Figure 9. (top) EEP apparatus for water adsorption. (bottom) Contraction isotherm observed during water adsorption of a P.O. mesoporous film. Zone I, before capillary condensation; zone II, contraction characteristic of the capillary condensation; zone III, progressive relaxation of the capillary stress. Reprinted with permission from ref 148. Copyright 2005 American Chemical Society.

the realization of similar analyses.^{146,217} Yet, if XRR is limited to the analysis of 500 nm thick films, the ellipsometry limit depends on the wavelength of the light source. The use of a UV-vis ellipsometers pushes this limit to a few micrometers, and the use of infrared wavelength extends it to about $50 \mu\text{m}$. In addition, IR light being sensitive to the vibrational behavior of molecules, IR-EP is an analytical tool extremely interesting, able to monitor the vibrational signature of the adsorbate during the adsorption and/or to perform a chemical analysis of the film with a spatial resolution.¹⁴⁷

So far, the very recent EP and EEP techniques (SOPRA²¹⁸) are developing very fast in laboratories and become reference techniques for the analysis of thin film porous networks.

3.2.4. Surface Acoustic Waves (SAW). Surface acoustic waves are generated and detected by interdigital transducers deposited directly on a piezoelectric substrate, with the device used as a feedback element in an oscillator circuit (Figure 10).²¹⁹ The frequency and propagation velocity of the SAWs are very sensitive to mass loading and propagation surface structure of the piezoelectric substrate such as some rugosity or the presence of a film (Figure 11).

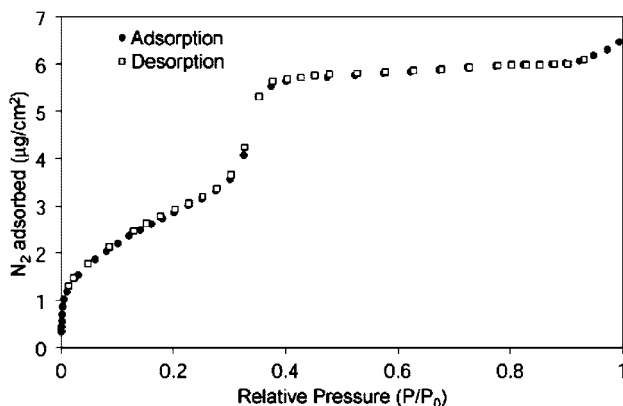
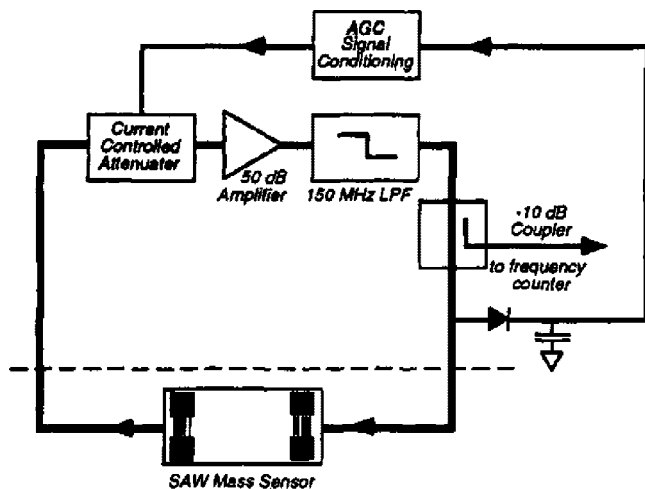


Figure 10. (top) Scheme of a SAW detecting system. Reprinted with permission from ref 220. Copyright 1993 American Chemical Society. (bottom) N_2 adsorption-desorption isotherm of a POMTF functionalized with COOH groups. Reprinted with permission from ref 221. Copyright 2003 The Royal Society of Chemistry.

SAW devices have been used in porous thin film characterization for more than 10 years.^{29,220,221} After deposition of the porous film onto the piezoelectric substrate (quartz usually), the SAW sensor is cooled at 77 K and used for classical N_2 physisorption.

In this case, the SAW sensing system is perturbed in two ways, by adding some weight and, usually in a minor proportion, by modifying the stiffness of the surface. The fractional addition of weight produced by N_2 adsorption modifies the SAW velocity v as given in eq 5

$$\Delta v/v = -C_m f_0 \Delta m \approx \Delta f/f_0 \quad (5)$$

where C_m is the calculated mass sensitivity (for ST-quartz $C_m = 1.29 \times 10^{-6} \text{ cm}^2 \text{ s g}^{-1}$),²²⁰ v_0 and f_0 are the unperturbed SAW velocity and frequency, respectively, and Δm is the change in surface mass density (mass/area). For small perturbations, $\Delta v/v_0$ can be approximated equal to the relative shift of the oscillation frequency. Measurements in the change in oscillation frequency as a function of N_2 partial pressure produce the adsorption-desorption isotherm $\Delta m = F(P/P_0)$ on which classical porosimetry models can be applied. No thickness limit exists on such a detection mode. However, the film has to be deposited and treated directly onto the piezoelectric substrate. Any film post-treatments able to damage the substrate of the

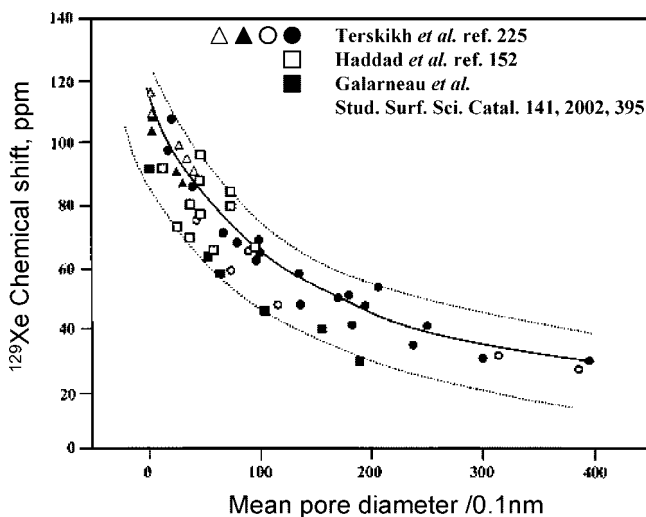
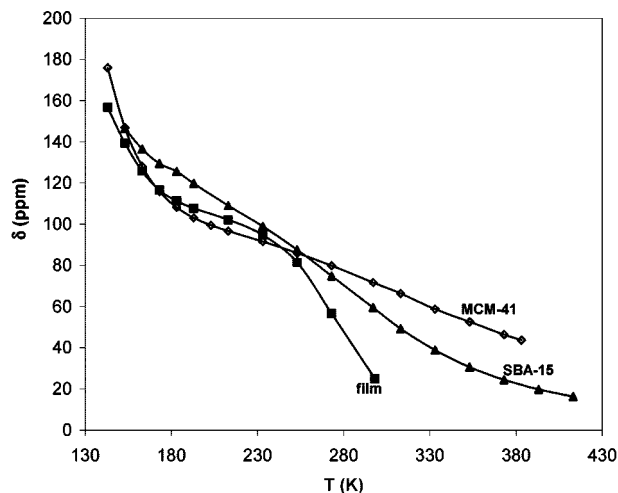


Figure 11. (top) Correlation between ^{129}Xe chemical shift and mean pore diameter of various periodically organized mesoporous materials. Reprinted with permission from ref 152. Copyright 2004 Elsevier. (bottom) Comparison of chemical shifts of mesoporous silica powders and film as a function of the temperature. Reprinted with permission from ref 227. Copyright 2004 Elsevier.

electrodes are then to be avoided (very high temperature treatments needed for the nanocrystallization of some films, for example).¹⁰⁹

When generated by a laser, the density and mechanical properties can be measured through the surface wave velocity using spectroscopic SAW (SAWS). In this case, the wave velocity v_f obtained data frequency f depends on the material density, the Poisson ratio, and the Young's modulus E . When detected at different distances from the wave generation point, a frequency dependent velocity dispersion curve is obtained and fitted. By knowing both substrate and film materials properties, the Young's modulus of the film can be determined. More detailed information is given in ref 222.

3.2.5. Optically Hyperpolarized ^{129}Xe NMR (OHPXe NMR). In the past 20 years, ^{129}Xe NMR has become a popular technique for the characterization of porous solids.^{223,224} However, application of thermally polarized ^{129}Xe NMR produces a relatively weak signal because of low concentration of adsorbed xenon and long relaxation time. An increase in sensitivity by a factor 10^4 can be achieved by using optical pumping techniques for the

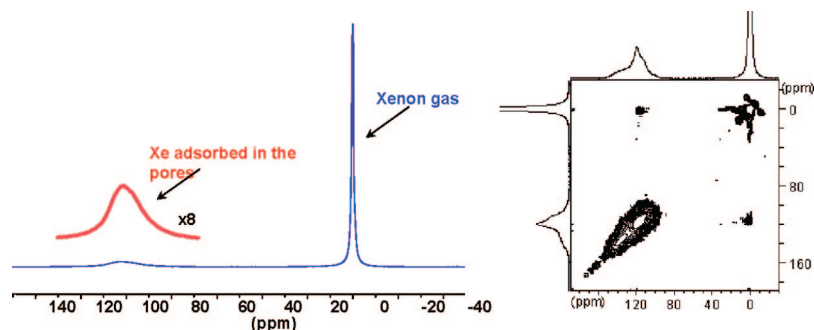


Figure 12. (left) 1D analysis of a silica POMTF and (right) 2D EXSY spectrum of ^{129}Xe on phenyl hybridized SiO_2 POMTF with mixing time of 0.1 ms. Reprinted with permission from ref 227. Copyright 2004 Elsevier.

production of hyperpolarized xenon, making OHPXeNMR a suitable technique for the investigation of the porous structure of thin films.^{151,152}

By adsorbing in a porous network, the chemical shift δ of ^{129}Xe is modified by the xenon-surfaces δ_{Surf} and xenon–xenon δ_{Xe} interactions as expressed in the eq 6

$$\delta = \delta_{\text{ref}} + \delta_{\text{Xe}} + \delta_{\text{Surf}} \quad (6)$$

where δ_{ref} is the chemical shift of the xenon gas at zero pressure ($\delta_{\text{ref}} = 0$). Following the analysis of Terskikh et al.,²²⁵ that is, assuming fast exchange conditions, that the xenon adsorption obeys Henry's law and that the observed δ is a dynamic average between the gas and the adsorbed states, one can express the chemical shift as a function of the pore diameter (eq 7).

$$\delta = \delta_{\text{Surf}} / [1 + D / (fK_{\text{ads}}RT)] \quad (7)$$

where the pore diameter D and K_{ads} is the Henry's constant and f is a factor depending on the geometry of the pores. The smaller the pore, the more shifted the signal. For microporous materials, empirical correlations have been proposed long ago.²²⁶ Although very simple, this δ - D correlation has to be taken with care attending that additional structural parameters can modify the chemical shift (presence of chemical heterogeneities such as Al^{3+} centers or organic groups or coexistence of microporosity and mesoporosity leading to strongly adsorbing sites).

According to the literature, pressure dependent and temperature dependent analyses can be performed on POMTFs. Pressure dependent experiments allow determining the presence of strongly adsorbing sites. As xenon pressure increases, a quasi constant chemical shift shows a homogeneous surface quality. On the other hand, a chemical shift moving at higher field is typical of the presence surfaces with different adsorbing strengths (such as micropores connecting some mesopores, for example).²²⁷

Temperature dependent experiments explore the exchange processes occurring between the free xenon, the xenon mobile into the pores, the xenon adsorbed at the surface, and if a hybrid film is investigated, the xenon absorbed within (adsorbed onto) organic domains.¹⁵³ The evolution of the variable-temperature spectra reflects the changes of adsorption constant with temperature. This experimental approach allows the probing of the porous network connectivity and of the proximity of adsorbing sites of different energies. Figure 12 gives the example of the dynamic investigation of a periodically organized silica film grafted with phenyl

groups via a 2D exchange ^{129}Xe xenon spectroscopy (EXSY) on which the exchange times of each type of xenon can be probed. The observed evolution of chemical correlations clearly indicates a hierarchical set of exchange processes following the sequence (from fastest to slowest): mesopore with free gas, mobile xenon in mesopores with xenon residing in the organic phase, free gas with micropores, and finally, between gaseous mobile xenon and xenon residing in the organic phase. Future developments of OHPXeNMR will likely allow determining of inhomogeneities, connectivity, and diffusion coefficient in hybrid and inorganic POMTFs.²²⁸

3.3. Electrochemical Investigations. Electrochemical techniques have been studied only recently on POMTFs. They allow an efficient probing of molecular dynamics in films and gels²²⁹ and are used to access the porous network accessibility and interconnectivity. However, for many applications implying the optimization of the diffusion (or retention) of a probe through the porous network of a film (modified electrodes, sensing, photovoltaic cell, photocatalysis or solution ultrafiltration, controlled drug release, etc.) these techniques are very valuable.

The classical analyses are cyclic voltammetry and chronoamperometry, one example of a wall-jet experiment have also been reported.^{230–235} Cyclic voltammetry monitors the oxidative and reductive behavior of a chemical probe when various potentials are applied between two electrodes. By extension, it also allows the accessibility of the film coated electrode by a selected electrolyte to be determined, thus investigating the influence of the synthesis parameters (chemical composition, coating process, thermal treatment, etc.) and the detection conditions onto the porous structure of the film and its transport properties.²³⁶ When coupled with intensity monitoring at different scan rates, the apparent diffusion coefficient (D_{app}), thus the charge transfer, can be obtained^{230,233} from the Randles–Sevcik equation (eq 8)

$$D_{\text{app}} = (p/0.44nFAC_{\text{Fe}})^2(RT/nF) \quad (8)$$

where n is the number of electrons per probe unit, A is the active area of the electrode, C_{Fe} is the volume concentration of probe within the film, p is the slope of the straight line I vs $(\text{scan rate})^\alpha$ relationship where α is the diameter of the solution jet, R is the gas constant, T is the temperature, and F is the faraday constant. The best porous structure can then be selected for each targeted application.²³¹

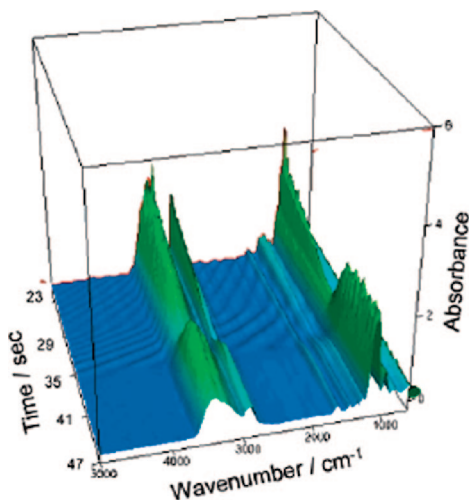


Figure 13. Rapid scan time-resolved FTIR monitoring of the formation of a periodically organized silica thin film by EISA. Adapted with permission from ref 238. Copyright 2006 American Chemical Society.

3.4. In Situ Fourier Transform Infrared. FTIR is powerful routine characterization technique analyzing the absorption of IR wavelength by local vibrational states and chemical bonds (bending, stretching, or rotating), usually in the energy range $400\text{--}4000\text{ cm}^{-1}$. Usually of limited sensitivity, this technique is often valuable for the characterization of POMTFs because their high surface area renders FTIR sensitive enough for detecting adsorbed species. FTIR is then used for quantification of organic functions (assessment of structuring agent departure, grafting of organic functions,¹⁹² organic molecule adsorption–desorption isotherms, complexation state of carboxylate groups, or less often, inorganic matrix hydroxylation and condensation states).¹⁸³

In situ FTIR is a very interesting evolution of this widespread technique.^{183,237} Employed to double the GI-SAXS experiments, a synchrotron source is used for rapid scan time-resolved FTIR to analyze the chemical composition of the film cast during the evaporation and mesostructuration processes.²³⁸ The time resolution is excellent (less than 0.2 s). In this case of a periodically organized silica film, solvent evaporation (before 38 s) and silica network condensation (after 38 s) were monitored between $800\text{ and }5000\text{ cm}^{-1}$ (Figure 13). The dynamic water content of the film can then be monitored (the time needed to equilibrate the water composition of the film with the environment relative humidity) and followed until the inorganic network was rigid. At laboratory scale, similar observations can be obtained by FTIR-spectroscopic ellipsometry with good time resolution (1 s), but experiments reported so far could only provide analysis of 2 min old films.¹²⁹ Although very little work was reported so far, time-resolved in situ FTIR investigations will probably develop very quickly in the optimization of the evaporation and post-treatment of organic–inorganic films.

3.5. Conclusive Remarks. To clarify the analytical approach of POMTs, the main usual and above described characterization techniques are compared in Table 1. The number of asterisks is proportional to the quality of the determination (*, poor; **, effective tool with occasional accuracy problems; ***, very good tool for this characteriza-

tion). Such a comparison was made to clarify which combination of fundamental techniques should be used for a complete description of POMTFs. Keeping apart characterization techniques dedicated to the analysis of a specific property, one sees that a complete set of tools can be achieved by coupling a mesostructured characterization tool (GI-SAXS or 2D SAXS WAXS), a porosity investigation tool (the best are EP and XRR porosimetry), vibrational spectroscopies, and any electron microscopy equipped with EDX analysis (HR-TEM being the more polyvalent). Hardness not included, the combination proposed above reaches a very high mean quality criterion of 2.8 asterisks for the characterization of conventional properties.

Although impressive, this combination is still incomplete. Indeed, none of the described approach is able to quantify precisely the crystallinity level of the mesoporous network. In 2003, the first periodically organized nanocrystalline thin films were reported.¹¹³ Since then, the crystallinity (completeness of the crystallization) is still difficult to determine with accuracy. Four techniques have been proposed. The first one implies using the area of a XRD diffraction peak as a reference fully crystalline film. The ratio of diffraction peak surface areas gives then directly the crystallinity of the film.²³⁹ Although simple, this approach should be considered as semiquantitative because it assumes that nanocrystals have the same mean size and orientation at all steps of the crystallization process. The second one is purely qualitative and uses a simple TEM investigation of the film using a dark field mode. The third option is to use Raman spectroscopy that can usually detect and separate the vibrational contributions of amorphous and inorganic networks. This approach is mainly qualitative. A fourth approach was recently proposed for TiO_2 films by Soler-Illia and co-workers.²¹³ It consists in analyzing the XANES curves of an amorphous film and a crystalline reference (a powder, for example) at the edge of the concerned metallic center. A deconvolution of the XANES profiles of the semicrystalline films and a comparison with references allows determining of the crystalline fraction. This method, sensitive to local environment of Ti centers, is semiquantitative and requires access to XANES facilities.

4. Periodically Organized Mesoporous Thin Films

4.1. Silica Thin Films. The first attempts to elaborate ordered mesoporous thin films involved silica as inorganic precursors only (most of the time, TEOS, TMOS, or inorganic silica sources). This could be explained by the discovery in 1971⁷ and good characterizations in 1990–1992 of MCM-41^{9,17} and FSM^{241,242} materials a few years earlier. On the other hand, the choice of surfactants was opened and synthesis of ordered mesoporous thin films were made with anionic, cationic, or neutral surfactant leading to materials with pore dimensions as a function of the chain length of the hydrophobic tail of the template and the headgroup size. For example, using a quaternary ammonium with a C16 alkyl chain (cetyltrimethylammonium bromide) generally results in pore diameter around 2–3 nm. Water-soluble triblock copolymer surfactants lead to materials with much larger pore dimensions (5–30 nm).

Table 1. Summary of the Main Characterization Techniques of POMTFs and Their Output in Terms of Structural and Textural Parameters

characterization techniques	thickness	porous volume	PSD	pore anisotropy	surface area	Young's modulus	hardness	meta-periodicity ^a	meso-periodicity	micro-periodicity	chemical composition	multilayer resolution
FTIR and ATR-FTIR											**	
EDX								**	**	*	**	*
XPS										**	**	
XRD									*	**		
RAMAN										**	*	
RBS		*									***	***
2D SAXS-WAXS				**					**	***		
GI-SAXS	*			**					***			
FE-SEM (EDX)	***	*	*	*				***	*			***
TEM and HR-TEM	***	*	*	***				***	**	*		***
AFM		*	*						**			
BET (N ₂ -Kr)		***	***		***							
EP	***	***	***	**	***	***		**				***
XRR and NRR ^b	***	***	***	**	**	***			**			**
SAW		**	***		***	***						
¹²⁹ Xe NMR			**								*	
PALS	**	**	*		*			*				**
UV-vis abs	*							**				
NI ^c						**	**					

^a Multilayer made of stacked POMTFs. ^b Equipped for porosimetry, periodical stacking of POMTFs forming 1D photonic crystals.^{193,240} (*) poor; (**) effective tool with occasional accuracy problems; and (***) very good tool for this characterization. ^c If good reproducibility can be obtained with this method, film mechanical properties are systematically over-estimated on thin films because of a contribution of the substrate.

As already reported in part 2, chemical solution deposition routes, involving evaporation induced self-assembly, are the most often used to synthesize ordered mesoporous thin films. From a chemical point of view, the synthesis of silica mesoporous thin films could be done in an acidic or basic medium. But the majority of thin films involve acidic catalysis. However, Anderson et al.^{89,243} formed thin films in basic conditions by dip or spin coating a solution of TMOS, CTAB, and methanol. The basic compound, NH₃ gas, was added after the deposition step to increase the condensation rate of silica. However, these thin films are composed of a network of small mesostructured particles rather than a continuous coating. The preferential use of acidic conditions lies in the morphology of silica species at low pH. It is well-known that the molecular-scale morphology of silica differs when grown above or below the isoelectric point (pH 2).⁶ Below pH 2, silica species result in branched polymeric structures, and above this pH, the species are denser and present a more particulate cluster morphology.

The ordered thin films (silica-alkyltrimethylammonium salts) were successfully synthesized in 1994 by evaporation of a simply deposited solution containing surfactant and soluble silica precursors derived from alkoxysilanes.⁹¹ In 1996, these thin films were also prepared by nucleation on solid substrates^{92,160} and at the air-water interfaces.^{160,161} Despite these different methods of synthesis, solvent evaporation induced self-assembly processes were the preferential method, even at the beginning, to produce ordered mesoporous thin films.^{27,29,89-91,243-254} Silicon alkoxides (TMOS or TEOS) were partially hydrolyzed by water under acidic conditions. Then, an aqueous solution of surfactant was added, and the mixture was stirred at room temperature. Then, the solution was spin coated on a glass substrate and dried in air to complete condensation of the silica. Finally, the vapor phase deposition technique has been recently used to generate silica mesostructured materials.¹³⁶

All these syntheses produced well-ordered mesostructured thin films presenting various structures which could be two-dimensional: 2D-hexagonal, lamellar, wormlike, or tridimensional (see Figure 5). Film thicknesses range from 50 to 2000 nm in general, and thicker films tends to bear structural non-homogeneities because of composition gradients created during drying (see part 5). Porosity, pores, and inorganic wall sizes are governed by the dimension of the micelles and the surfactant/Si molar ratio adjusted in the solution. In general, triblock copolymers lead to thicker pore walls, bearing microporosity, than smaller ionic surfactant. It has been shown that the stability of the thin films was also structure dependent.²³¹ The most often obtained and reported 2D-hexagonal structure collapses in the presence of water, while the tridimensional phases (*Pm3n* and *P6₃/mmc*) exhibit longer lifetimes. Similar trends have been found for mechanical properties.^{255,256} Moreover, thin films made with triblock copolymers (F127) are less stable than those prepared with ionic surfactants (CTAB) as a result of the microporosity created by the penetration of the PEO chain into the silica atomic network.^{148,231} Methods to overcome these lack of hydro- and mechanical stabilities are a post-densification in the presence of TEOS vapor²⁵⁷ or one pot incorporation of a transition metal cation. Indeed, a recent study showed that Zr (or Al)-loaded SiO₂ mesoporous thin films are much less likely to dissolve in simulated body fluid than the equivalent pure SiO₂ films.²⁵⁸

Final pore size depends on micellar template size as conventionally evidenced by TEM, SAXS, XRD, SEM, and more recently by positron spectroscopy.¹⁷⁴ However, many micelle chemical modifiers may be added in the initial solution to adjust the pore size and morphology. Typically, ionic surfactant micelles are strongly dependent on the ionic strength of the solution and on the size of the directly interacting ions. A hydrophobic agent such as TMB or TIPB²⁵⁹ or alcohol cosolvent such as *n*-BuOH²⁶⁰ was successfully use to enlarge the F127 micelles size and thus the related pore dimension of a silica films. Pore size can

also be doubled (e.g., from 6 to 13 nm in diameter) when PPO agent is added to a F127/TEOS solution prior to coating.²⁶¹

4.2. Mixed Transition Metal (TM) Silicon Oxide Thin Films. The creation of transition metal (TM)-Si mixed oxide frameworks imposes a chemical challenge, because of the marked differences in hydrolysis–condensation behavior of TM and Si cations that usually lead to phase segregation. Homogeneous Ti–Si mesoporous thin films have been reported for Ti contents up to 20%.²⁶² Higher metal loadings result, generally, in phase segregation. A critical issue in the synthesis of TM–Si mixed mesoporous thin films is thus the chemical homogeneity of the inorganic walls. Its control is achieved by tuning the kinetic of inorganic hydrolysis and condensation reactions of both cations, while keeping the compatibility of the inorganic network with the organized template. In the literature, several approaches have been developed to either increase or decrease the kinetics of these reactions. For silica precursors, a prehydrolysis step is often required before mixing it with the transition metal precursors. In contrast, the kinetics for the hydrolysis and condensation reactions of transition metals have to be slowed down by either chelating it or decreasing the pH of the solution.

Beside the control of the kinetics of the hydrolysis and condensation reactions of Si and TM, the water content in the films has to be tuned to allow the existence of Si–O–M bonds.²⁶³ However, the use of mixed alkoxide precursors in nonaqueous conditions avoids the use of water. Mesoporous oxide thin films with a mixed silica/zirconia framework have been synthesized by a two-step dip-coating method.¹⁰⁶ In this approach, the freshly dip-coated films are immediately treated by a short water vapor treatment to form an organized mesophase in which Si–O–M bonds exist. The composition of these thin films is varied from silica-rich (100–70%) to zirconia-rich (100–70%). These films of optical quality are highly organized and oriented, stable, and exhibit amorphous mixed frameworks presenting good dispersion of both cations at the molecular level. Si-doped zirconia matrixes modify the inorganic network, improving the thermal and chemical stability of the mesostructure. A “library” of varied compositions and tunable mesostructures (cubic *Im3m*, 2D-hexagonal *p6m*, local hexagonal, lamellar) has been established with F127, P123, and Brij 58 as templates.

4.3. Non-silica Oxide Thin Films. Mesoporous nonsilica oxide materials prepared as powders have received tremendous attention by the research community since their announcement by Antonelli and Ying^{24,25} and a few years later by Yang et al.²² in 1998. They pointed out the interest of using amphiphilic poly(alkylene oxide) block copolymers as structure-directing agents to organize porous inorganic networks. However, none of the reported results demonstrated the possibility of making organized mesoporous thin films. Additionally, the thick walls are mainly constituted of domains which are not crystallized. It further appears from these works that obtaining high crystallinity in the pore wall imposes severe experimental conditions since collapsing of the meso-ordering was systematically observed during the thermally induced crystallization.

The chemical nature, the mesostructure, the pore size, and the physical properties of various mesoporous inorganic thin films, prepared from 1998 to present, are listed in Table 2 together with the template and the inorganic precursors employed. In the early 2000, the first stable nonsilica-based (TiO₂) mesoporous ordered thin film, with optical quality, was reported.⁹⁶ It was made using the EISA of conventional Pluronic-type copolymers with Ti^{VI} molecular complexes and oligomers, stabilized in a mixed water and ethanol solution by a high acidity. The inorganic precursor was selected to be TiCl₄ since its hydrolysis liberates protons that are responsible for the high acidity and for the consequent stability of the resulting hydrolyzed molecular inorganic moieties. Moreover the HCl formed upon reaction of TiCl₄ is eliminated after evaporation of solvent as a result of its high volatility. A very slow and careful thermal treatment follows to eliminate the template and to stabilize the amorphous mesoporous titanium oxide network. In 2003, significant advances have been made in understanding crystallization processes in mesoporous thin film formation by developing in situ characterization techniques (SAXS/WAXS).^{264,265} The crystallization of mesoporous anatase was then achieved with F127, as structuring agent promoting the transformation of the initial bcc mesostructure to the grid-like open mesostructured (see part 5).⁹⁸ This first achievement opened the door to the wide family of nanocrystalline oxide mesoporous thin films. Most of these mesoporous films were prepared from traditional templates such as Brij58, P123, and F127 using chloride salt precursors hydrolyzed in an EtOH/H₂O mixture or alkoxide dissolved in EtOH/H₂O/HCl, which led to a similar type of stabilized inorganic intermediates.^{96–98,100,113,128,140,264,266} These different works also underlined the importance of tuning the relative humidity to control the formation of the mesostructure during drying. High quality and reproducible nanocrystalline POMTFs are obtained when a good control of the chemical, processing, and treatment conditions is reached especially for Pluronic-type templates. On the other hand, many attempts, not reported here, led to homogeneous mesoporous layers with a poor degree of mesoporosity order. For instance MnO₂ mesoporous films with poor ordering but showing supercapacitor behavior were synthesized on a Pt electrode in the presence of F127.¹³²

Recently, the development of a novel family of templates such as poly(ethylene-*co*-butylene)-*b*-poly(ethylene oxide) (“KLE” polymers) and poly(isobutylene)-*b*-poly(ethylene oxide) (PIB-*b*-PEO), which are chemically and thermally more stable than the pluronic family, allows the synthesis of a variety of mesoporous thin films in less drastic experimental conditions. Highly ordered *Im3m* TiO₂ mesophases were thus obtained with a very limited control on the processing conditions. The higher hydrophobic contrast achieved in these templates gives them the ability to self-assemble faster and in a broader range of solvent.¹⁰⁷ Additionally, their high thermal stability due to the hydrophobic core of the micelle (i.e., 250–300 °C) allows almost completely the inorganic amorphous inorganic network to be dehydrated before organic total decomposition, preventing mesoporosity collapsing. One must also take into account

Table 2. Physical Properties of Inorganic Porous Organized Mesoporous Thin Films

material composition	template	inorganic precursor	mesostructure	wall structure	pore size (nm)	wall crystallite size (nm)	specific surface area ($\text{m}^2 \text{g}^{-1}$)	thickness (nm)	physical properties references
Fe_2O_3 , FeOOH	PIB-PEO, KLE	$\text{FeCl}_3 \cdot 7\text{H}_2\text{O}$	bcc arrangement	hematite	10	7–10	150		magnetic ¹¹⁴
TiO_2	F127, Brij58, Brij56, P123, KLE	$\text{Ti}(\text{Cl})_4$	$Im3m$	anatase	2.5–8	6–12	140–200	100–300	photocatalysis ^{96,98,100,107,272}
	P123	$\text{Ti}(\text{OEt})_4$	2D-hexagonal wormlike 2D-hexagonal 3D-hexagonal $R\bar{3}m$	anatase	7.6 18.5; 6.7	8.8 5–8	206	150	photocatalysis ^{273,274}
	P123	$\text{Ti}(\text{OEt})_4$	$Im3m$	amorphous					photocatalysis ^{22,104}
	Brij 56, Triton X-100, F127	$\text{Ti}(\text{Cl})_4$	$Im3m$	anatase	5.5 nm	7.5			photocatalysis ¹⁵⁰
	P123	$\text{Ti}(\text{OPr}^i)_4$	not ordered	anatase		17–23		300	photocatalysis ²⁷⁵
	P123	$\text{Ti}(\text{OPr}^i)_4$	$Im3m$	anatase	4.6	6.1	113	400	photocatalysis ²⁷⁶
	P123	TEOT	lamellar	amorphous				300–400	photocatalysis ¹⁰¹
			2D-hexagonal	anatase	4	3–8		200–500	
	P123	TiCl_4	cubic	anatase	6.5	2.4	205		semiconductor ⁹²
			cubic						
Al_2O_3	P123	AlCl_3	cubic	amorphous	7		105		dielectric ⁹²
	KLE22, KLE23	$\text{AlCl}_3 \cdot 6\text{H}_2\text{O}$	cubic	$\gamma\text{-Al}_2\text{O}_3$	6	5			dielectric ¹⁰⁹
CeO_2	KLE	$\text{CeCl}_3 \cdot 7\text{H}_2\text{O}$	distorted bcc	cubic	9–10	7–10		170–200	dielectric ^{111,267}
	KLE, LI	$\text{CeCl}_3 \cdot 7\text{H}_2\text{O}$	bimodal (spherical worm-like)	cubic	6×16 2.5–3	5			
ZrO_2	KLE	ZrCl_4	distorted bcc	cubic	10	10			dielectric ¹¹¹
	F127, Brij58	ZrCl_4	2D-hexagonal	tetragonal	2.5–8		140–200	300	dielectric ^{56,97,100}
	P123	ZrCl_4	cubic	tetragonal	5.8	1.5			dielectric ⁹²
Eu_2O_3	KLE	EuCl_3	bcc arrangement	bcc Eu_2O_3 structure	11	16–22			luminescence ¹¹⁶
			grid-like morphology						
$\text{ZrO}_2\text{-CeO}_2$	KLE	$\text{ZrCl}_4/\text{CeCl}_3 \cdot 7\text{H}_2\text{O}$	distorted bcc	cubic	~10	2–4			ref 111
$\text{ZrO}_2\text{-CeO}_2$	F127	$\text{ZrCl}_4/\text{CeCl}_3 \cdot 7\text{H}_2\text{O}$	2D-hexagonal	cubic	8	7–9		300	ref 97
$\text{ZrO}_2\text{-Y}_2\text{O}_3$	F127	$\text{ZrCl}_4/\text{YCl}_3 \cdot 6\text{H}_2\text{O}$	2D-hexagonal	cubic	8	7–9		300	ref 97
SnO_2	KLE	SnCl_4	cubic	cassiterite	14	5–6			ref 108
	no template	SnCl_4		cassiterite	5–7 (tubular)		65–112		ref 277
	P123	SnCl_4	cubic	cassiterite	6.8	3	180		semiconductor ⁹²
HfO_2	KLE	HfCl_4		monoclinic	15	10			semiconductor ¹¹²
	P123	HfCl_4	cubic	amorphous	7		130–160 105		ref 22
BaTiO_3	KLE	$\text{SrCl}_6 \cdot 6\text{H}_2\text{O}$, BaCl_2	$Im3m$	perovskite	12	10–20			ferroelectric ^{104,105}
SrTiO_3	KLE	TiCl_4 , CoCl_2	$Im3m$	tetragonal	12	10–20			piezoelectric
MgTa_2O_6	KLE	$\text{Mg}(\text{OH})$	$Im3m$	anatase, rutile, or ilmenite	12	10–20			superconductor

Table 2. Continued

material composition	template	inorganic precursor	mesostructure	wall structure	pore size (nm)	wall crystallite size (nm)	specific surface area ($\text{m}^2 \text{g}^{-1}$)	thickness (nm)	physical properties references
$\text{Co}_x\text{Ti}_{2-x}\text{O}_{2-x}$	KLE	$\text{Ta}(\text{OC}_2\text{H}_5)_5$	$Im3m$		12	10–20			
NiTiO_3	KLE	NiCl_2	$Im3m$						
Al_2TiO_5	P123	$\text{AlCl}_3/\text{TiCl}_4$	cubic	amorphous	8		270		dielectric ²²
ZrTiO_4	P123	$\text{ZrCl}_4/\text{TiCl}_4$	cubic	amorphous	8		130		materials with negative thermal expansion properties
ZrW_2O_8	P123	$\text{ZrCl}_4/\text{TiCl}_4$	cubic	amorphous	5		170		
$\text{SiAlO}_{3.5}$	P123	$\text{SiCl}_4/\text{AlCl}_3$	cubic	amorphous	6		310		refs 22 and 278
$\text{SiAlO}_{3.5}$	P123	$\text{SiCl}_4/\text{AlCl}_3$	cubic	amorphous	10		330		
SiTiO_4	P123	$\text{SiCl}_4/\text{TiCl}_4$	cubic	amorphous	5		495		
WO_3	L62, P123	WCl_6	disordered pores	monoclinic	4–10	10	156–138		photochromism, sensor ²⁷⁸
	SDS (electrodeposition)	W metal powder	disordered pores	hexagonal (oriented [0001])	5–10	5–20		177	electrochromism ²⁷⁹
	SDS (electrodeposition)	WO_3	worm-like or lamellar structure		2.5	10	45	800	photocatalysis, electrochromism ¹²⁴
					2.5 wall thickness, 1.5 interlayer space				
	TMDD				4–5				
	F127	WCl_6	3D vermicular cubic	monoclinic	3.7	6–7	145		electrochromism ²⁸⁰
		WCl_6			5	10–15	150–180	140	sensor, electrochromism ¹¹²
	P123	WCl_6	not ordered cubic	monoclinic	5	3.8	143		Li insertion, sensor ²⁸¹
		WCl_6		monoclinic	2	2	125		ref 22
TiO_2/WO_3	F127	tungsten(V) pentaethoxide, titanium tetraisopropoxide	cubic or worm like (8 mol % WO_3)	anatase + WO_3 amorphous	10	≤ 1		300	photocatalysis ¹²⁰
Ta_2O_5	P123	TaCl_5	cubic	Ta_2O_5 nucleation started	3.5	≤ 1	165		semiconductor ²²
Nb_2O_5	P 123	NbCl_5	cubic	Nb_2O_5 nucleation started	5	≤ 1	196		semiconductor ²²
In_2O_3	KLE	SnCl_4 , $\text{In}(\text{III})$ acetylacetonate	cubic	bixbyite	ellipsoidal 16×8	7–8			sensor, conductor ¹²⁵
Y_2O_3	PHB-PEO		$Im3m$		11.5				dielectric ²⁸²
Nd_2O_3	PHB-PEO		bcc		12.5				dielectric ²⁸²
ZnO	SDS, CTAB	$\text{Zn}(\text{NO}_3)_2 \cdot 6\text{H}_2\text{O}$	lamellar			1.5			semiconductor ¹³⁰

Table 3. Physical Properties of Mesoporous Other Non-Oxide Thin Films

material composition	template	inorganic precursor	mesostructure	wall composition	pore size (nm)	wall crystallite (nm)	physical properties	references
TiPO, AlPO, ZrPO, NbPO, CePO	P123	anhydrous metal chloride or alkoxide	<i>Im3m</i> , <i>p6m</i> , <i>P63/mmc</i> , <i>1a3d</i>	Me/P = 1	4–8		proton conductor	283, 284
ZrPO	P123	Zr(OPr) _n	<i>c2mm</i>		3.3		proton conductor	122
AlPO	F127, F108, Brij56	AlCl ₃	<i>Im3m</i> , <i>p6 mm</i>	Al/P = 1				285
TiN, TiN _{1-x} O _x	F127	TiCl ₄ (NH ₃ treatment)	grid-like		5–8	10–14	photocatalysis	286
Pt, Ni, Pd, Sn, Co	Brij56, Brij76, Brij78	Acetate or chloride	Hexagonal or lamellar	Pt, Ni, Pd	5–10			15, 26, 169, 287–289
CdTe, CdSe, CdS	C ₁₆ EO ₈	CdSO ₄ , TeO ₂	hexagonal	CdTe, CdSe, CdS			semiconductor	290, 291

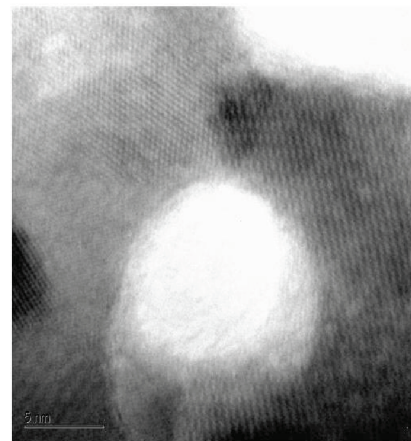


Figure 14. HRTEM image of a nanocrystalline Eu₂O₃ POMTF. Reprinted with permission from ref 116. Copyright 2007 Institute of Physics.

that large micelles (10–40 nm) are usually associated with these templates, thus producing larger walls, smaller pore curvature, and larger mechanical stability upon network crystallization. Matrixes that were difficult to stabilize with conventional templates were easily prepared, together with those already obtained with conventional templates (e.g., HfO₂, CeO₂, ZrO₂).^{107,108,111,112,114,119,126,267–270} The best example of the efficiency of these templates was shown by Kuemmel et al.¹⁰⁹ who managed to stabilize γ -Al₂O₃ nanoparticles, of 5 nm in size, into a well-ordered three-dimensional contracted fcc mesostructured network up to 900 °C. This achievement was associated with the perfect sequential steps involving first EISA, followed by drying, dehydration, stabilization of the amorphous oxide, decomposition of the template, and delayed crystallization into γ -Al₂O₃ at 900 °C. This represents the highest thermal stability reported so far for nanocrystalline metaloxide mesostructured thin films. Taking the advantage of this new family of template, CeO₂ mesostructured thin films were also synthesized.^{111,126} These films exhibit highly crystalline pore walls and ordered arrays of mesopores. Finally, WO₃ and SnO₂ thin films with a periodically ordered mesopore structure and variable degrees of crystallinity have also been prepared.^{108,112} The HRTEM image in Figure 14 offers an excellent illustration of a 10 nm large nanopore formed inside the Eu₂O₃ nanocrystalline network.¹¹⁶ The crystalline state of the network is clearly visible through the presence of reticular plans.

Another benefit of this new family of template arises when oxide composites, or solid state phases, of POMTFs had to be prepared. The formation of highly organized mesoporous yttria–zirconia, ceria–zirconia, and ilmenite POMTFs was reported in 2003 with conventional Pluronic templates.^{97,105} Mesophases have also been formed by controlling the quantity of water inside the coating during the aging step, and cubic structures were stable up to 700 °C. The use of KLE copolymer as directing agent in these systems provided also mesostructured ceria–zirconia films with crystalline pore walls.¹¹¹ Compared to previous works,⁹⁷ the pore size is larger while the particle size in the pore wall is smaller. Changing the nature of the template allows the formation of nanocomposite systems with controlled structural (pore and

particle) size, which in turn tunes the physical properties of these porous materials.

Finally, multicationic inorganic mesoporous thin films with perovskite (SrTiO_3) and tetragonal MgTa_2O_6 structures have been obtained from metal–chloride precursors and KLE-type polymers, through the specific control of the self-assembly and dehydration kinetics so as to prevent cation demixion (see part 5.2.2.).¹⁰⁴ This class of mesoporous thin films is expected to offer all the attributes for ferroelectricity, piezoelectricity, adjustable band gaps, and high temperature superconductivity. These results on multicationic and/or nanocomposite mesoporous thin films offer new compositional and design space to explore.

A variety of metal oxides have thus been synthesized by a careful control of the sol–gel chemistry, the nature of the template, the deposition process, and finally the crystallization of the inorganic wall. However, not all the compositions have been successfully prepared through EISA. In particular, the table highlights the difficulty of synthesizing mesoporous thin films of M^{2+} ions of the late 3d transition metals ($\text{M} = \text{Ni}^{2+}, \text{Co}^{2+}, \text{Cu}^{2+}$), even if ternary oxides such as ilmenites ABO_3 ($\text{A} = \text{Ni}^{2+}, \text{Co}^{2+}$ and $\text{B} = \text{Ti}^{4+}$) were successfully prepared. In the case of Zn^{2+} , the use of electrodeposition coupled with a templating approach resulted in the successful synthesis of organized mesoporous ZnO films.^{130,271} This result is significant as it represents the first example of the synthesis of mesostructured thin films containing only metal ions in the 2+ oxidation state.

The physical properties of these various inorganic porous organized mesoporous thin films are reported in Table 2.

4.4. Nonoxide Thin Films (Table 3). Besides mesoporous metal oxides, metal phosphates have also been reported in the literature using a triblock copolymer, P123, combined with anhydrous metal chloride or alkoxide (Table 3). These new mesoporous materials exhibit large channels of cages (4–8 nm), very high thermal stabilities (800 °C for aluminophosphate (AlPO), 700 °C for zirconophosphate (ZrPO), 400 °C for cerium phosphate (CePO)), and homogeneous compositions.^{283,284} These studies mention just the possibility of making these mesoporous materials under various morphologies such as films, monoliths, fibers, and so forth. However, no exhaustive studies on the films characterization have been reported. Recently, Nishiyama et al.¹²² have shown that the framework of mesoporous zirconium phosphate thin films can be stabilized via vapor treatment of phosphoric acid and ammoniac before calcination. This postvapor treatment is necessary to enhance the thermal stability of this periodic structure up to 500 °C. These films exhibit high proton conductivity in the plane parallel to the film surface. Mesoporous aluminophosphate thin films with tunable cubic and hexagonal pore arrangement have been achieved using a variety of nonionic templates.²⁸⁵ Using ^{27}Al and ^{31}P NMR, the authors pointed out a transition from an amorphous aluminophosphate gel to a well-defined phosphate with 4-coordinated Al centers.

Another example of nonoxide mesoporous thin films with complex compositions is the synthesis of nanocrystalline mesoporous N-doped titania films. The introduction of nitrogen into the mesoporous anatase, TiO_2 , allows the

synthesis of $\text{TiN}_{1-x}\text{O}_x$ with $0 \leq x \leq 1$ compounds. In these compounds, titanium exhibits different oxidation states.²⁸⁶ Microstructural studies indicate that the ordered mesoporosity is maintained until 700 °C, where TiN_xO_y nanodomains begin to form.

The use of sol–gel methods to prepare a wide range of mesoporous inorganic thin films has emerged rapidly over the past six years, and it is evident that nonoxide thin films can benefit greatly from this existing work.

Mesoporous elemental metals, for example, Pt, Pd, Ni, Co, and Sn, have also been synthesized by block copolymer templating (Table 3).^{15,26,169,170,287,290,292} Attard et al. reported the synthesis of Ni, Pd, Pt, and Sn mesoporous metal electrodes through electrochemical deposition in presence of a template.^{15,26,169,170} These materials are interesting for fuel cells for the electrochemical hydrogenation of organic species.

The liquid crystal templating strategy was also extended to fabricate mesostructured CdTe , CdS films with excellent optical properties.^{290–293} These films exhibit uniform cylindrical pores organized in a hexagonal array and strong optical birefringence at energies above and below the bandgap.

4.5. Using Non-Amphiphilic Templates. Ionic surfactants are environmentally nonviable, and quality block copolymers are expensive. This is a reason why the use of something other than amphiphilic templates is one of the interesting alternative components entering the processing of POMTFs. Cellulose has been used to prepare TiO_2 ²⁹⁴ and SiO_2 films though the EISA approach.²⁹⁵ While films present calibrated nanoporosity, no meso order could be achieved. Supramolecular assemblies of oligomeric chains, which were formed through a very slow sol–gel process, were used as the self-templating agent for SnO_2 film formation upon surfactant-free solution dip coating.²⁷⁷

5. Mechanism of Formation of POMTFs

Whatever the selected method of preparation, three main steps are involved in the preparation of POMTFs. The first step consists of selecting the chemical precursor, the catalyst, the templating agents, and the solvents. The solvent dissolves the different precursors to obtain a homogeneous and stable solution. The second step is the deposition process that drives both templating and inorganic precursors (or intermediates) to combine so as to obtain a homogeneous layer with specific final mesostructure. Ideally, this latter is composed of an interpenetration of both phases in an ordered mesostructure strongly attached to the substrate surface. Because the first step is to eliminate the templating agent to liberate the porosity and to second stiffen the network, a third and final necessary step of treatment has to be conducted. The latter can be of chemical or physical nature and may, in a specific case, be a smart sequence of them. Mastering these three steps is a prerequisite to precisely adjust the nanostructuration and the physicochemical properties of the final layers. Chemical conditions are obviously the most important one. A small part will briefly recall the selection of the more classical chemicals because this subject has been widely discussed in the previous part 4 for pure inorganic materials and in the following part 6 for the hybrid materials. In terms

of the self-assembly mechanism, literature delivers mainly reports concerning EISA because it is the most commonly used technique to prepare POMTFs nowadays. These mechanistic studies aim at (i) isolating the chemical and processing critical parameters, (ii) identifying their role on the self-assembly mechanism, and (iii) optimizing them to improve the structural characteristics for a specifically targeted application. The effect of the thermal treatment on the final structure (crystallinity, mesostructure, layer cohesion) is also an important issue that has already been mentioned in part 4.3 and will be discussed in detail in a following part dedicated to final modification of the layer. The last section will be dedicated to the combination of the template approach with other types of processing methods to form complex hierarchically structured layers such as micropatterns, multimodal porosity or oriented porosity, and heterogeneous ultrathin mesoordered layers (nanopatterns). This latter hot topic of how to master the formation of vertical pores allowing the complete direct accessibility between both interfaces will be addressed in a more detailed paragraph, since it remains one of the most important challenges of the POMTF field.

5.1. Inorganic Precursors and Template. The main templating agents that have been used to process POMTFs are amphiphilic ionic or nonionic molecules or polymers. Among them are CTAB, Brij, and commercially available block copolymers: F127, P123 (PEO-PPO-PEO), or PS-POE. The reader interested in a more complete presentation of possible surfactants will find a complete set of physicochemical information in the relevant literature.^{1,296,297}

One observes that around 90% of the works reported in the literature on mesoporous films concerns silica matrixes, while most of the rest is dedicated to TiO₂, and only a few papers report about other matrixes (see part 4). Almost all silica mesoporous films are prepared from TEOS in acidic and aqueous media while more conventional texturing agents are CTAB or polyethyleneoxide based block copolymers. Non-silica mesoporous films were mainly obtained as oxide from chloride precursors and PEO (polyethyleneoxide) based block copolymers. Because of the more delicate chemistry associated to these type of materials, obtaining the first mesoporous transition metal oxide films with ordered porosity required greater efforts and more time than silica. Self-assembly occurs upon evaporation with a strict control of humidity and thermal treatment sequence. Eventually, crystallization of the ordered network could be reached with the same system upon careful thermal treatment.

5.2. The Evaporation Induced Self Assembly (EISA)
Method. 5.2.1. *CTAB and PEO-Based Copolymer Binary Systems.* In the EISA approach, the templating agent and the inorganic precursors are gathered in the same solution, for which chemical conditions (i.e., composition, stoichiometry, addition of polymerization catalyst or inhibiting agent, aging time, etc.) are adjusted so as to favor homogeneous dispersion of both parts. The latter solution is then cast on the substrate through conventional chemical solution deposition (CSD) by either spin, dip, meniscus, or spray coating processes as shown in Figure 3. The self-assembly is triggered during evaporation of the latter deposited solution

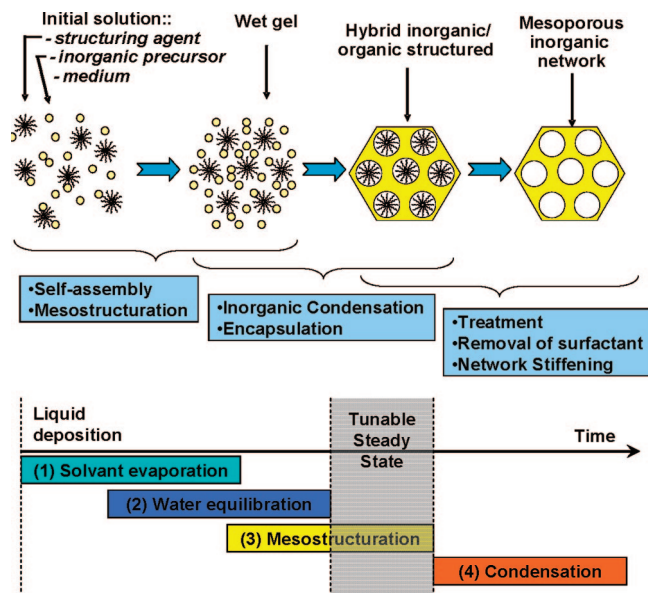


Figure 15. Scheme illustrating the templating approach combined with the various steps involved in the evaporation-induced self-assembly process during thin film formation by liquid deposition techniques.

layer just after deposition on the substrate and is thus governed by the progressive departure of the volatile components. This is a complex dynamic step that involves at least four simultaneous or subsequent mechanisms that may be governed by totally different parameters.^{128,129} These are: (1) the fast evaporation of the solvent; (2) the film water content equilibration with the atmosphere; (3) the formation and stabilization of the template/inorganic biphasic homogeneous layer; and (4) the consolidation of the inorganic network through consolidation. In addition, these steps are either thermodynamically or kinetically governed and do not necessarily take place in the given precise order with possible overlapping along the process of thin film deposition. This overall complex transformation can be simply seen as a straight polycondensation of the inorganic precursors around the organic micelles (or mesophase) freezing the latter liquid crystal mesostructure (see Figure 15).

The only prerequisite to a homogeneous highly ordered stable hybrid material is that step (3) must be completed before step (4) is too advanced. Also, one must keep in mind that evaporation takes place at the atmosphere/wet film interface, creating concentration gradients that are responsible for potential nonhomogeneities. Indeed, the structuration can be assimilated to a frontier of transformation progressing from the atmosphere interface toward the substrate interface, and step (3) is completed when this frontier has reached the solid surface.²⁹⁸

Detailed studies of such a complex mechanism have been conducted for various mesostructured films (i.e., SiO₂/CTAB,^{129,139,298,299} SiO₂/Pluronic,^{98,299} TiO₂/Pluronic,^{113,140} TiO₂/KLE¹⁰⁷), and organically modified SiO₂ films,⁵⁵ using in situ time-resolved SAXS analyses. Ellipsometric FTIR spectroscopy,¹⁴⁷ conventional FTIR,^{238,300} interferometry,^{6,299} fluorescence spectrophotometry,³⁰¹ and X-ray reflectivity¹⁴⁴ were also used to assess these transformations. It was shown from these in situ studies that the critical parameters to adjust are the inorganic precursor degree of condensation (solution

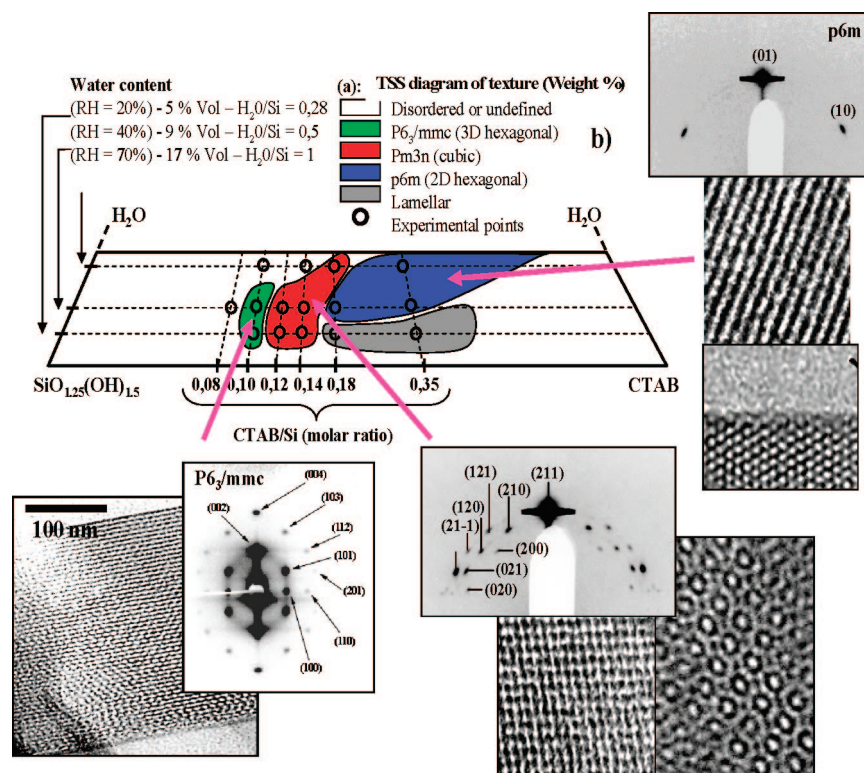


Figure 16. Texture diagram corresponding to the TSS local minima for the TEOS/CTAB system in HCl/EtOH/H₂O media and upon dip-coating in controlled humidity. Reprinted with permission from ref 129. Copyright 2004 Wiley—VCH Verlag GmbH & Co. KGaA. TEM and GI-SAXS patterns are reported to illustrate the various obtained phases.

aging time, concentration, and catalysis), the organic template/inorganic volume fraction, the presence of water that depends on the solution composition and on the atmosphere relative humidity, the film thickness, and the evaporation speed. The self-assembly seems to be followed by a critical state where the inorganic system is not condensed enough (still flexible) and where its composition is in equilibrium with the environment.

During the step (3), a tunable steady state (TSS)¹²⁹ is reached where a change in the atmosphere composition results in a modification of the film composition inducing potentially a modification of the mesostructure (see Figure 15). Many other works came to complete this first feature and confirmed these tendencies for most of the systems. The role of water on the micellar curvature during EISA was evidenced by in situ SAXS.^{98,129} While several structures were reported with the same solution but in different relative humidity,^{302,303} water up-taking was confirmed by other groups using GI-SAXS experiments.³⁰⁴

Water molecule intercalation at the organic/inorganic interface depending on the pH has been investigated by solid-state NMR in homologous powder systems, underlining its critical role in the mesophase curvature stabilization.³⁰⁵ The influence of the evaporation rate on the roughness, due to the Marangoni effect,³⁰⁶ and on the structure homogeneity^{141,299} was confirmed to be a crucial point. The initial solution composition such as the ratio of template on inorganic precursor, the dilution, the pH, and the aging time have also to be precisely adjusted to control the structure. To summarize these latter works, a larger template leads to larger pores, while increasing the template/inorganic volume

ratio leads to a higher density of pores and narrower pore walls. Obviously this latter ratio has an effect on the type of mesostructure finally obtained since different surface curvature and geometry may be adopted to minimize the interfacial energy. Examples of mesostructures obtained with SiO₂ are given in Figure 5. Texture diagrams depending on the initial stoichiometry have been proposed for CTAB/TEOS,^{129,307} CTAC/TMOS,³⁰⁸ PEO-PPO-alcane/TEOS,³⁰⁹ or Pluronics/TiCl₄^{98,129} systems. Other investigations showed the importance of the solution aging time, especially for silica based systems, on the mesophase as a result of variation of condensation degree (Figure 16).^{307,309–312} Some studies reported the role of the substrate interface nature and topography on the mesostructure formation; even if structural deviations were observed depending on the substrate, no trends and critical parameters could be clearly identified.³¹³ The only unambiguous effect of solution/substrate interface has been shown by Miyata and Kuroda for the lateral alignment induced by polyimide surface rubbing.³¹⁴

5.2.2. Polycationic systems. When more than one type of inorganic precursor is used, such as when ternary oxide materials want to be prepared, the self-assembly step (3) must be completed as fast as possible so as to rapidly proceed to step (4), before inorganic phase separation takes place as a result of the differences in solubility and in condensation kinetics. Several ternary oxide phases with certain stoichiometry have been prepared such as Zr^{IV}Y^{III}, Zr^{IV}Ce^{IV},⁹⁷ Si^{IV}Zr^{IV},¹⁰⁶ or Nb^VTi^{IV}.¹¹⁷ Inversely, when cations with highly different oxidation states must be associated, fast conditions must be applied. Perovskite SrTiO₃, Ilmenite CoTiO₃, or tetragonal MgTa₂O₆ were prepared with a precise

control on the conditions of chemical, processing, and thermal treatment steps.¹⁰⁴ On the other hand, the latter inorganic precursor demixion previous to step (4) may be useful if a multiphase network is required. Indeed, this phenomenon has been used to prepare POMTF with both anatase and ilmenite nanocrystallites cohabitating in the mineral framework from Ni^{II} precursors.¹⁰⁵

5.3. Final Treatment. As-prepared thin films are hybrid xerogels where the organic template domains are embedded into the inorganic matrix which is, at this stage, wet and poorly condensed. Making them useful as porous matrixes requires the stabilization of the inorganic network and the removal of the organic phase. Several treatments can be combined (e.g., thermal, chemical, extraction, UV, etc.). The more universal, and probably the more efficient for pure inorganic systems, is the thermal treatment that allows simultaneously the dehydration, the decomposition of the surfactant, the condensation,^{176,315,316} and for some systems, crystallization.^{102,113}

5.3.1. Thermal Treatment. As described previously, the thermal treatment is a very important step since it conducts first to the stabilization of the hybrid mesophase, which is composed of an ordered micellar arrangement embedded within a stable amorphous inorganic medium. The second evident goal of the thermal treatment is the decomposition and elimination of the organic micelles, which liberates the porosity. Two points have to be addressed here: first, one must be assured that the removal of the micelles takes place when the inorganic network is rigid enough to prevent collapsing of the whole porous mesostructure. Second, one must keep in mind that thermal decomposition in the presence of Lewis acid centers results in a stabilization of carbonate species anchored by complexation on the oxide surface. The full elimination of organic is allowed at a higher temperature than that of the decomposition of the template (e.g., typically 600 °C for TiO₂ materials).^{315,317,318} The third aim of the thermal treatment concerns crystallization of the network, which often requires high temperatures. This stabilization is accompanied by the unidirectional contraction of the network,^{176,317,319} already initiated during the drying process.³²⁰ For instance, 2D-hexagonal structure transforms into triclinic or 2D-centered rectangular (*C2m* space group) mesostructure,⁹⁸ while *Im3m* with [110] orientation transforms to orthorhombic mesostructure.³¹⁷ In addition, this anisotropic contraction results in the formation of ellipsoidal pores.¹⁴⁸ As expected, an increase of mechanical properties is associated with the thermal treatment and has even been quantified for CTAB and Pluronic SiO₂ templated films by nanoindentation.³²¹ It has even been reported that phase transformation may be induced through thermal treatment. Transformation from 2D-hexagonal *p6m* to cubic *Ia3d* silica thin films was attributed to the decomposition of organic moieties.³²² Unfortunately, an in situ 2D-SAXS investigation of the transformation is still required to confirm such a transformation.

5.3.1.1. Thermally Induced Crystallization. Crystallization occurs through nucleation and growth of crystallized nuclei and is followed by diffusive sintering if a sufficiently high

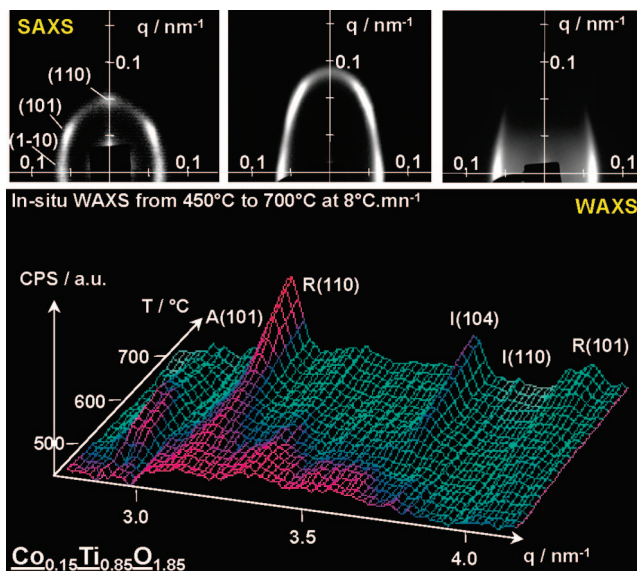


Figure 17. Typical in situ simultaneous SAXS/WAXS experiment, aiming at assessing the modification of the mesostructure (SAXS) during the crystallization (WAXS) of the inorganic network upon thermal treatment. CoTiO₃, ilmenite, and TiO₂ anatase/rutile phase transformation associated with the formation of the grid-like structure. Reprinted with permission from ref 104. Copyright 2004 MacMillan Publishers Ltd.

temperature is maintained long enough. To retain a high degree of pore ordering upon crystallization, one must favor homogeneous nucleation but prevent extensive diffusive sintering.

A fast nucleation is preferred since it is associated with a greater number of seeds created homogeneously into the inorganic network.¹⁰² Crystallization of the inorganic matrix is often accompanied by the deterioration of the quality of the mesoporosity as a result of template elimination and the atomic rearrangements associated with the various metal oxide phase transformations. Careful control of the thermal treatment conditions is thus required to prevent extensive modification of the porosity to prepare well-ordered nanocrystalline mesoporous thin films.

In situ time-resolved simultaneous SAXS/WAXS experiments were performed to assess the influence of the thermal treatment on the mesoporous order during calcinations of TiO₂ films. The latter experiment allowed the condition of treatment to be optimized and important modification of the mesoporosity interconnection to be observed.¹¹³ Indeed, heterogeneous nucleation followed by particle growth and diffuse sintering induces pore merging in TiO₂/PEO-based copolymer film systems. When starting from *Im3m* [110]-oriented domains, an interesting grid-like structure, with high accessibility from the film surface, is obtained. Similar types of modification were also observed upon crystallization of [110]-cubic *Im3m* mesostructure TiO₂,³²³ ZrO₂,¹⁰⁰ Nb₂O₅,¹¹⁷ TiO₂,^{107,324} SnO₂,¹⁰⁸ NiTiO₃,¹⁰⁵ CoTiO₃/TiO₂ (see Figure 17) and SrTiO₃.¹⁰⁴ Crystallization of amorphous PB-*b*-PEO templated Al₂O₃ into gamma phase did not modify the fcc mesophases and occurs at very high temperature. This behavior is due to the combined effect of the high specific surface area and the mesoporosity.¹⁰⁹ Besides the stabilization of metastable phase at high temperature, the ordered mesoporosity may influence the crystallization kinetics, and preferential

orientation of the nanocrystals within the inorganic network can be obtained. Such behavior was observed for crystals with an anisotropic unit cell such as MoO_3 and Nb_2O_5 .¹²⁷

5.3.1.2. Using Thermally Stable Block Copolymers. When thermally stable templates (i.e., copolymers composed of polystyrene or polybutadiene for the hydrophobic block) are used, a stable intermediate hybrid phase can rapidly be obtained. This is related to the fact that dehydration and precondensation of the inorganic network can be triggered with temperature increasing since the polymer core remains in the cavities withstanding the shrinkage of the network.¹⁰⁷ The crystallization of the inorganic wall has less effect on the porous mesostructure when these copolymers are involved.^{109,325} This is related to their relative thermal stability and/or to the larger dimension of the walls, usually formed with these templates. This latter does prevent extensive diffuse sintering. This is likely associated with the lesser surface to volume ratio that is diminishing the destabilization effect of the surface energy contribution during the thermally induce transformation. Many different pure metal oxide POMTFs were prepared with this type of block copolymer as already reported in part 4.3 and in Table 2.

5.3.2. Template Extraction. Extraction of templates can be performed when thermal treatment is not possible. Specific solvents and methods have to be adjusted depending on the system. Once again, one has to be certain that the network has been prestabilized enough before processing. Ionic surfactants such as CTAB can be leached out from SiO_2 films by simple acidic washing with medium polarity solvents, while Pluronic copolymers require stronger conditions that are attained with Soxhlet extraction with EtOH.¹⁷⁶ Using supercritical conditions is an elegant way of eliminating these types of template without involving cracks as a result of the lack of surface tension and liquid/vapor interface.³²⁶ This technique is also well appropriated to exotic templates. Indeed, fluorinated surfactants can be successfully eliminated from silica based films in CO_2 supercritical conditions.³²⁷

5.3.3. Physico-Chemical Treatments. Chemical treatments can be also applied to eliminate the template. This protocol is especially used when a fragile organic group has been incorporated into the film during solution deposition. In general, the inorganic network needs to be reinforced before leaching of the surfactant without collapsing of the mesoporosity. Irradiation with ultraviolet light of SiO_2 CTAB-templated films (O_3 oxidation process) under O_2 atmosphere has shown to be efficient as a pretreatment to further condense silica.³²⁸ The NH_3 atmosphere is also commonly used to condense the silica network before elimination of the template at high temperature. This treatment helps to prevent too high contraction and to keep a high porosity.^{143,176,261} UV irradiation is a soft and effective method to simultaneously eliminate PEO-based block copolymers and further condense the silica network.³²⁹ Chemical treatment may also be used to modify the surface of the mesoporosity after elimination of the template. One example is the silylation of SiO_2 mesoporous thin films with alkyl groups to make the surface of the pore hydrophobic for low- k applications. These modifications can be done either in vapor

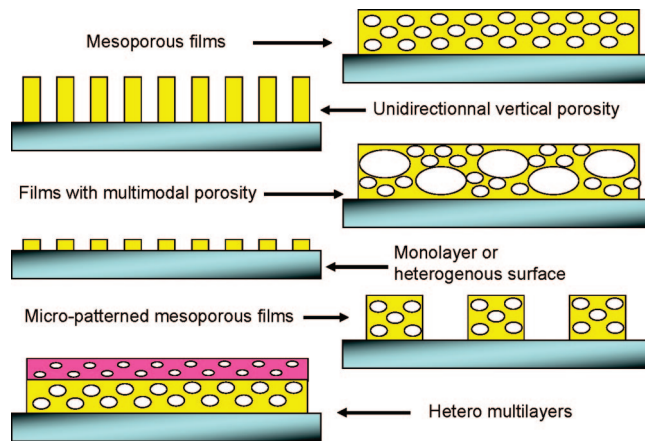


Figure 18. More complex architectures of mesoporous films.

phase^{156,330} or in solution. Additionally, the in situ elaboration of nano-objects into POMTF has been reported. In general, the POMTF pores were selectively impregnated, and reactions in the pores are in *certain* cases needed. For instance, mesoporous silica thin films were modified with magnetic iron nanoparticles by infiltrating the pores with iron acetate followed by reduction under H_2 atmosphere.³³¹ Post-treatment of POMTFs is widely used to modify the surface of the porous network. This subject is developed in more detail in part 7.

5.4. Complex Architectures for Mesoporous Thin Films. For some specific applications, such as integration on “lab-on-chip” designs, controlling multifunctionality, obtaining anisotropic properties, and so forth, other morphological characteristics have to be added to the materials; see Figure 18. These could be mastered by combining processing techniques. The following part explains some formal and recent achievements to the fabrication of POMTF films with some complex architectures (Figure 18).

5.4.1. Surface Micropatterning. When the adsorption, the hydrolysis, and the condensation of TEOS is allowed on SAM premicropatterned substrates and in presence of CTAC, mesoporous SiO_2 patterns were synthesized through a bottom up approach.^{168,332} A top-down approach has also been applied, since regions of mesoporous films can be selectively eliminated using lithography-based method. Plasma etching has been applied to form macropatterns of a complex stack system, containing a SiO_2 mesoporous film as one layer component.²³⁷ More recently, EISA of micellar templates was combined with controlled evaporation and photoinduced condensation at a wet liquid layer surface to produce well-ordered wrinkled microstructures of TiO_2 .³³³ Other physical methods, such as electron-beam³³⁴ or soft³³⁵ lithographies, allow pluronic templated SiO_2 waveguides or TiO_2 nanopatterns of submicronic motifs to be obtained. An overview of these patterning techniques has been recently reviewed.³³⁶ Brinker’s group demonstrated the possibility, using serial rapid printing procedures, to form hierarchically functionalized hybrid mesostructures on several substrates in a few seconds.^{337,338} The rapid-prototyping procedures, that is, micropen lithography, ink-jet printing,³³⁹ and dip-coating of pat-

terned self-assembled monolayers, employ readily available equipment and provide a link between computer-aided design and self-assembled nanostructures.

5.4.2. Multimodal Porosity. Templating techniques can be combined with other techniques to produce porous films with more than one type of porosity. One of the simplest ways is to use two different types of template. Infiltration of a macro-latex beads sedimented layer with a typical infiltration solution containing TEOS/F127 leads to bimodal macro-meso porosity.^{340,341}

5.4.3. Oriented Pore Channels. Coatings that would present channel pores with a single orientation are of great interest because of their ability to tune transport into a single direction. Among these mono-oriented pores, coatings bearing vertical (perpendicular to the surface) pores are the most interesting ones since they can act as a barrier with controlled permeation, where electrons, atoms, molecules, or polymers can cross without lateral diffusion. Different methods were investigated to obtain such an interesting geometry using the template approach. However, making the elongated micelles rise perpendicular to the interface was shown to be a real challenge as a result of the enthalpy driven stability of the hydrophilic outer part of the micelles interacting with the more energetic air/solution and solution/substrate interfaces. This area is still in its infancy, and promising results emanating from confinement effects, surface modification, and mesophase alignment via external fields demonstrate that new advances on oriented POMTFs can be expected.^{183,342–346}

The first attempt was made on a typical silica (TEOS)/CTAB system in presence of ferrofluid nanoparticles and a strong magnetic field.¹⁷⁷ Such a combination only managed to disrupt the preferential alignment of the mesochannels with both interfaces or facilitate alignment with the interface,³⁴⁷ which already occurs naturally. A similar disorientation of F127 micelles was obtained in a strong (12 T) magnetic field without ferrofluid particles.³⁴⁸ Via a different approach, Boissière et al. grew 250–500 nm thick silica membranes at the top layer of a γ -alumina 0.2 μm porous tubular support.^{349,350} Mesoporous silica layers are synthesized onto the surface of γ -alumina through an interfacial reaction between a silica condensation catalyst (NaF) impregnated into the γ -alumina porous support and the hybrid micelles present in the surrounding solution.³⁵¹ This approach did also promote the orthogonal growing of cylindrical pores aligned mostly normal to the support. This interfacial growing method is, however, limited to the deposition onto porous substrates. More recently, it was reported that very thin (less than 70 nm thick) TiO_2 or SiO_2 films can be prepared with “tilted cylindrical nanopore arrays” in the presence of P123 upon EISA on a PEO-*b*-PPO modified substrate.^{352,353} However, in view of the initial structure and of the final GI-SAXS signature it is very probable that the authors formed the grid-like structure first obtained and reported for TiO_2 films upon thermal treatment and from very similar initial *Im3m* mesostructure systems.¹¹³ Even then, thicker films with such a grid-like structure have been reported for various different oxides [HfO_2 , SnO_2 , SrTiO_3 , etc.]. Coating substrates with polymers has been proposed to force alignment of the channel pores in the same direction. Kuroda et al.

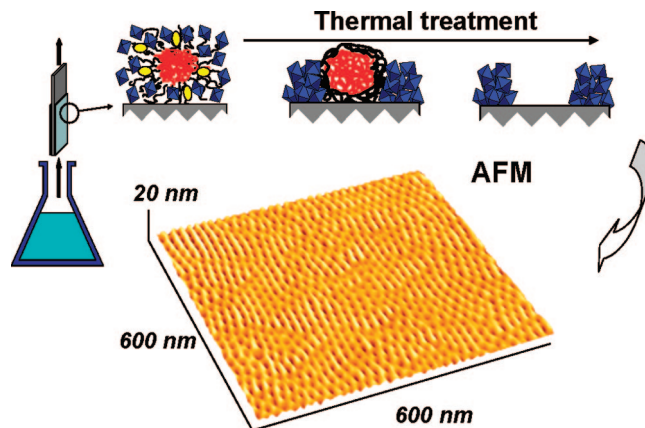


Figure 19. Nanoperforated layer of TiO_2 deposited on a SiO_2 surface. The AFM image reveals 12 nm in diameter craters highly ordered under hexagonal arrangement. Reprinted with permission from reference 362. Copyright 2007 American Chemical Society.

used a rubbing-treated polyimide film to favor alignment of the channels in the direction of the rubbing (parallel to the surface of the substrate).^{314,354,355} However, they recently showed that decreasing the template to inorganic ratio leads to the expected transformation from 2D hexagonal to 3D hexagonal structure.³⁵⁶ Similar polymer induced preferential orientation has been shown using a photo-cross-linkable polymer^{328,357} or a photochromic azobenzene-containing liquid crystalline³⁵⁸ layer on top of the substrate. The best achievement of vertical pores is reported for several hundred of nanometer thick silica films made from PS-*b*-PEO copolymers and silsesquioxane SSQ source of silica.³⁵⁹ Solutions of these were spin coated on a hydrophobic surface, and the wet film was allowed aging in a hydrophobic saturated atmosphere of chloroform and octane. Perpendicular orientation is stabilized by the low interfacial energy at both film interfaces. Cross-linking silica and copolymer elimination is then thermally triggered to liberate the porosity. TEM pictures confirmed such orientation, but no X-ray evidence is providing proof for long-range ordering.

5.4.4. POMTF Monolayers or Ceramic Nanopatterning. “Monolayers” of mesoporous films can be seen as perforated grids that are laying on a flat surface. The surface is thus accessible through discrete perforations that are calibrated in size and have controlled dispersion, ordering, and density. They constitute robust systems that have the unique combination of ceramic properties and nanostructured and ordered heterogeneous surfaces. The first report of such nanopatterns concerned TiO_2 networks deposited on SiO_2 surfaces.³⁶⁰ They were prepared by EISA (dip-coating) of highly diluted TiCl_4 solution in the presence of PB-*b*-PEO copolymers (see Figure 19).

A precise control of the quantity of deposited nonvolatile components in addition to the evaporation conditions is required. Other works were then reported from different groups on similar systems, but these nanoperforated layers have poor organization²⁶⁸ and the thickness is not well-controlled.³⁶¹ A more recent work isolated the critical parameters and showed that various interesting patterns could be obtained with matrixes other than TiO_2 such as Al_2O_3 and ZrO_2 and with different kinds of commercial copoly-

mers.³⁶² When deposited on conducting surfaces, one ends up with nanoelectrode arrays (NEA) that present highly interesting electrochemical behaviors³⁶³ and constitute a novel nanostructured heterogeneous substrate for complex nanocomposites architecture elaboration.

6. Hybrid Mesoporous Films

Hybrid mesostructured thin films could be classified into two general classes following the nature of the interaction existing between the organic and the inorganic parts.⁴ Class I corresponds to hybrid systems in which organic compounds (molecules, oligomers, or low molecular weight organic polymers) are simply embedded in inorganic matrixes. On the contrary, class II corresponds to hybrid organic–inorganic in which organic and inorganic components were both bonded through stronger covalent or ionic-covalent chemical bonds. It is worth mentioning that doped materials (Class I) involve most of the time a host–guest relationship with included species whereas the functionalized ones (Class II) imply a deeper relation since supplementary organic compounds participate more actively to the materials.

6.1. Doped Hybrid Mesoporous Thin Films and Nanocomposites: Class I. In the literature, examples of doped mesostructured hybrid films (Class I) are scarce compared to grafted ones (Class II). Historically, they result from *in situ*^{29,249,364,365} or steady-state^{246,247,366–369} investigations with fluorescent dyes on local environments provided by as-synthesized thin films, that is, before removal of template. These studies are based on specific spectroscopic responses (fluorescence polarization, solvent-sensitive emission band, lifetime, excimer/monomer emission) of fluorescent dyes toward polarity, rigidity/microviscosity of their direct environment. Briefly, it was shown that hydrophobic dyes are incorporated in the hydrophobic part of micelles.^{29,246,249,366,367,370} These dyes do or do not interact with the polar head groups of surfactant.^{247,367–370} On the other hand hydrophilic dyes as the ClRe(CO)₃–2,2′-bipyridine are incorporated in the silica framework and inside the ionic interface composed of water and polar head groups of surfactants.³⁶⁵ The specific localization of dyes in thin films was used to study the energy transfer occurring between two dyes localized in the organic part.^{247,371–373} It is noteworthy that even if these investigations involved low amount of probes usually, a high loading was reached (up to 1 pyrene for 5 CTAB, that is to say 0.05 pyrene for 1 TMOS) without dye aggregation and without loss of mesostructure order.^{246,366} These studies revealed that the mobility of dyes inside thin films are usually restricted^{246,247,249,364–366} especially when compared to free micelles in solution but increase with temperature.³⁶⁶ This loss of mobility was assigned to the confined state of micelles in mesostructured thin films. However, it has been demonstrated recently^{368,369,374} that a single dye could explore the mesostructure over a wide range in a relatively short time (up to several micrometer in 500 s). This mobility also appears to depend on the phase present in the pores since dye motion is observed for as-synthesized thin films and calcined films rehydrated under high humidity conditions on the contrary to dry calcined films.³⁷⁴ This difference of mobility between all these studies cited above is most probably due to the difference of observation time-

scale (much longer for the last three ones) and to the difference of diffusion rate of the mesophase considered (diffusion is much faster in a 2D-hexagonal phase compared with the most often studied: a lamellar phase).

Another approach to mesostructured thin films of class I consists in incorporating dyes molecules in calcined silica/titania mesoporous thin films. These films are synthesized via a simple immersion of films inside dye containing solutions.^{250,375–378} To increase the loading and in some extent to limit leaching of the dyes, aluminosilica thin films were also tested.³⁷⁹ These latter thin films showed a better adsorption ability toward a cationic photochromic dye than pure silica ones due to specific anionic sites provided by the incorporation of aluminum in the inorganic network. In addition, the concentration of the dye in thin films was higher than in solutions whatever the solvent considered and without aggregation. Finally, after dye absorption in these films, the chromophore mobility is high enough to perform photoisomerization reactions.

Besides optical properties that mesostructured thin films could exhibit after dyes doping, these materials were successfully used as host matrixes to elaborate new hybrid nanocomposites. In this case, mesoporous thin films serve as nanoreactors for chemical reactions. The simplest reaction was the synthesis of rare earth ion complexes in the same time that mesostructuration occurs.³⁸⁰ They were also used as an efficient template to synthesize carbon nanotubes.^{381–383} The synthesis of carbon nanotubes involves three steps. It implies first the synthesis of mesoporous thin films followed by a calcination step. Thin films were deposited onto conductive substrates as indium tin oxide glass (ITO) or gold layer. Once the surfactant was removed, a small amount of metal as catalyst (Co³⁸¹ or Fe³⁸²) was electrodeposited into the bottom of the pores of mesoporous thin films. Metal precursors could also be incorporated in the starting sol and reduced in H₂/N₂ flow after a calcination step.³⁸³ Then carbon nanotubes were synthesized at high temperatures (~700–750 °C) via catalytic decomposition of alcohol vapor³⁸¹ or acetylene gas.^{382,383} It is noteworthy that this procedure implies working preferentially with a three-dimensional mesophase (here, *Im3m* or *Ia3d*) since the 2D-hexagonal phase is more fragile and tends to collapse^{148,231} and molecular transport from the top to the bottom of thin films is favored with the 3D mesophase.²³¹ Following this synthesis procedure, the highly aligned carbon nanotube arrays grew from the bottom to the top of pores with a very uniform diameter corresponding to the pore diameter and hollow open ends. As carbon nanotubes are hollow with open ends, it is also possible to fill them with metal by electrodeposition reaction leading to metal nanowires (here Fe) encapsulated in carbon nanotubes.³⁸² The same approach was used to elaborate other hybrid nanocomposites with growth of polymers (polyethylene) inside the pores.³⁸⁴ After deposition and calcination steps, the mesoporous thin films were immersed in solutions containing the catalysts: dicyclopentadienyltitanium dichloride and methylaluminumoxane. The polymerization took place via addition of ethylene monomers in the gas phase at room temperature. A simpler and more efficient alternative to synthesize hybrid polymer mesoporous

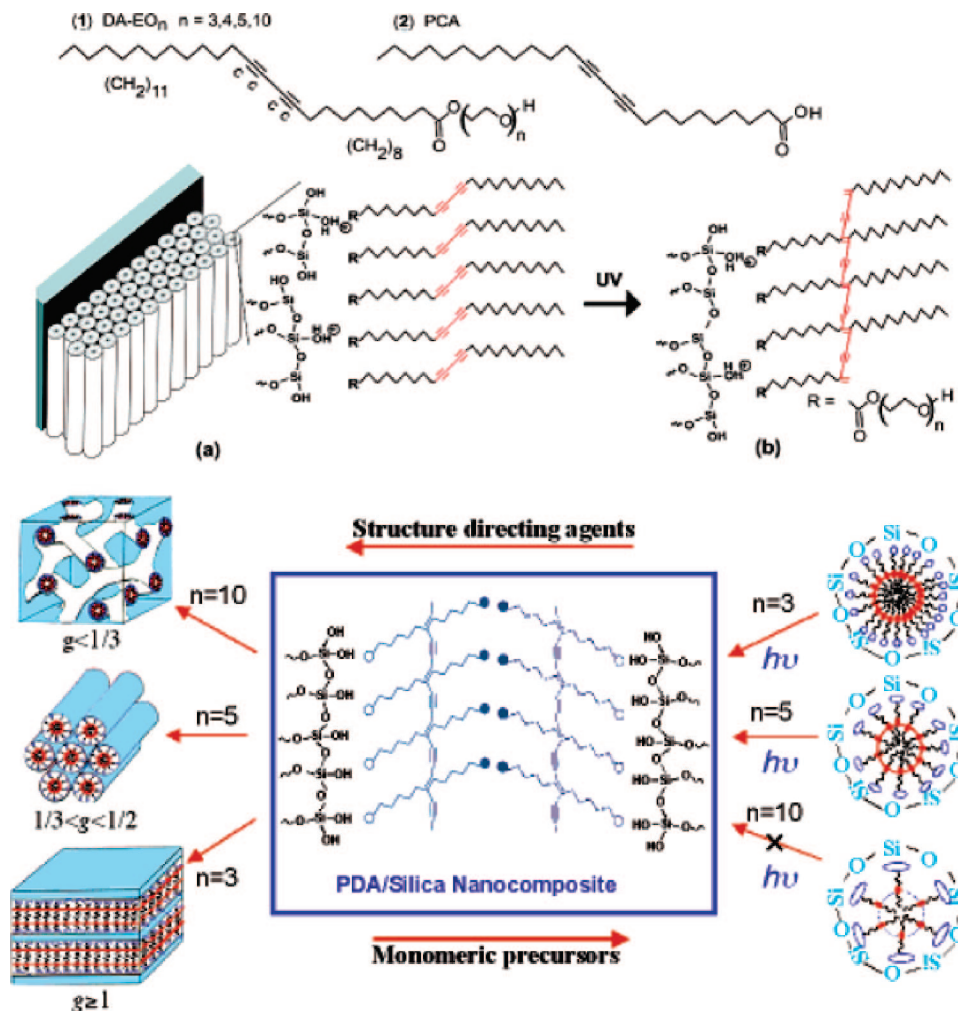


Figure 20. Top: Molecular structures of DA surfactants (1 and 2) and polymerization of DA/silica nanocomposites. (a) Film cross section near the final stage of drying shows an oriented hexagonal mesostructure and hypothetical arrangement of DA surfactants adjacent to the cylindrically structured silicic acid framework. (b) Hypothetical structure of polymerized PDA/silica nanocomposite formed upon exposure to UV light and continued acid catalyzed siloxane condensation. Bottom: Increasing the number, n , of EO subunits comprising the hydrophilic surfactant headgroup resulted in the formation of higher-curvature mesophases: lamellar ($n = 3$) → hexagonal ($n = 5$) → cubic ($n = 10$). Adapted with permission from refs 388 and 389. Copyright 2001 MacMillan Publishers Ltd. and copyright 2003 American Chemical Society.

thin films was done by Coakley et al.³⁸⁵ and Jang et al.³⁸⁶ Here, polymers were spin coated on the top of the calcined mesoporous titania thin film. An adapted heat treatment (above glass-transition temperature, T_g) allowed the infiltration of polymers inside the pores. The authors³⁸⁵ demonstrated that polymers fully penetrated inside the mesoporosity from the top to the bottom of thin films. They suggested that the conformational entropy loss of polymer due to its confinement in pores was compensated by a strong enthalpic interaction between the highly polarizable chains of the polymer and the polar titania surface. In fact, they proposed that a chain of the polymer could infiltrate the mesoporosity only if some of its segments are able to absorb on the walls of the titania surface. Once inside thin films, the polymer chains presented a different conformation compared to neat films of polymers; in mesoporous thin films, they are coiled and unable to π -stack. The last way reported^{387–389} is undoubtedly the most elegant one and consists of a “one-pot” synthesis, that is, all the components of thin films (surfactant, inorganic precursors, solvents, catalysts, monomers) are mixed together in the same starting sol. This “one-pot” procedure has been also used to synthesis hybrid

polymer–nanocomposite of class II.^{248,390–393} The first attempt was to use polymerizable amphiphilic diacetylene molecules as both structure-directing agents and monomers.^{388,389} By tailoring the size of the oligo(ethylene glycol) headgroup of the diacetylene-containing surfactant, they synthesized conjugated polymer/silica nanocomposites with hexagonal, cubic, or lamellar mesophases (Figure 20).

The EISA process^{27,29} allowed a rapid and uniform incorporation of organic monomers within a highly ordered inorganic environment. The polymerization of diacetylene units initiated by ultraviolet light converted the colorless mesophase into a blue polydiacetylene–silica nanocomposite. By changing the number, n , of EO subunits comprising the hydrophilic surfactant headgroup it was possible to tune the resulting mesophase: lamellar ($n = 3$), hexagonal ($n = 5$), and cubic ($n = 10$). This could be explained by the surfactant packing parameter^{2,394} $g = v/a_0l$ where a_0 is the surfactant headgroup area, v the surfactant volume, and l its tail length. Then an increase of “ n ” values reduces the value of g favoring then the formation of higher curvature mesophases. However, large headgroups ($n = 10$) also served as spacers, preventing polymerization of the pure DA–EO₁₀ surfactant.

To overcome this problem, addition of surfactants with smaller headgroups (e.g., 1 with $n = 3$ or 5, or 2) was necessary to form PDA in the cubic system.

It was observed previously, via fluorescent investigations, that micelles of surfactants are more packed in mesostructured thin films than in solution.^{246,247,249,364–366} Indeed, the authors did not observe DA polymerization in Langmuir monolayers and trilayers of neat DA while polymerization occurred in the lamellar mesophase. In both systems, the diacetylenic surfactants are organized into highly oriented planar configurations with the EO headgroups disposed toward the hydrophilic interface, either water (Langmuir films) or polysilicic acid (nanocomposites). The explanation about this different behavior toward polymerization cannot involve the lamellar organization itself. The authors postulated that Langmuir films did not polymerize because the reactive DA moieties were spaced too far apart on the contrary to the hybrid lamellar mesophase. Closer spacing of the EO headgroups (and correspondingly the diacetylenic moieties) within the self-assembled nanocomposites (lamellar, hexagonal, or cubic) may be resulted from attractive interactions (Van der Waals interactions, H bonding, etc.) between the EO headgroups and the silica network. The nanostructured inorganic host altered the diacetylene polymerization behavior, and the resulting nanocomposites showed unique thermo-, mechano-, and solvatochromic properties. The second attempt is more conventional since surfactants and monomers are distinct compounds³⁸⁷ (this approach was also used to form class II polymer nanocomposite thin films via introduction of a silylated coupling agent in the starting sol^{248,390–393}). In this case, two monomers were used: 2,5-diiodothiophene and acetylene. The first one was solubilized in the starting sol with a catalytic complex, and the second one was incorporated in the gas phase with triethylamine at room temperature under pressure. This procedure lead to a cubic mesostructured conjugated poly(2,5-thienylene ethynylene)/silica nanocomposite. All the literature cited above involves organic molecules or polymers as the organic part of hybrid materials. Recently, Baca et al.³⁹⁵ immobilized successfully living cells in mesostructured thin films. However, the encapsulation of living organisms in matrixes requires overcoming serious difficulties in cell viability throughout the synthesis process. It implies, for example, biocompatible surfactants. Indeed surfactants used in templated mesoporous silicas are detergent monomers that insert into cell membranes and lead to their solubilization, inducing rapid cell death. Thus, standard surfactants were replaced by phospholipids, which are integral components of the cell membrane. The choice of phospholipids species must be done with respect to three parameters: they should (i) present minimal disruptive electrostatic interactions with cell membranes, (ii) be soluble in water, and (iii) have sufficiently small critical packing parameters g to direct the formation of high curvature 3D (hexagonal or cubic) lipid–silica mesophases. However, even if diacylphosphatidylcholines were identified as suitable templates, the incorporation of living cells markedly altered the mesostructuration process in several ways. During the EISA process, cells rapidly organized around themselves a lipid-rich shell

excluding largely silica. Moreover, *S. cerevisiae* globally altered the sequence of mesophase development during the EISA process leading to a 2D hexagonal mesophase instead of a 3D hexagonal/cubic one. On the contrary to conventional organic moieties, living cells are dynamic structures able to sense and respond to their environment.

As solvent evaporates, the concentration of osmolytes in the system increases. Stationary-phase cells can release up to 35% of their cellular water volume in response to a change in turgor pressure (the pressure of the cell contents against the cell wall) in the cell membrane, which would increase the volume of water in the surrounding lipid shell by more than 60%. The resulting pH gradient that develops around the cell in turn affects both the local lipid interface and the host lipid/silica matrix. This pH gradient favors both conversion of lipid bilayers into ordered lamellar mesophase (instead of the 3D hexagonal/cubic phase expected) and enhancement of silica condensation around cells hindering diffusion of silica oligomers. Despite all the potential applications described above of doped-mesostructured thin films (Class I), the localization of the organic components in the micellar part and/or the opened pores of mesostructured thin films could limit their potential applications mainly due to the high tendency of organic molecule leaching. Then it is most of the time necessary to graft organic molecules via covalent or iono-covalent bonds to the matrix.

6.2. Functionalized Hybrid Mesoporous Thin Films: Class II. **6.2.1. Grafting Routes.** Two grafting routes are commonly used to incorporate organic functionalities into POMTFs: the “one-pot” synthesis and the postfunctionalization. The first one, that is, “one-pot” synthesis, involves a co-condensation step between a functional inorganic precursor, generally an organosilane, with an inorganic precursor (typically TEOS or TMOS and less frequently transition metal oxides) in the presence of templates. In this case the mesostructuration process and functionalization take place at the same time. In the second one, that is, postfunctionalization, chemical modifications come off once mesostructuration and calcination steps are achieved, via solution impregnation or vapor treatment through chemical bonds with silanol or M–OH groups covering the pore surface. The “one-pot” synthesis was largely dedicated to functionalize silica POMTFs while postfunctionalization was used with silica and TMOs matrixes. However, the “one-pot” synthesis of transition metal oxide has been recently reported either via the use of organosilane precursors^{393,396,397} or with a complexing/chelating agent.^{192,398} In this latter case, the complexing/chelating agent, trifluoroacetic acid, was randomly distributed within the inorganic framework and was rather used to control the rate of titania condensation.⁵

Despite the fact that postfunctionalization was widely exploited to modify properties of mesoporous powders (for an overview on functionalization of mesoporous powders, see the following reviews: refs 43 and 44), the most frequent route leading to functional POMTFs is the “one-pot” synthesis. In fact, this approach allowed POMTFs bearing a vast choice of organic functions to be synthesized (for a more detailed description of functional groups incorporated into POMTFs, see the following review: ref55). These functional

Table 4. "One-Pot" Synthesis versus Postfunctionalization⁶⁰

"one-pot" synthesis	postfunctionalization
tailor compatibility R-MX _n and MX _n	tailor surface-R-MX _n interactions and reactivity
network consolidation temperature limited by the thermal stability of organic groups	high preconsolidation temperature (calcination step possible) before grafting, leading to a more stable inorganic network
localization of organic groups in the pores and/or embedded in the framework depending on the nature of the organic groups	organic groups grafted mostly on pore surface
organic groups have a role in the mesostructuration process (e.g., polarity, condensation catalysis, cosurfactant, etc.)	mesostructure is determined before organic group incorporation
relatively homogeneous dispersion of organic groups	pore blocking possible
limited by chemical compatibility	limited by diffusion plus pore blocking
one-pot synthesis, one or more functions, lower control of dispersion	one postgraft, one function, successive possible

groups could be chemically inert, such as, for example, alkyl chains^{399–403} or aromatic groups,⁴⁰³ but also more reactive as aminoalkyl,^{337,338,396,403–405} methacryloxypropyl,^{392,403} cyanoalkyl,^{190,221} and so forth, or presenting intrinsic properties such as silylated dyes^{337,338,403,406} which could serve as sensors^{337,338,407–410} or more sophisticated materials as nanovalves.^{236,411} The co-condensation route generally leads to a more homogeneous distribution of organic functionalities into mesoporous matrixes with a high control of the stoichiometry. The final materials exhibit a small decrease of the pore sizes and pore volume only. However, the synthesis could be more delicate because of different effects of organic functions on the mesostructuration process of POMTFs.^{55,60} The influence of organic functions generally limits the organic/metal molar ratio which is often restricted to 20%. However, higher loadings of organosilanes in POMTFs, from 50 to 100%, were achieved either by a careful control of hydrolysis–condensation steps^{412–414} or by using hybrid bridged silsesquioxanes^{28,64,415} and methyl-triethoxysilane.^{401,416}

On the other hand, postfunctionalization overcomes some difficulties related to the "one-pot" synthesis. Since mesostructuration process and grafting are two distinct steps, the influence of organic functionalities is seriously restricted. Moreover, the thermal treatment at high temperature (>500 °C) allowed by the absence of organic functionalities favors more stable matrixes. However, this method often leads to a quite low loading, an inhomogeneous distribution of the functional groups inside matrixes, a decrease of the pore volume, and even in extreme cases, a complete closure of the pores.⁴³ Moreover, depending on the postgrafting conditions (impregnation), the inorganic network could be partially damaged due to capillary stresses or chemical cleavage of M–O–M bonds. Recently, another alternative route, vapor infiltration treatment, was successfully tested without reducing the pore size and with an increase of mechanical strength. Briefly, neat surfactant mesophases¹³⁶ or as-synthesized silica thin films^{330,402,417} were first coated on a substrate and a subsequent organosilane or hexamethyldisilazene vapor treatment was then applied leading to functionalized POMTFs. This subsequent vapor treatment has been also realized on calcined POMTFs.^{418,419} A similar method has been developed recently using supercritical carbon dioxide as the synthesis medium.¹⁵⁷ In Table 4 are reported the advantages and drawbacks of both methods.⁶⁰

Although the vast majority of functionalized mesostructured thin films are obtained via "one-pot" and postfunctionalization pathways, combined routes have been investi-

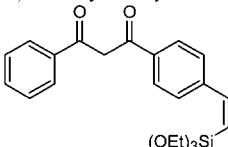
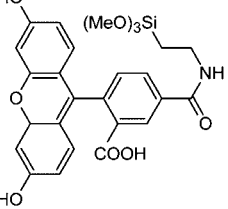
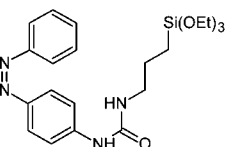
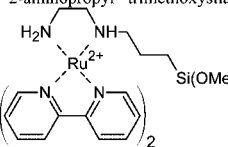
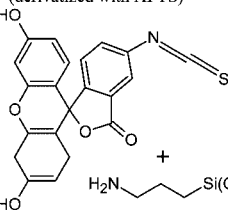
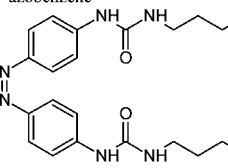
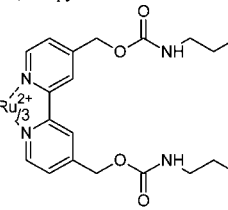
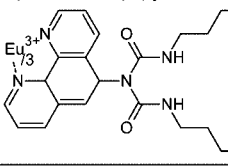
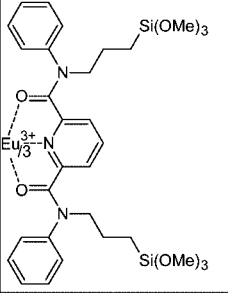
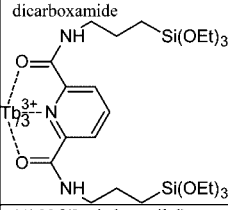
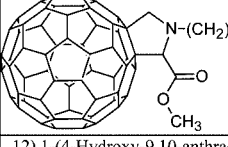
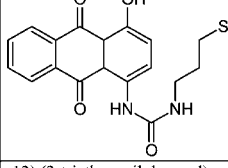
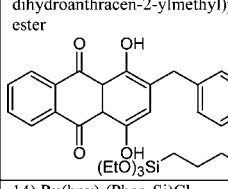
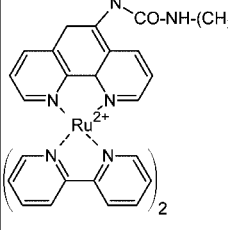
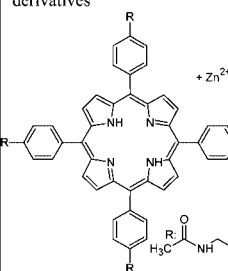
gated. This combined approach could occur when organosilanes are not commercially available. Instead of synthesizing the desired organosilanes before film synthesis, some authors elaborated hybrid thin films through co-condensation or a postfunctionalization procedure with an organosilane bearing a reactive function (typically amino,^{235,337,338} thiol,⁴²⁰ cyano,⁴²¹ and iodo²³⁵ groups). After removal of surfactant, the postmodification involving the reactive function anchored into thin films and the organic molecule (fluorescein derivative,^{337,338} ferrocenecarboxylic acid,²³⁵ azobenzene derivatives,⁴²¹ β -cyclodextrin⁴²⁰) could take place. This combined approach presents the advantages both to avoid the synthesis of organosilanes and to limit the influence of organosilanes (often bulky) on the mesostructuration process.

6.2.2. Co-Condensation or "One-Pot" Synthesis. The "one-pot" synthesis has been used to synthesize almost exclusively hybrid silica-based mesostructured thin film via co-condensation of organosilanes with TEOS or TMOS. However, Soler-Illia et al.^{396,397} reported recently the one-pot synthesis of highly ordered hybrid mesoporous thin films (M_{1–x}(SiR)_xO₂) obtained by co-condensation of organotrialkoxysilanes (R-Si(OEt)₃ with R = propylamine, propylthiol, and phenyl) with transition metal chloride (MCl₄ with M = Zr or Ti). Such mixed oxide hybrid matrixes allow a further selective functionalization with metal chelating agent leading to bifunctional materials. Bifunctionalization could also be achieved with pure silica matrixes by a one step procedure.^{370,415,422}

Data concerning one-pot synthesis of mesoporous thin films are gathered in Table 5. The non-commercial available organosilanes, the surfactant and experimental conditions, the nature of the mesophase, and the targeted applications are reported.

Although the one-pot synthesis presents several advantages compared to postgrafting, this approach is somehow complicated and several difficulties exist in addition to the control of the main parameters related to the EISA process. For example, the presence of organosilanes presenting different reaction rates and self-assembly can modify or even hinder mesostructuration. Moreover, an increasing proportion of organosilanes in the reaction mixture favors homocondensation reactions to the detriment of cross-linking co-condensation reactions with the silica precursors leading to an inhomogeneous distribution of different organic functionalities in the framework. In addition to that the temperature of the network consolidation step should be adapted

Table 5. Non-Commercial Organosilanes and Properties of Resultant Thin Film Mesophases

Functional organosilanes	Properties / applications (ref)	
1) Triethoxydibenzoylmethane 	Heavy metals sensor ⁴⁰⁸ BF ₃ sensor ⁴²³	
2) Dye-NH(CH ₂) ₃ -Si(OCH ₃) ₃ Dye = 5,6-carboxyfluorecein, succinimidyl ester (5,6-FAM, SE) 	pH sensitive ^{337,338}	
3) 4-(3-triethoxysilylpropylureido) azobenzene 	Smart gas masks, membranes, controlled release systems, externally controlled micro/nanofluidic-channel systems ^{236,411}	
4) Ru(II) 2,2'-bipyridine-2-aminoethyl-2-aminopropyl-trimethoxysilane 	^{370,424}	
5) Fluorescein isothiocyanate (derivatized with APTS) 	Optical solid-state pH sensors ⁴⁰⁷	
6) 4,4'-bis(3-triethoxysilylpropylureido) azobenzene 	Optomechanical actuation ⁴²⁵	
7) Silanized Ru(II) 4,4'-hydroxymethyl-2,2'-bipyridine 	^{370,426}	
8) Silanized Eu(III) phenantroline 	Nonlinear optical materials, tunable solid-state lasers ⁴²⁷	
9) Eu(III) bis(N,N'-phenyl 3-trimethoxysilylpropyl)-2,6 pyridine dicarboxamide 	^{370,373}	
10) Tb(III) N,N'-bis-(3-triethoxysilylpropyl)-2,6 pyridine dicarboxamide 	^{370,373}	
11) N-[(3-triethoxysilyl)propyl]-2-carbomethoxyfulleropyrrolidine 	Optically encoded information storage for read only materials (ROMs) ⁴²⁸	
12) 1-(4-Hydroxy-9,10-anthraquinone-1-yl)-3-(3-triethoxysilylpropyl) urea 	Intrinsic optical bistability investigations ⁴²⁹	
13) (3-triethoxysilylpropyl)carbamic acid 4-(1,4-dihydroxy-9,10-dioxo-9,10-dihydroanthracen-2-ylmethyl)phenyl ester 	Intrinsic optical bistability investigations ⁴²⁹	
14) Ru(bpy) ₃ (Phen-Si)Cl ₂ 	Oxygen Sensor ⁴¹⁹	
15) Metalloporphyrin or porphyrin derivatives 	TNT Sensor ^{410,430}	

to the organic compounds present inside the matrixes. In the following sections, an overview of the main results reported by the literature will be developed.

6.2.2.1. Chemical and Processing Parameters (EISA Parameters). The EISA method, which is used in almost all the syntheses of functionalized and mesostructured silica thin films, implies a homogeneous starting sol. However, when the silylated probe is poorly soluble or insoluble in the alcoholic sol, segregation or aggregation can take place. This phenomenon may be due to an insufficient hydrolysis of the organosilane precursor, resulting in hydrophobic species. In some cases, the precursor can be insoluble regardless of the hydrolysis time. To overcome these problems, a prehydrolysis step of the organosilane in a weak acidic medium⁴³¹ and/or the use of a cosolvent are required.

The choice of cosolvents is limited: the cosolvent must not only dissolve the desired organofunctional molecule but also be miscible with the starting sol without causing organosilane gelation and affecting neither the film optical quality nor the mesostructuration. Moreover, the cosolvent must present evaporation ability close to that of ethanol and ensure a good wettability toward coating substrates. In addition to that the amount of cosolvent in the initial sol should be adapted to avoid phase separation during the evaporation process (higher than the quantity needed to solubilize the organosilane especially when its boiling point is lower than that of ethanol). The cosolvent most commonly employed in the literature is the tetrahydrofuran. This cosolvent, used in place of ethanol or in a mixture with ethanol, has been successfully employed for preparing well-organized thin films with monomers,^{388,389,392} β -diketones,⁴⁰⁸ C₆₀ and quinizarine derivatives,^{428,429} bridged silsesquioxane,⁴²⁵ or MTES-based matrixes.⁴⁰¹

The presence of organosilanes could also modify the hydrolysis–condensation rates of silica species. For example, organosilanes bearing a basic function, typically an amino group, catalyze hydrolysis and condensation reactions of the silica precursor and can yield the fast gelation of the sol. Acidic conditions in EISA are important to make films which present good (optical) quality, which is a very important feature for applications in optics and optical sensors. To avoid basic catalysis of silica species, amino groups are first usually neutralized with a strong acid prior to the addition of the silica precursor.^{403,404,432} A subsequent treatment of the films with ammonia could allow the recovery of the amino group through deprotonation of the ammonium.⁴⁰³ However, the gelation process could not be always hindered. For example, high loading of ruthenium complexes in the initial sol leads to gel formation.³⁷⁰ On the other hand, the presence of methyltriethoxysilane in hybrid MTES–TEOS⁴³³ thin films or vinyltriethoxysilane with TMOS²⁵¹ slows down the polycondensation of silica. This is beneficial since hybrid MTES–TEOS mesostructured thin films are highly ordered and defect-free.^{183,433–435} A recent approach leading to well-ordered hybrid POMTFs with a high content of organosilanes has been developed. A majority of the hybrid POMTFs results in one step co-condensation, i.e. organosilanes and inorganic precursors (TEOS/TMOS) are mixed at the same time in the initial sol, but this one step co-condensation gives

usually poorly organized hybrid POMTFs at high loading of organosilanes. Some authors^{337,338,370,408,429} reported an alternative “one-pot” synthesis highlighted by Matheron et al.^{412–414} This synthesis is based on a pre-hydrolysis–condensation step of TEOS followed by the addition of organosilanes just prior the sol deposition. These conditions limit considerably the condensation of organosilanes before film deposition.^{412–414} This “delayed” synthesis modifies the main EISA parameters as surfactant/inorganic precursor molar ratio and the optimum relative humidity within the dip-coater. It was observed that the CTAB–TEOS mesophase diagram was shifted toward higher CTAB/TEOS ratio and that this shift increased with the organosilane content. Typically, a 3D-hex mesophase obtained for a CTAB/TEOS ratio of 0.08 with pure TEOS is shifted to 0.16 for 20% of MTES (MTES/TEOS ratio = 1/4) and to 0.20 for 50% (MTES/TEOS ratio = 1/1). In the same time, the increase of MTES content in thin films (from 0 to 50%) causes a decrease of the optimum relative humidity (RH) value (from 65 to 40% in the case of a 3D-hexagonale mesophase). These changes of optimum RH values were explained by the necessity to obtain rapid gelation of the deposited sol to stabilize 3D mesophases (3D-hexagonal and 3D-cubic) which do not exist in the phase diagram of CTAB with water and ethanol. This “delayed” procedure allowed well-organized hybrid POMTFs with high content of methyltriethoxysilane, MTES (50%); vinyltriethoxysilane, VTES (30%); and trifluoropropyltrimethoxysilane, TFP TES (20%) to be synthesized.⁴¹⁴

6.2.2.2. Localization of Grafting Compounds. To control the final properties of functional thin films, it is of great importance to localize perfectly organosilane species in the mesostructure and to address a specific compound to a specific place. The localization of such species inside the mesophase has been investigated either directly by spectroscopic techniques such as fluorescence,^{370,424,426,427} UV–visible absorption,^{408,429} and micro-Raman¹⁹⁰ spectroscopies and/or indirectly by studying structural changes induced by the incorporation of probes (e.g., variation of the lattice parameters,^{190,403} phase transition,^{190,403,408,429} formation of mesophase at very low surfactant/TEOS ratio⁴³¹).

With regards to mesostructured thin films made with ionic surfactants such as CTAB, the structure can be divided into three main regions:^{370,424,426} the silica framework (Figure 21a zone I), the ionic interface formed by the charged surfactant heads, the hydrosilylated silica surface (Figure 21a zone II), and the organic region composed by the hydrophobic core of the micelles (Figure 21a zone III).

This organic/inorganic phase separation is also obtained with nonionic surfactants such as triblock copolymers (i.e., poly(ethylene oxide)–poly(propylene oxide)–poly(ethylene oxide), PEO–PPO–PEO)-based thin films. However, in this case, the limits between the three phases, silica wall, hydrophobic PPO block, and hydrophilic PEO block are less defined mainly because of interpenetration of the PEO and silica networks.⁴³⁶

According to the literature, the silylated functions can be classified into two categories:

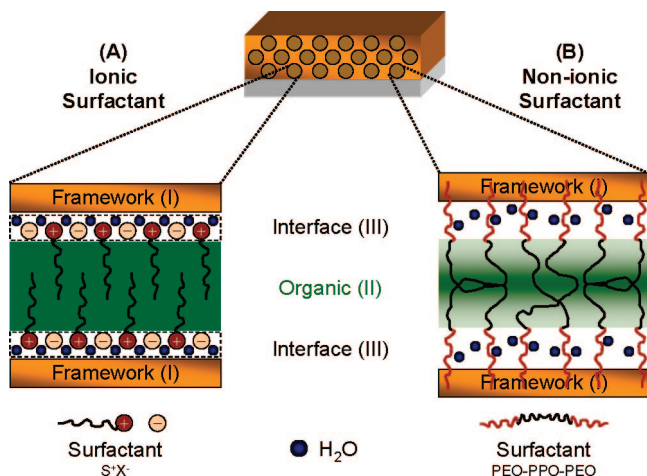


Figure 21. Structure of the mesostructured thin films made with (a) ionic surfactants and (b) nonionic surfactants. Reprinted with permission from ref 55. Copyright 2005 The Royal Society of Chemistry.

(i) Monosilylated compounds, $F-S-Si(OR)_3$, constituting the most common category studied (with $-OR$ being condensable groups, F the functionality, and S the spacing group).

(ii) Multisilylated probes of general formula $F(S-Si(OR)_3)_n$ mainly composed of $(OR)_3Si-F-Si(OR)_3$ bridged silsesquioxanes and rare earth complexes with silylated organic ligands.

The localization of organosilanes is governed by their physicochemical properties. Several factors have to be taken into account such as the hydrophilic/hydrophobic balance of the organosilane molecule, the number of anchoring functions ($-OR$)₃, the length and the nature of the spacing group (group S between the functionality F and the anchoring function $-Si(OR)_3$), and the nature of the functionality F (hydrophobic, hydrophilic, ionic, polar, apolar, aromatic, for example).

A general tendency is commonly observed with probes presenting multiple trialkoxysilane functionalities. They are mainly incorporated inside the inorganic network, as was observed with multisilylated rare earth complexes^{370,424,426,427} or even compose the walls of the framework as observed with hybrid bridged silsesquioxanes^{28,64,157,415} (and also the monosilylated methyl-triethoxysilane^{401,416}) leading to mesostructured thin films with concentrations as high as 100% in organosilanes.

However, most of the common organosilanes are monosilylated with a general formula $F-S-Si(OR)_3$. Such molecules possess two different groups, one carrying the functionality and the other being the condensable groups. Both groups simultaneously interact with two different regions of the mesostructure. The condensable $-OR$ groups allow the formation of chemical bonds between the molecule and the framework. It is interesting to point out at this stage that even if most studies reported in the literature concern pure silica frameworks, the use of such compounds is also compatible with organosilica frameworks (bridged bistralkoxysilanes⁴¹⁵); or surprisingly, with transition metal oxides like ZrO_2 or TiO_2 .^{396,397} The localization of the functionality F is mainly governed by the “philicity” concept (or “like”

dissolves “like”) but also by specific interactions such as cation- π ⁴³⁷ or ionic.³⁷⁰

Generally, the solubilization of lipophilic molecules occurs in the hydrophobic micelle core and the placement of hydrophilic molecules either in the ionic interface or in the framework. For example, Nicole et al.⁴⁰⁸ investigated the incorporation of a hydrophobic chelating agent in thin films: a silylated β -diketone. β -Diketones are well-known to exist mainly in two tautomeric forms in equilibrium. As the keto-enol equilibrium is extremely solvent-sensitive and as the ketone and enol forms present two distinct UV-visible spectra, it was possible to determine spectroscopically the placement of the silylated β -diketone in thin films. Indeed, the absorption spectra of the β -diketone in thin films, whatever the mesophase studied ($Pm3n$, $p6m$, lamellar), have the same aspect as that of the probe dissolved in THF, indicating that β -diketone environment is apolar, suggesting their localization inside the hydrophobic core of the micelles. On the other hand, Zink et al.^{370,424} observed that the localization of a silylated ruthenium complex positively charged depended on the surfactant charge. In SDS (anionic surfactant) based thin films, the ionic complex resided in the ionic region at the interface between the organic and inorganic regions, while, in mesostructured thin films made with cationic surfactant (i.e., CTAB), the complex was located in the silica network. These results suggest that the electrostatic repulsion between the positively charged Ru complex and cationic CTAB headgroups makes the ionic region less hospitable than the silicate matrix, thus forcing the Ru complex to enter into the silicate matrix. Cagnol et al.⁴⁰³ noticed that the structure of the final mesophase depended on the loading rate of (2-phenylethyl)trimethoxysilane in thin films. For low amounts of organosilanes, the mesostructure was not modified, presenting a cubic structure ($Pm3n$), whereas for high amounts of probe, a 2D-hexagonal ($p6m$) phase was formed. Such phase transitions are commonly observed when the $[CTAB]/[SiO_2]$ ratio increases,¹²⁹ inducing a decrease in the curvature of the micelles. It is generally agreed that two kinds of sites are available when a molecule is solubilized inside micelles: one near the polar head and the other between alkyl chains in the hydrophobic core of the micelles.^{438,439} It has been shown⁴⁴⁰ that the first sites occupied by aromatic compounds are near the polar head of CTAB surfactants due to specific interaction between the π system and the quaternary ammonium.^{437,441,442} Once the first sites are saturated, the solubilization occurs in the hydrophobic part of the micelles, inducing a decrease of the curvature of the micelles and causing a phase transition. However, the length and the nature of the spacing group, S , could hinder the natural placement of hydrophobic functionality inside the micelles. For instance, with the same functionality (i.e., phenyl group) and the same relative amount of probes, no variation of mesophases was observed with the phenyltriethoxysilane, on the contrary to the (2-phenylethyl)trimethoxysilane.⁴⁰³ This result could be explained by a physical impossibility of the aromatic functionality to fully reach the hydrophobic part of the micelles in the case of the phenyl precursor, thus “preventing” the swelling of the micelles and the decrease of the interface curvature. This

geometrical criterion is in balance with all other parameters described previously.

Consequently, the role of the organic function during the self-assembly is complex, mainly because the key parameter leading to a particular mesophase is not always predictable. The functionality and the spacing group may interact with the silica wall, with the surfactant headgroup, and with its hydrocarbon tail, affecting in some cases the curvature of the hybrid interface.

6.2.2.3. Mesopore Modifications. We have seen previously that spectroscopic techniques (i.e., absorption, UV–visible, or fluorescence spectroscopies) are a useful tool to determine the placement of organosilanes inside mesostructured thin films. Nevertheless, the incorporation of such compounds inside thin films could also cause structural changes, from variations of the lattice parameters to phase transitions, and even allows the formation of a mesophase for a (very low) molar ratio of surfactant/silica leading to an amorphous thin film without organosilanes. All these changes give an indirect proof of the localization of the organosilane inside mesoporous thin films.

The changes of the lattice parameters with an increasing amount of organosilane could be an indication of its preferential localization at the ionic interface, near polar heads of the micelles.^{190,403} In the system CTAB–TEOS, the incorporation of a positively charged organosilane, 2-(trimethoxysilyl)ethylpyridinium, induced the formation of a 2D-hexagonal phase (*p6m*), regardless of the loading ratio.⁴⁰³ The authors observed a progressive increase of the interlayer distances $d(01)$ with the increasing incorporation of protonated ammonium functions. This observation also occurred with the two other positively charged groups studied (i.e., 3-(2,4-dinitrophenylamino)propyltriethoxysilane and 3-aminopropyltriethoxysilane). These results could be primarily attributed to the cationic character of the incorporated functions. Usually, in acidic conditions, the bromide is intercalated between the ammonium headgroup and the silica wall through electrostatic interactions.⁴⁴³ In this case, the electrostatic repulsion between the two positively charged groups (i.e., the polar head of the surfactant and the functionality, F, of the organosilane) governs the formation of the mesophase with a main localization of the probe in the ionic interface, even if a swelling effect could be involved. These results are in agreement with the spectroscopic study of the group of Zink concerning the localization of a positively charged silylated ruthenium complex in CTAB-based mesoporous silica thin films.³⁷⁰

The incorporation of probes could also lead progressively to a deconstruction of the mesophase with few changes in the lattice parameters, as in the case of 3-cyanopropyltriethoxysilane from a well ordered 2D-hexagonal structure to a worm-like phase.¹⁹⁰ This modification could be explained by a solubilization of the cyanopropyl groups inside the surfactant micelles. Another example of phase transitions was reported with the incorporation of bulky hydrophobic compounds.^{408,429} The addition of increasing amounts of dibenzoylmethane/quinizarine derivatives for a fixed CTAB/silica molar ratio induces mesostructural evolutions in thin films. The following sequence was observed: cubic phase

(*Pm3n*) < mixture of cubic (*Pm3n*) and 2D-hexagonal (*p6m*) < pure 2D-hexagonal phase < lamellar phase. Such phase transitions are explained in terms of variation in the packing parameter g . The increase of the packing parameter can be due to solubilization of large species preferentially in the hydrophobic part of micelles during evaporation of solvents, leading to an increase of the total volume associated to the surfactant chain. This mechanism is supported by the UV–visible experiments performed on hybrid thin films.^{408,429} In this case, the incorporation of large species causes direct phase transitions without modifications of the lattice parameters.

This co-solvent effect allows the formation of a mesophase for conditions at which mesostructured thin films are not usually obtained (i.e., very low surfactant on silica ratio). The synthesis of mesoporous thin films with 10 mol % of perfluoroalkylsilanes with long chains, typically tridecafluoro-1,1,2,2-tetrahydrooctyltriethoxysilane and heptadecafluoro-1,1,2,2-tetrahydrodecyltrimethoxysilane, have been achieved⁴³¹ with sol containing a ratio of CTACl/Si ~ 0.004 . It is interesting to point out, following the phase diagram of CTAB/Si/H₂O ternary system,¹²⁹ that the lowest ratio CTAB/Si leading to the formation of mesostructured thin films is equal to 0.10. Moreover for this last ratio, we could expect only a 3D-hexagonal mesophase (*P6₃/mmc*), which is a structure with a higher curvature of the micellar interface than the 2D-hexagonal phase (*p6m*) observed with the addition of the perfluoroalkylsilanes. This result suggested that perfluoroalkylsilanes also act as a structure-directing agent when the reactant was mixed with a small amount of surfactant. Indeed, hydrolyzed perfluoroalkylsilanes carrying hydrophilic silanol head groups and long hydrophobic perfluoroalkyl chains can clearly be amphiphilic molecules.

We have seen that the function, F, could develop direct interactions with surfactant head groups. These interactions increase the area of the surfactant's headgroup, promoting higher curvature of the micelles promoting *Pm3n* structure. The opposite effect on the curvature would be obtained by increasing the volume of the hydrophobic micelle core (swelling effect). However, in a particular system, one has to keep in mind that the effect of each function is more subtle and cannot be sketched by only these two extreme effects.

6.2.3. Postfunctionalization Route. The other route leading to hybrid POMTFs consists of postgrafting organic functions onto a stabilized inorganic network. The difference of reactivity between silica and TMOs implies distinguishing these two matrixes toward postfunctionalization. Indeed, grafting on silica matrixes involves covalent bonds due to condensation reactions with organosilanes species which are also able to react on themselves. On the contrary, TMOs matrixes are functionalized via ionic-covalent bonds with complexing/chelating agents which can only react with inorganic matrixes. Moreover, the strength of bonds, from ionic-covalent to covalent, could influence dramatically the properties of the resulting hybrid matrixes in terms of diffusion, accessibility, and homogeneity. The grafting of silica could be considered as irreversible while functionalization of TMOs is based on complexation equilibria. Such differences render silica matrixes much more sensitive to

pore blocking due to extensive condensation of silica species. This problem has been limited by new postfunctionalization treatments: vapor infiltrations of organosilanes or hexamethyldisilazane on as-synthesized POMTFs.

From this short overview, it appears that two main parameters are of great importance for obtaining a homogeneous distribution of organic functions in POMTFs: (i) the accessibility of the porosity (large diffusion of molecules inside the whole film) and (ii) the reactivity of the molecules toward matrixes and among themselves. The diffusion properties essentially depend on the mesophase (two-dimensional or three-dimensional), the pore interconnection (presence of restrictions or no interconnection, for example), the pore size, and the pore morphology (spherical, cylindrical, ellipsoidal, for instance).

Postfunctionalization could be also used to elaborate bifunctional POMTFs.^{396,397} Briefly, in the first step, a hybrid $M-(RSi)O_2$ POMTF ($M = Ti, Zr$ etc.) is created by one pot co-condensation of MCl_4 and $RSi-(OEt)_3$. The second function R' is added by postsynthesis treatment with an organic $R'-G$ molecule, in which G is a complexing group, able to selectively attach to the transition metal sites (Ti, Zr , etc.), which are freely accessible. This approach allows then both a good homogeneity of the first function (organosilane species) due to "one-pot" synthesis and a high dispersion of the second function (complexing/chelating molecules) due to the properties of postfunctionalization with TMOs.

6.2.3.1. Postgrafting on Transition Metal Oxide Matrixes. Examples of nonsilica functionalized mesoporous materials are scarce, even if methods for the synthesis of transition metal oxide films have been developed, either for MO_2/M_2O_3 ^{16,39,56,233,444,445} or mixed oxide frameworks,^{57,58,106,446} by a general evaporation-induced self-assembly (EISA) procedure. The feasibility of incorporating organic molecules within mesoporous zirconia thin films by postsynthesis grafting was demonstrated by Crepaldi and co-workers.⁵⁶ The production of hybrid POMTFs is often based on the postsynthesis functionalization of titania or zirconia mesostructures with organic bifunctional molecules F-G, which contain a desired F group and a suitable grafting group ($G =$ phosphonate, phosphate, carboxylate, acetyl acetonate, etc...) capable of performing complexation of the transition metal centers. This procedure leads to highly ordered, nonsilica hybrid POMTFs with organic functions at the pore surface. An important aspect of these films is that the anchoring of the organic groups can be varied, from strong and inert (phosphate, phosphonate) to relatively labile (carboxylate), leading to a great flexibility in the attachment of organic functions, which can be advantageous for several different applications (e.g., sensors, controlled release systems). However, the postfunctionalization of TMO thin films is not straightforward, and particular attention has to be paid to aspects such as surface chemistry, diffusion within pores, dissolution, etc. Another important issue is the integrity of modified mesoporous transition-metal oxides under solvent flux (i.e., function leaching), due to the fact that functions are grafted via coordination or ionic-covalent bonds to the pore wall.

In these studies,^{56–58,396,445} mesoporous films with 2D hexagonal or cubic mesostructures were prepared by EISA,

using a triblock copolymer (Pluronic F127) or Brij-58 [$C_{16}H_{33}(CH_2CH_2O)_{20}OH$] templates. The films were thermally stabilized by several postsynthesis treatments until complete removal of the template. A typical functionalization experiment was performed by dipping a calcined mesoporous film, previously rinsed with ethanol, into a continuously stirring solution of the chosen molecule in THF, acetone, or water.

Kinetics experiments showed that molecule incorporation occurs in two steps and that over 80% of the incorporated functional groups enter the pore system within 5 min. The remaining 20% are gradually incorporated, and saturation is reached between 60 and 120 min. It has been also observed that the function incorporation depended on the mesostructure: cubic 3D mesostructures ($Im3m$) are more accessible than their $p6m$ 2D hexagonal counterparts. This difference is attributed to the presence of pores open to the surface in the cubic phase that were absent in the $p6m$ mesostructure.^{57,58} Moreover, the pores in the cubic phase are interconnected because of the development of large size necks upon thermal treatment and shrinkage of the original mesostructure.¹¹³ Shrinkage of the $p6m$ system results in tubular pores with an elliptic section; however, no new pore interconnections are created, and molecules have to diffuse from pore to pore through defects in the mesostructure (e.g., boundaries between organized domains).

The trends issuing from leaching experiments demonstrate that the anchoring strength follows the complexation strength of the grafting group, that is, $R-O-PO_3^{2-} \sim R-PO_3^{2-} >$ dicarboxylate $>$ carboxylate, for groups with high solubility in the leaching solvent.^{57,58} The transport of the grafting molecule to the inner pores of transition metal oxide POMTFs could follow a sequence of adsorption–desorption–diffusion. Hence, a higher complexation ability of the grafting group should result in slower incorporation of the organic function.⁵⁷ The solvent also plays an important role, particularly favoring the desorption step. For example, the leaching rates of mercaptosuccinic acid are higher at low pH, where the acid is fully protonated, and therefore the carboxylate anchoring groups become more labile.⁵⁸ An interesting characteristic of these hybrid POMTFs is that, contrary to the irreversible grafting observed in mesoporous hybrid silica, anchoring groups with different strengths can be selected to obtain a wide variety of responses, from strongly attached functions to functions that can be liberated by external stimuli (pH). Moreover, transition metal oxide POMTFs could be also processed as multilayer stacks with silica or hybrid silica POMTFs and were selectively functionalized by complexing molecules.^{193,446}

6.2.3.2. Postgrafting on Silica-Based Matrixes. As described previously, the most commonly employed method to functionalize mesostructured silica thin films is the one-pot synthesis. However, some studies employing postfunctionalization have been reported either via vapor phase infiltration^{330,402,413,417–419,421,447} or via immersion in a solution.^{235,405,420,448–451} It is interesting to notice at this stage that the majority of postfunctionalized silica POMTFs are devoted to (ultra) low- k materials, especially those made via vapor phase infiltration.

In the postfunctionalization via immersion procedure, thin films were calcined and stirred in dry toluene, ethanol, or dichloromethane solution containing organotrialkoxysilane or hexadimethylsilazane species under refluxing conditions. The reaction time was varied from 4 to 24 h. Finally, thin films were washed with solvent and dried at low temperature. In the alternative route, that is, vapor infiltration, POMTFs before^{330,402} or after^{402,413,417–419,421,447} the calcination step are exposed to grafting molecule vapor in a closed vessel at moderate temperatures (150–165 °C depending on the grafting molecule).

It was observed that postgrafting in some cases led to materials presenting pore restriction⁴⁴⁸ (bottle ink pores) or to a total blocking of the porosity.⁴⁰⁵ On the contrary the vapor infiltration techniques especially on as-synthesized POMTFs prevent the usual shrinkage of pores due to calcination, allow densification of walls and thus an increase of mechanical and hydrothermal stabilities of POMTFs, and limit the usual reduction of pores due to grafting.^{330,402}

7. Properties of Thin Films and Potential Applications

POMTFs with their unique properties, e.g., versatile framework nature (single or multioxides, crystalline or amorphous structure, hybrid organic–inorganic, etc.), high surface area, modulable pore dimension and shape (cylindrical, spherical, ellipsoidal, etc.), tailored surface (organic or inorganic, inert or active), and high processing and handling abilities have offered to scientists a land of opportunities. For instance, the pore filling of polymers gave birth to new hybrid polymer nanocomposites (class I^{384,385,387–389,452} or class II,^{248,385,390,391,393,452} see section 6) presenting synergistic properties (i.e., increase of hardness,²⁴⁸ environmentally responsive materials,^{390,391} photovoltaic devices by interpenetration of organic and inorganic semiconductor networks^{385,452}). As a result of their perfectly calibrated pore dimensions and shapes, POMTFs have been used as nanoreactors for the growth of nanocrystals/nanoparticles/nanowires and carbon nanotubes.^{381–383} Several strategies have been developed to elaborate these nano-objects: incorporation of precursors during the synthesis^{453,454} of POMTFs (“one-pot” procedure), just after the deposition step³³¹ or after the calcination step by impregnation,^{449,455–460} or electrochemical^{118,382} and pulsed laser deposition¹⁸⁰ techniques. It is interesting to notice that the synthesis of nanocrystals resulting from “one-pot” incorporation involves PEO-containing surfactants which are well-known for their chelating properties of metallic centers.⁴⁶¹ These nano-objects, essentially metal nanoparticles (gold,^{81,84,118,449,462,463} silver,^{180,455,459} and iron³³¹) or semiconductor nanocrystals (CdS,^{454,460} CdSe,⁴⁵⁴ PbS,⁴⁵⁶ Cd_{1–x}Zn_xS,⁴⁵³ and Cd_{1–x}Mn_xS^{457,458}), present very interesting properties useful in the fields of optics^{453,456,460,463} and photocatalysis.⁴⁵⁵ An innovative approach was recently developed by the Brinker group.^{81,84} They reported the synthesis of a new nanocrystal mesophase (face-centered cubic lattice) through self-assembly of gold nanocrystal micelles with silica oligomers. In this case, preformed gold nanocrystals were first functionalized with alkanethiol ligands and next stabilized by CTAB surfactant molecules. Other POMTF-based nanocomposites could also be synthesized by

particles/living cells³⁹⁵ (see section 6) embedding inside the matrixes. These studies involved titania,^{464–467} gold^{48,468,469}/platinum⁴⁷⁰/palladium⁴⁸ particles, and zeolite beta nanocrystals.⁴⁷¹ This particle embedding allowed the formation of new sensors,^{468,469} catalysts,^{48,470} photocatalysts,^{464,466,467,470} and photovoltaic cells.⁴⁶⁵ In this section, we will focus on the more developed applications of POMTFs. Since some applications are intimately linked to the intrinsic properties of the framework nature (low *k* dielectrics with silica and photocatalysis with titania), this section on applications will be divided into two subsections: silica-based POMTFs and metal transition oxide POMTFs.

7.1. Applications and Properties of Silica-Based Thin Films. Most of the studies devoted to the applications of silica-based POMTFs involves hybrid POMTFs (class I or class II, see section 6). Although some studies have dealt with potential applications concerning absorption of polluting species such as organophosphorus compounds,^{415,472} grafting sites (typically –NH₂ or –COOH groups) for binding biomolecules such as enzymes, antibodies, and other proteins^{221,404} or creating synthetic ion channel devices,^{221,404} the majority of research is dedicated to the study of applications in the field of sensors, low *k* dielectrics, photonic devices, environmentally responsive materials, and permselective membranes for gas separation or with switchable permeabilities for polymer ultrafiltration.

7.1.1. Sensing Applications. In the literature three main transduction with POMTF sensors giving birth to (i) electrochemical sensors, (ii) optical sensors, and (iii) quartz crystal microbalance-based sensors. Electrochemical sensors involve usually pure inorganic POMTFs (silica or tin oxide) whereas optical sensors and QCM-based sensors involve hybrid silica-based POMTFs.

7.1.1.1. Electrochemical Sensors. Electrochemical sensors were used to detect simple molecules in gas phase as water,^{450,473–478} alcohol,^{473,479–481} ammonia,⁴⁵⁰ NO,^{482,483} NO₂,^{481,483–485} and H₂,⁴⁸¹ or metal ions (Pb²⁺) in aqueous phase.⁴⁴⁸ The first electrochemical POMTF sensors were reported simultaneously by Innocenzi et al.^{478,479} and Domansky et al.⁴⁵⁰ In the first case, pure silica POMTFs were deposited by dip-coating on substrates with metallic interdigitated electrodes. The working properties of these sensors are based on current variations in the films as a function of the sensing species (here water and alcohols^{473–479}) concentration and mobility. These current intensity variations (more than four magnitude orders) were attributed to a protonic conduction (Grotthus model⁴⁸⁶) due to protonated water ions in an “ice-like” layer configuration formed on the pore surface.^{473–476} This explanation was supported by an optimum calcination temperature around 400 °C which preserves a sufficient amount of surface silanols favoring the adsorption of water molecules. Besides, these sensors present a large sensitivity to alcohols (methanol, ethanol, 2-propanol, butanol-1) at room temperature and the possibility to discriminate between the different alcoholic species.⁴⁷⁹ Interestingly, the authors highlighted the role of porosity since thin films obtained without surfactant showed only a very low current variation to relative humidity.^{476,478} Capacitance-based sensors were also investigated with pure

or hybrid silica-based POMTFs.^{450,482,487} Briefly, POMTFs serve as insulator between a metallic conductor and a semiconductor. Variations of the POMTFs dielectric constant which result from physical and/or chemical adsorption of the target gas inside the pores leads to changes of the capacitance. These capacitance variations are measured by an inductance–capacitance–resistance meter⁴⁵⁰ or by a lock-in amplifier (surface photovoltage technique, SPV).^{482,483} Such devices allowed good detection of water,⁴⁵⁰ ammonia,⁴⁵⁰ NO,^{482,483} and NO₂⁴⁸² gases. The response could be modulated by the functionalization of POMTFs. For example, HDMS-treated POMTFs displayed a better dynamic range of the response toward relative humidity than pure silica POMTFs which are more sensitive to high humidity levels.⁴⁵⁰ Moreover, SPV-type gas sensors exhibited a sensitivity to NO and NO₂ gas at very low concentrations (1 ppm) to very high concentrations (50 and 100 ppm). The authors observed also that the sensing performance depended strongly on the mesostructure of the POMTFs: a cubic structure is more efficient than a 2D-hexagonal one due to its bicontinuous structure.^{482,483} NO₂ gas sensing was further improved by doping silica POMTFs with tin oxide.^{484,485} In fact, tin oxide is a well-known semiconductor material used to detect both reducing and oxidizing gases via SnO₂ conductivity changes.^{488,489} However, in these studies, the effect of SnO₂ is rather a catalytic effect due to its low content in thin films (Sn/Si molar ratios = 0.005–0.03). Pure tin oxide POMTFs were successfully tested as selective gas sensors for ethanol and H₂.^{480,481} Compared with polycrystalline tin oxide sensor, they displayed a better sensitivity toward these last two gases and a better selectivity to other interferential gases (such as methane, butane, CO, and gasoline). These results were explained by the high surface area of tin oxide POMTFs compared with commercial polycrystalline tin oxide materials which provide more surface sites available for oxygen and target gas adsorption. Yantasee et al.⁴⁴⁸ tested the applicability of a thiol-functionalized POMTF as an electrode sensing layer in the aqueous phase. The process of absorptive stripping voltammetry detection of Pb(II) using the thiol-functionalized POMTF electrode involves several steps. The preconcentration step results in an accumulation of Pb(II) ions on the surface of the nanopores by complexation with the thiol groups of the surface. During the detection step accumulated Pb(II) ions desorb from the thiol-functionalized POMTF surface in an acidic medium (e.g., 0.1 M HNO₃) and diffuse to the surface of the gold electrode. The authors demonstrated that functionalized mesoporous thin films with high binding site density, due to high surface area of the mesoporous structure, lead to high sensitivity and large dynamic range for metal ion sensing.

7.1.1.2. Optical Sensors. Historically the first POMTF optical sensors were reported simultaneously in 2000–2001 by two research groups.^{337,338,407} These sensors resulted of the functionalization of silica POMTFs (class II, see section 6) with pH-sensitive dyes (fluorescein derivatives). This functionalization ensures that the dye is covalently anchored onto (or within) the SiO₂ wall during mesostructure synthesis. Wirsberger et al.⁴⁰⁷ synthesized the sensor by reacting

fluorescein isothiocyanate with 3-aminopropyltriethoxysilane and adding it to a F127 block copolymer film preparation. These sensors operated by recording the emission of the anchored fluorescein dye. The thin film sensors acted analogously to the dye in solution, except that the pK_a value was shifted from 6.4 in solution to ~7.3 in the thin films. The response time of the mesoporous hybrid thin films was about 7 s for a 95% change in the emission intensity. This response time is much shorter than the value measured in sol–gel glasses.^{490–492} The fast response time was attributed to the high porosity of the dye-carrying mesoporous thin film, since the open pores enable a fast diffusion of the solution toward the dye molecules. Brinker and co-workers used microfluidic approaches to produce a similar pH sensor.^{337,338} They first patterned amine-modified cubic mesoporous silica using selective dewetting of patterned surfaces made by surface assembled monolayers, SAMs. The sol was prepared by adding aminopropyltrimethoxysilane to a TEOS/Brij-56 sol. Selective dewetting during dip-coating followed by calcination results in a patterned, amine-functionalized, cubic mesoporous film. The moderate calcination allowed the removal of the surfactant while maintaining the amine functionality. The dye conjugation reaction was realized by immersion in a solution of 5,6-FAM SE (5,6-carboxyfluorescein, succinimidyl ester). Finally, solutions of different pH were placed on the pads and transported to the cell by capillary flow. Comparison with solution fluorescence spectra indicated that dye molecules covalently attached to the mesoporous framework retain similar features to those in solution. Later, POMTFs functionalized with triethoxysilyldibenzoylmethane (SDBM) compound exhibiting a high selectivity and sensitivity to metal cation pollutant as uranyl were developed by Nicole et al.⁴⁰⁸ They observed also a short response time of the sensor, around 30 s, and an uranyl detection limit relatively low, 1 ppm, if we consider the simple absorbance variation sensing method used. It is interesting to point out that amorphous sol–gel functionalized thin films synthesized without surfactant did not show efficient detection of any tested metallic cations. Other crucial sensor parameters such as reversibility and reproducibility have been investigated. A simple treatment in solution with acetylacetone permits regeneration of the films with good preservation of their sensing properties, even after several complexation–regeneration cycles. The same SDBM-functionalized POMTFs were successfully used as selective sensor for boron trifluoride, a gas commonly used in semiconductor industries. In this case, SDBM molecules form a fluorescent complex with BF₃ while neither SDBM nor BF₃ are fluorescent.⁴²³ Larger silylated dyes were incorporated in silica POMTFs allowing the detection of oxygen gas⁴⁰⁹ or vapors of explosives as TNT^{410,430} via fluorescence quenching. In the case of TNT detection, the authors observed an important effect of the mesostructure on the sensor response. Here again, a three-dimensional mesophase exhibits the best response compared to a two-dimensional one. Moreover, thin films synthesized without surfactants present a very low quenching efficiency proving then the importance of the mesostructure on the detection ability. Optical sensors based on hybrid POMTFs of >class I were

also reported for the detection of Cu^{2+} in the aqueous phase,^{493,494} the determination of pH,⁴⁹⁵ and the detection of methanol vapor.³⁷² Surprisingly, for these sensors of class I working in aqueous media, the leaching of the dyes was hardly observed. This could be explained by their solubilization in the micelles of surfactant.^{493–495} Although hybrid POMTFs functionalized with dyes are the most common optical sensors reported in the literature, some authors investigated other ways. For example, Goettmann et al.^{468,469} encapsulated phosphine-stabilized gold nanoparticles inside silica POMTFs. They were able to detect thiols and small phosphines via UV–visible absorption technique. These compounds induced variations of the plasmon band position of gold nanoparticles. Pure inorganic POMTFs coupled with optical polarimetric interferometry techniques allowed the detection of simple gases as ammonia or water.^{496–500} Recently, multilayer stacks of TiO_2 and SiO_2 POMTFs functionalized¹⁹³ or not.²⁴⁰ They were investigated for the detection of water, alkanes, and alcohols. Organic functions added to the pore surface allowed the response to change, permitting tailoring of the selectivity toward small-size molecules such as water.¹⁹³

7.1.1.3. (Quartz Crystal Microbalance)-Based Sensors. Examples of QCM-based sensors involving POMTFs are scarce. From a general point of view, quartz crystal microbalance consists of a quartz disk with double sides coated with metal electrodes. Upon modification of the electrodes with sensitive receptor molecules, QCM devices can be used as sensors for chemical and biochemical analysis. The immobilized receptor molecules selectively capture the associated analytes, which lead to the changes of the oscillation frequency and oscillation quality of the QCM. To improve sensitivity of QCM-based sensors toward benzene and ethanol vapor, Palaniappan et al.^{420,501} coated, on the QCM crystals, hybrid silica-based POMTFs functionalized with β -cyclodextrin. The authors observed that the sensing performance of the QCM was enhanced by the introduction of the hybrid POMTFs on the electrodes. On the contrary to the usual flat electrode surface that limits the amount of immobilized receptor molecules per unit area, POMTFs provide higher available receptor sites leading to an increase of sensitivity.

7.1.2. Low- k Dielectric Properties of POMTFs. Dielectric materials with a low dielectric constant k are currently in demand for future integrated circuits. By extension of the pristinely used isolating layers of microelectronics, SiO_2 ($k \sim 3.8$) is one of the materials investigated in this direction. However, as devices are becoming smaller, lower dielectric constants are required ($k \leq 2$). One of the most promising applications of these mesoscopically ordered silica films is their use as insulators in integrated circuit devices due to their low dielectric constant.⁵⁰² Indeed, the strategies to lower the dielectric constant are limited. Usually two issues are targeted: (i) increase the porosity and (ii) decrease the molecular polarizability of the matrix (for a better understanding of low dielectrics see the excellent review in ref 222). However, the effect of the global density (number of molecules per unit of volume, which determines porosity of films and density of the wall) on the dielectric constant film is stronger than the effect of molecular polarizability, since

reducing the density allows the reduction of the dielectric constant to the extreme value close to unity (corresponding to the dielectric constant of the void). It is thus obvious that mesostructured thin films, with their large porosity, are promising candidates as low k materials. Further lowering of the k value can be accomplished by replacing the Si–O bond with a less polarizable bond such as Si–R, thus introducing alkyl or fluoroalkyl groups in the matrix. In addition to that, the introduction of such organic groups in the matrix provides a hydrophobic environment which limits the parasite adsorption of highly polarizable water molecules in pores. Therefore the different approaches involve the modification of either the nature of the walls (i.e., bridged polysilsesquioxanes^{28,64,157} or methyltriethoxysilane^{157,401,416}) or the pore surfaces with one-pot synthesis functionalization of perfluoroalkoxysilanes^{419,431} or trimethylchlorosilane.⁵⁰³ A post-treatment with hexamethyldisilazane^{157,418,447,450,451,503} / 1,3,5,7-tetramethylcyclotetrasiloxane⁴¹⁹ or trimethylethoxysilane³³⁰/trimethylchlorosilane⁵⁰⁴ could improve the hydrophobicity of thin films by reacting with silanols. However, despite numerous claims, low- k property alone is useless since low- k application is always a compromise between porous volume, mechanical stability, hydrophobicity, system processibility, and dielectric constant.⁴¹⁶ For example, the presence of organic groups inside POMTFs leads to a decrease of the thermal stability of the POMTFs which could have a dramatic effect for their integration into the copper interconnect process. In fact, organic groups can be decomposed during various high-temperature integrated circuit processes (Cu metallization), thus leading to devastating damage to the interconnect structure. Chen et al.⁴¹⁷ studied the thermal stability of POMTFs postfunctionalized with HDMS into a Cu/nitrided Ta/POMTFs/Si wafer device (from the top to the bottom). They observed that the decomposition of trimethylsilyl groups in the hybrid POMTFs became obvious around 450 °C. However, decomposition-induced chemical degradation seemed not to cause any film crack and interfacial failure in the Cu-metallized POMTFs, even for the sample annealed at 600 °C. They also noticed that Cu diffusion into the POMTFs could be completely retarded in the Cu/[Ta(N)]-metallized POMTFs annealed at 400 °C. The diffusion of species inside the porosity of POMTFs could also be seriously limited by the coating, via plasma treatment, of a hydrogenated amorphous silicon carbide layer⁵⁰⁵ or the deposition of a very thin layer (5 nm) of nonporous silica⁵⁰⁶ at the surface of POMTFs.

7.1.3. Photonic Applications of POMTFs. Here again, most of the studies reported concern hybrid POMTFs. It was underlined in section 6 that the hydrophobic regions provided by the core of micelles were compatible environments for organic dopants such as dyes, enhancing their overall solubilities and preventing their aggregation. In addition, the rigid inorganic framework protects and stabilizes the embedded species. The intrinsic optical and mechanical properties of such materials coupled with their unique architecture, that is, organic/inorganic phase separation organized on the nanometer scale, allowed scientists to investigate several promising application fields. For example, researchers took advantage of the high loading ability of dyes with reduced

aggregation or dimerization inside mesostructured thin films for elaborating materials exhibiting amplified spontaneous emission.^{335,398,507–510} In addition, the versatility of the thin film processing allowed the deposition of these films on various substrates such as PDMS elastomeric molds on silicon wafer for waveguides,^{335,508} glass microscope slides,^{398,509,510} and optical fibers.⁵⁰⁷ By using different inorganic matrixes (silica or titania) and depending on the substrate used (glass slides or silicon wafers), the refractive index of doped thin films was tuned to synthesize efficient waveguides.³³⁵ Finally, this approach led to a dye-doped mesostructured silica distributed feedback laser.^{398,511} Generally, the doping of mesostructured thin films could be done with various dyes during the synthesis leading to materials exhibiting various properties. For example, it was observed that mesostructured thin films were excellent hosts for silylated dyes,⁴⁰⁶ fullerene derivatives,⁴²⁸ photochromic dyes,^{379,512} photosynthetic pigments,^{513,514} or photoconductive polyphenylvinylene polymers.^{424,426,515} They could also serve as optical data storage.⁵¹⁶ Furthermore, they presented an anti-Stokes luminescence property when doped with rhodamine 101.⁵¹⁷ The particular nano-organization of organic and inorganic domains inside POMTFs allowed energy transfer to occur between two organic dyes. This energy transfer could happen when the two dyes were both located in the micelles of surfactant³⁷¹ but also when the dyes are located into two different spatially separated regions: the first one incorporated in the micelles and the second one located in the framework.³⁷³ It is interesting to point out that dye fluorescence in POMTFs is usually greater than the one observed in amorphous film due to the high solubilization ability of micelles and less interactions with inorganic framework.³⁷³ Recently, hybrid POMTFs functionalized with quinizarine derivatives were used to investigate an intrinsic optical bistability phenomenon (two stable responses exhibited by a system under the same optical excitation).⁴²⁹ Also, incorporation of semiconductor particles as PbS into POMTFs led to POMTFs presenting high optical nonlinearity properties.⁴⁵⁶

7.1.4. Environmentally Responsive POMTFs. To expand the range of accessible properties, various organic functional groups have been covalently incorporated onto the pore surfaces of mesoporous materials. However, these modifications have provided mainly “passive” functionality, such as controlled wetting properties, reduced dielectric constants, or enhanced adsorption of metal ions. By comparison, materials with “active” functionality would enable properties to be dynamically controlled by external stimuli, such as pH,³⁹⁰ temperature,^{236,390,411} or light.^{236,411} The Brinker group^{236,411} reported the synthesis of nanocomposite POMTFs functionalized with photoresponsive azobenzene-containing organosilanes. Azobenzene derivatives were selected because their *trans* ↔ *cis* isomerization is UV sensitive. UV irradiation of the *trans* isomer causes transformation to the *cis* isomer. Removal of the UV radiation, heating, or irradiation with a longer wavelength switches the system back to the *trans* form. This isomerization changes the molecular dimension of the organic molecule (molecular length of the *cis* isomer is shorter than that of the *trans* isomer, Figure 22).

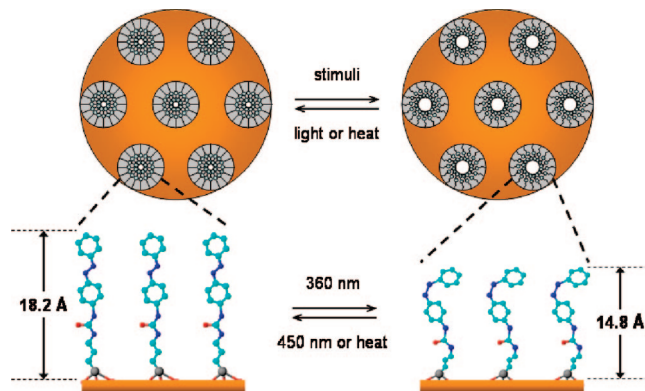


Figure 22. Photoresponsive nanocomposites prepared by EISA. Atom labels: C, cyan; O, red; N, blue; Si, grey; H atoms are omitted. Adapted with permission from refs 236 and 411. Copyright 2004 American Chemical Society and 2003 Wiley–VCH Verlag GmbH & Co. KGaA.

To demonstrate optical control of mass transport, chronoamperometry experiments were performed using an electrochemical cell working electrode modified with an azobenzene-functionalized nanocomposite membrane (Figure 23a).²³⁶ The chronoamperometry experiment used ferrocene dimethanol (FDM) and ferrocene dimethanol diethylene glycol (FDMDG) as electrochemical probes and provided measurement of mass transport properties through the nanocomposite hybrid membrane (Figure 23c). During electrolysis at constant potential, the effective pore size limits the diffusion rate of probing molecules to the electrode surface. Under dark conditions, the azobenzene moieties are predominantly in their extended *trans* form. Upon UV irradiation ($\lambda = 360$ nm), azobenzene moieties isomerize to the more compact *cis* form which increases the diffusion rate and, correspondingly, the oxidative current (Figure 23b). Likewise, exposure to visible light ($\lambda = 435$ nm) triggers the reverse *cis*–*trans* isomerization of the azobenzene moieties, which decreases the current to the pre-UV exposure level. Moreover, it was observed that increasing the volume of the diffusing analyte decreased the overall mass transport, leading to some selectivity for this nanocomposite.

Another example of environmentally responsive mesostructured hybrid films is that of polymer/silica nanocomposite³⁹⁰ with lamellar mesophases, which swell/deswell upon change of pH or temperature due to the presence of anchored polymers into the interlamellar space. Polymers such as poly(methacrylates) and poly(*N*-isopropylacrylamide) (PNIPAM) show a pronounced response toward changes in pH and temperature, respectively. To study the thermoresponsive behavior, the hybrid POMTFs were immersed in water at temperatures around the PNIPAM phase transition temperature. Temperature change induced a significant shift of the lamellar *d* spacing due to the phase transition of the confined NIPAM/DM copolymers around 30 °C. This lamellar *d* spacing shift can be explained by the swelling/deswelling property of the organic part but does not imply any variation of the silica layer thickness. The magnitude of the swelling/deswelling response could be increased by heating and cooling over a larger temperature range (between 10 and 50 °C instead of 30–40 °C). The swelling/deswelling process is reversible and takes approximately 5 h, which is comparable to that of bulk systems. The pH sensitive nanocom-

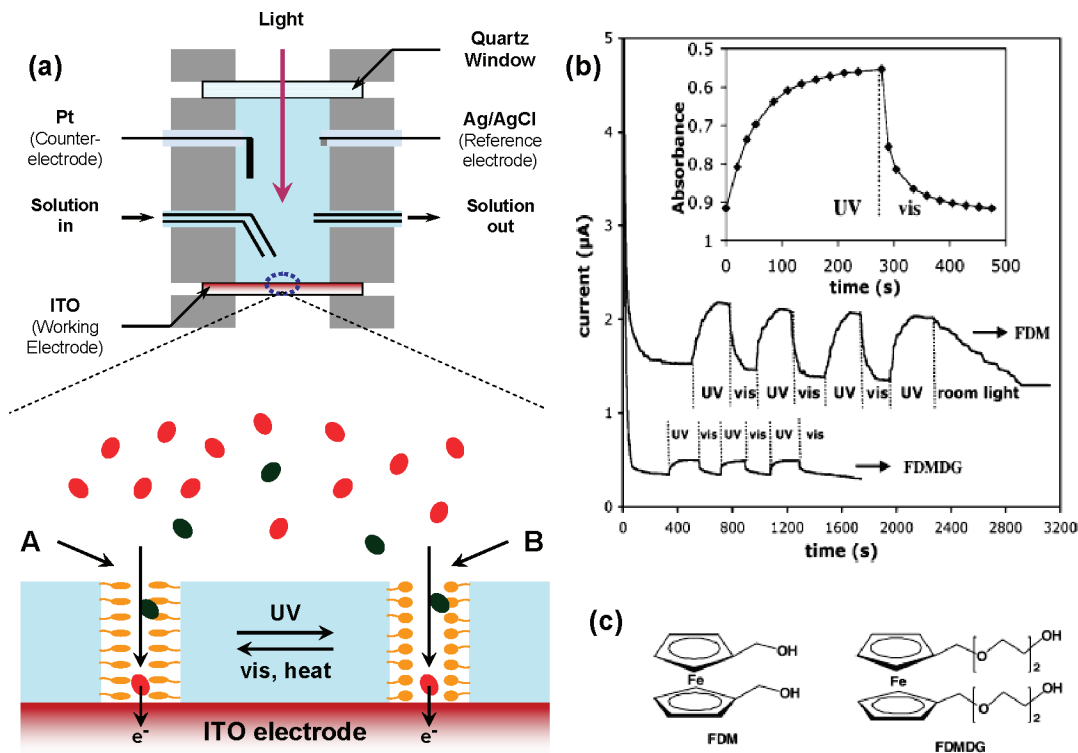


Figure 23. (a) Schematic drawing of the electrochemical cell (top) and mass transport of probing molecules through the photoresponsive nanocomposite membrane integrated on an ITO electrode (bottom). (A) Diffusion through smaller pores with azobenzene ligands in their *trans* configuration; (B) diffusion through larger pores with azobenzene ligands in their *cis* configuration. Legend: red ovals (FDM or FDMDG, see part c), green ovals (FDM⁺ or FDMDG⁺), orange ovals (azobenzene in *cis* form), orange elongated oval (azobenzene in *trans* form). (b) Current–time, *I-t*, behavior of a photoresponsive nanocomposite film under alternate exposure to UV (360 nm) and visible light (435 nm). (Last cycle uses room light, 400–700 nm.) Inset is the absorbance at 356 nm ($\pi-\pi^*$ transition of the *trans* isomer) of the same film immersed in the buffer solution containing 1 mM FDM. (c) Electrochemical probes: ferrocene dimethanol (FDM) and ferrocene dimethanol diethylene glycol (FDMDG). Adapted with permission from refs 236 and 411. Copyright 2004 American Chemical Society and 2003 Wiley–VCH Verlag GmbH & Co. KGaA.

posite films containing poly(dodecyl methacrylate) (PDM) were also studied in water. Poly(methacrylates) are hydrogels showing pronounced changes in chain conformation upon (de)protonation of the carboxyl groups. The authors observed an appreciable decrease of the lamellar *d* spacing with the decrease of the pH (from pH = 9 to pH = 4) probably due to partial hydrolysis of the ester functions of the polymer. In this case too, the swelling/deswelling process was reversible over several cycles.

7.1.5. POMTFs as Permselective Membranes. Inorganic membranes are semipermeable barriers that prevent two phases from getting into contact. They must be permselective to allow only some components of one phase to diffuse into the other, which explains why their transport properties depend on their microstructure, especially their pore size distribution and their connectivity.⁵¹⁸ An additional requirement lies in the effective separation layer thickness, which must be as thin as possible to allow a proper separation without decreasing the diffusion flow below unacceptable values. To overcome the mechanical strength requirement for easy handling, the actual separation layer is always deposited onto one or several stacked macro- to mesoporous layers, and the successful synthesis of an inorganic membrane requires the ability to build thin, continuous, homogeneous, and defect-free layers onto porous rough supports.

Gas Permeation Application. In the first work, Nishiyama et al. reported the preparation of a membrane made of MCM-48 mesoporous material with a three-dimensional pore

structure impregnated within a stainless steel or a porous alumina support under hydrothermal conditions.^{519,520} Very thick films were formed (50 μm), and no gas separation property was proven.

In a different approach, silica POMTFs made by EISA were deposited by Tsai and co-workers at the surface of a commercial 5 nm porous γ -alumina membrane as an underlying layer of high porous volume and low pore tortuosity.⁵²¹ Both these properties and the almost perfect surface quality of the POMTFs allowed the subsequent deposition of a 30 nm thick defect free perm-selective microporous silica layer (pore size between 0.3 and 0.4 nm). The resulting top dual layer ameliorated significantly the membrane quality (no pinhole defects resulting in higher selectivity between CH₄, H₂, He, and CO₂ gases) and attained higher gas permeation fluxes (thinner filtration layer allowed) if compared to the simple top layer. A typical multilayer membrane top coated with POMTFs is shown in Figure 24.

The same approach was reported for preparation of a mesoporous sublayer onto an anodized alumina support.⁵²³ Here again, the periodically ordered layer failed in exhibiting separation properties. Nevertheless, several groups attempted to prepare POMTFs with permselective properties (which implies crack free films with a porous network open from one to the other side of the POMTF). The same EISA strategy was used for deposition of a 2D-hexagonal silica POMTF where preferential pore alignment (parallel with the porous substrate) was disturbed by seeding the deposited

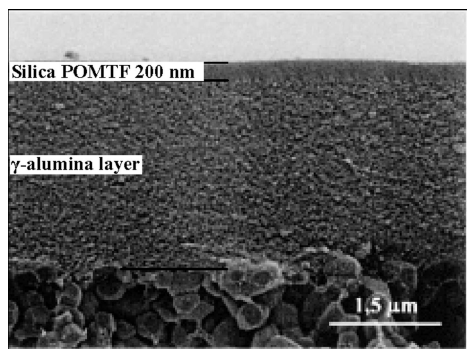


Figure 24. SEM picture of a silica POMTF deposited at the top of two asymmetric layers of γ -alumina membrane. Reprinted with permission from ref 522. Copyright 2001 Elsevier.

solution with silica colloids. N_2 permeation measurements proved the beneficial effect of the seeding over the permeation flux, but no separation property was shown.⁵²² More recently, a multistep aerosol deposition procedure was reported for the preparation of 1 μm thick silica POMTFs with disordered cubic structure. N_2 , He, and CH_4 permeation measurements proved that, after four depositions, the membrane exhibits very few defects.⁵²⁴ No separation property was presented.

Ultrafiltration (UF) of Polymer Solutions. The first application of POMTFs as pH responsive UF membrane was reported by Boissière and co-workers.^{349,350} They reported a 250–500 nm thick MSU membrane was grown at the top layer of a γ -alumina 0.2 μm porous tubular support via through an interfacial reaction between a silica condensation catalyst (NaF) and hybrid micellar building units made of silica precursors and nonionic surfactants.³⁵¹ Unlike other periodically organized membranes, this layer exhibited cylindrical pores aligned mostly normal to the support. Upon filtration property investigations, it appears that the combined effect of the silica nature of the membrane, whose surface charge can be easily adjusted by changing the pH, and the nonconnected cylindrical shape of the pores provided a new pH-responsive retention property, as proved by the filtration of polyoxyethylene polymers (PEO) with different molecular weights. Depending on the filtration conditions, a rejection rate of 80% and a steep cutoff at 2000 Da can be obtained or, on the reverse, polymers three times bigger than the pore diameter can diffuse through the membrane. This unknown filtration mechanism was explained in light of both topology of the porous network and pH-dependent interactions between PEO polymers and silica porous media.⁵²⁵

More recently, the direct coupling of separation and photo-oxidation was performed by depositing a TiO_2 POMTF from a solution containing block copolymers, already made anatase colloids, and molecular precursors.^{526,527} After thermal treatment, the semicrystalline membrane exhibited photo-oxidative properties versus methylene blue and a cutoff surprisingly low in the micropore range (1.6 nm). This work is one of the very rare examples of the preparation of periodical mesoporous transition metal oxide films using some nanobuilding blocks (route B1 in Figure 1).

7.2. Applications and Properties of Nonsilicate POMTFs. This part concerns the properties of nonsilicate periodically organized mesoporous thin films. Although

relatively few inorganic mesoporous thin films have been investigated, these materials have, nonetheless, already demonstrated unexpected electrochemical, catalysis, and photocatalysis properties. The flexibility and low cost of the processes involved to synthesize them, sol-gel chemistry and processing, allow specific compositions to be developed with highly organized mesopores, so that the solid network can be tailored to the specific properties while the mesoporous network serves as an efficient pathway for molecular transport and/or as “host material” for “guest material” with controlled properties. In this part, we will describe the recent research on inorganic mesoporous thin films as new materials in photocatalysis, photovoltaic, batteries, and electrocatalysis. We also wish to emphasize in our discussion that inorganic mesoporous thin films offer another contribution to electrochemical and catalysis science and technology—one beyond that of providing new materials or architectures. Because mesoporous thin films innately magnify the surface-to-volume fraction of a material, they are also tools that can amplify the critical phase of any electrochemical system: the interface.

7.2.1. Photocatalyst. Mesoporous thin films have been investigated as photocatalysts since their conception in 1998. They offer more active sites per gram for gas/solid interactions than dense materials can. The continuous organized mesoporous network on TiO_2 mesoporous thin films facilitates the flux of reactant molecules that access the catalytically active “internal surface” area. The rates of catalytic reactions that are transport-limited rather than kinetically limited would be improved by what a mesoporous thin film innately provides: ready mass transport of reactants to an increased area of catalytic surface.

The efficiency of photon-energy conversion in these systems readily depends on the crystallinity and the structure of the inorganic network forming the pore wall.^{528,529} Tang et al.⁵²⁹ have shown that highly crystalline and ordered mesoporous TiO_2 thin films exhibit a 2.5% photoconversion efficiency for the water photolysis at zero-bias and under Xe lamp illumination of 40 $\text{mW}\cdot\text{cm}^{-2}$.

Another important consideration for photocatalytic properties is the pore size and its distribution. For example, a cubic mesoporous film would offer higher photocatalytic efficiency than a hexagonal one since the mesopore channels of cubic mesostructures are open on the surface of the films regardless of the mesophase orientation, whereas those of the 2D hexagonal mesophases are parallel to the substrate and are not widely open on the films' surface. However, the surface is partially accessible through mesodomain edges, defects, and microporosity within the inorganic wall in these mesophases. Moreover, recent works¹⁵⁰ have shown that the photocatalytic properties in these mesoporous films are more efficient when the porosity is high and completely accessible to water, oxygen, and adsorbed species and when nanoparticles and pores have dimensions of 7.5 and 5.5 nm, respectively (Figure 25). Such fully open and optimized geometry, addressed as grid-like, is obtained upon crystallization of highly ordered mesoporous films having $Im3m$ initial structure with [110] preferential orientation of the domains. The porosity evolution, associated to such a grid-

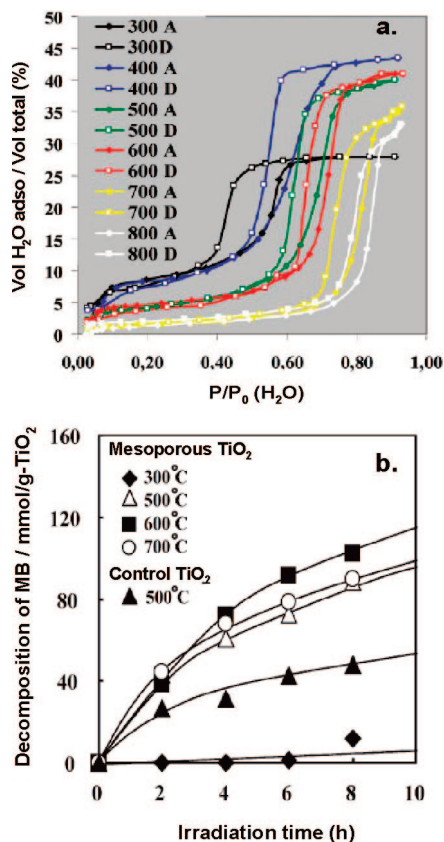


Figure 25. a. Adsorption–desorption isotherms plotted for TiO₂ mesoporous thin films calcined at various temperatures (curves A and D represent adsorption and desorption curves, respectively, preceded by the temperature of treatment). b. Photodegradation of methylene blue over TiO₂ films calcined at various temperatures and under UV light irradiation. Adapted with permission from ref 150. Copyright 2006 The Royal Society of Chemistry.

like transformation, was followed by ellipsometry porosimetry at different temperatures of calcination. The corresponding isotherms, given in Figure 25, show the opening of the structure and the stabilization of the porous network between 500 and 600 °C. The highest decomposition of methylene blue (MB) and lauric acid are obtained after this stabilization, when mesoporous TiO₂ films were heat-treated at 600 °C. These conditions correspond to the best compromise found to obtain high crystallinity together with the optimal open grid-like structure.

However, the literature covering the influence of the film porosity on the photoactivity is very poor because it is difficult to change for example the porosity of the films without altering the crystallinity or the grain size of the TiO₂ crystallites that are also known to have a drastic impact on the film properties. Furthermore, a comparison of the numerous results reported by many different authors is almost impossible. This is due to the absence of a careful characterization of the film porosities and the different conditions and methods reported for the measurement of the photocatalytic efficiencies.^{275,530–533} However, this question still remains an important issue since it should allow the optimization of the films mesostructure toward their applications, keeping in mind the limitation arising from the film mechanical properties. Recently, Allain et al.⁴⁶⁶ developed a versatile approach for the elaboration of TiO₂ based

photocatalytic coatings, allowing a separate control of the film porosity and the TiO₂ microstructure. This synthesis involved TiO₂ colloidal particles and silica mesoporous structure. The resulting materials consisted of ~50 nm aggregates of anatase TiO₂ primary particles (7 nm) embedded in a mesoporous silica network. The efficiency of the photocatalytic reactions was measured by a quantum-yield efficiency of 1.1%. The high photoactivity was attributed to a close proximity between the organic molecules and the surface of the TiO₂ crystallites as well as high water and oxygen diffusion rates through the ordered, interconnected porous network. Wark et al.⁵³⁴ have also demonstrated the benefit of organized mesoporous thin films of titanium dioxide for the degradation of methylene blue. They exhibit higher photocatalytic efficiency than the classic TiO₂ films synthesized from colloidal solutions. The photocatalytic efficiency does also depend on the films thickness; thicker films are substantially more active. Finally, they pointed out that a hydrophobization of the films surface is highly beneficial, in particular with reagents more hydrophobic than methylene blue. Yu et al.⁵³⁵ correlated their high photocatalytic activity for mesoporous TiO₂ thin films to the controlled size of TiO₂ particles of ~15 nm, the high surface area, and the surface roughness of these films.

To create more active and durable photoelectrodes or photocatalysts, the TiO₂ mesoporous network has been explored as “host” for metals.^{470,536} Indeed, the incorporation of metallic nanoparticles into a semiconductor mesoporous framework allows the electron migration from the semiconductor surface to the metal to be improved, suppressing electron–hole recombination. Anderson et al. have reported that the incorporation of silver nanoparticles into the TiO₂ mesoporous network increases the photocatalytic activity for oxidation of stearic acid.⁵³⁶ Furthermore, the metal clusters are encapsulated and stabilized in the robust pore channels of the mesoporous TiO₂ films. Such metal–TiO₂ composite mesoporous thin films have been reported to be efficient in the catalytic oxidation of CO to CO₂. No deactivation, during either heating or the prolonged operation period, was observed. The metal particles are embedded in the mesonet-work and interact with the anatase–TiO₂ network of nanocrystals, forming numerous semiconductor-metal nanoheterojunctions. Using this concept, Wang et al.⁴⁷⁰ have prepared metal–semiconductor nanocomposites with good catalytic and photocatalytic activities. In these mesoporous composite thin films, the Pt–TiO₂ nanoheterojunctions promote the separation of charge carriers on UV-excited TiO₂, thus significantly improving the photocatalytic activity of porous Pt/TiO₂ composites toward killing bacteria cells of *M. Lylae*.

Mixed oxide composite materials have also been reported to be more efficient photocatalysts than pure substances, because some new active sites are generated. This is mostly due to the interactions between TiO₂ and the dopant oxides (WO₃, ZrO₂). They also exhibit improved mechanical strength, thermal stability, and higher surface area. The preparation of TiO₂-based composite mesoporous materials has been extensively studied.^{104,105,371,398,537–539} Pan and Lee¹²⁰ have reported that the incorporation of WO₃ into TiO₂ helps to improve the ordering of the mesopore structure,

because WO_3 retards the crystallization of TiO_2 to the anatase phase. The photocatalytic activity of composite mesoporous films for 2-propanol was higher than that of mesoporous and nonporous TiO_2 films derived from a typical sol–gel method. This enhancement can mostly be attributed to the increase in surface acidity ($\text{PZC TiO}_2 = 6$; $\text{PZC WO}_3 = 2$), induced by the presence of WO_3 oxide on the surface of the pores. The benefit of WO_3 nanoparticles inserted in TiO_2 rutile mesoporous thin films has been also demonstrated for the degradation of toluene by UV or visible light.⁵³⁹ The high quality of the WO_3/TiO_2 interfaces reached in these nanoarchitectures allows a fast charge transfer between the two semiconductors and an efficient charge separation and recombination hindering, implying a high photocatalytic efficiency.

Recent works underscore the opportunity to fabricate nanocrystalline mesoporous N-doped titania films.²⁸⁶ Doping TiO_x with nitrogen is a very interesting approach for increasing photocatalytic activities of titania-based mesoporous thin films since the band gap of anatase is decreased. The decomposition of lauric acid coated on mesoporous N-doped titania films has been studied under visible light irradiation to evaluate their photocatalytic activity. Moreover, this decomposition was measured by the evolution of the water contact angle on the surface of the N-doped titania, since these oxides, highly hydrophobic, exhibit photoinduced hydrophilic features as well as photodecomposition of lauric acid under irradiation in the visible light. These studies pointed out that the films nitrided at 500 °C exhibit the highest photocatalytic activity. These films contain an optimal surface concentration of nitrogen since the oxygen vacancies are still not important enough to promote the recombination of the photogenerated electrons and holes. These N-doped TiO_2 POMTFs are really efficient photocatalysts working in both the UV and the visible ranges.²⁸⁶

7.2.2. Photovoltaic. Some mesoporous materials and architectures have been proven to present interesting behavior for photovoltaic cells; however, these trends may not be representative of real cell as they have been shown in ex situ measurement, and confirmation in an actual photovoltaic cell is thus necessary.

The dye-sensitized solar cells (DSSC) with nanocrystalline TiO_2 layers have been studied by several groups.^{215,378,385,452,470,540–546} It is now well established that TiO_2 nanocrystalline layers exhibit improved light-to-electricity conversion efficiency compared to TiO_2 microcrystalline layers. The solar conversion efficiency of nanocrystalline mesopores is even higher than for nanocrystalline thin films, as detailed below. Electrochemists and materials scientists now have an opportunity to study how surface to volume ratios and the morphology of solid and pore on the nanoscale influence photovoltaic behavior. The efficiency of these systems depends, in particular, on the nature of the electrolyte. Literature data show that the solar cells with corrosive liquid electrolyte exhibit cell efficiency around 8–10% while the ones with “solid” electrolyte (which includes ionically conductive gels, inorganic p-type conductors, and molecular and macromolecular organic hole-conductive polymers) have an efficiency of 1–4%. Although

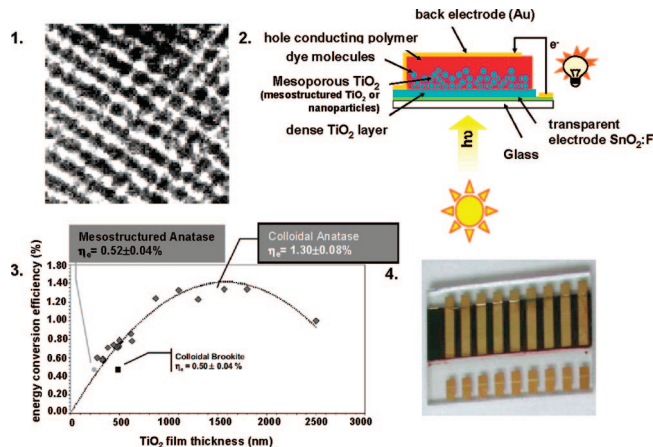


Figure 26. 1. Transmission Electron micrograph of a mesostructures anatase film's surface. 2. A schematic of the experimental setup used for testing mesostructured films (from ref 540). 3. Power energy conversion efficiency for different types of TiO_2 : colloidal anatase-based (\diamond), colloidal brookite-based (\blacksquare), and mesostructured anatase-based TiO_2 film (\bullet) as a function of porous TiO_2 layer thickness (reprinted with permission from ref 540; Copyright 2006 Wiley–VCH Verlag GmbH & Co. KGaA). 4. Prototype cells.⁵⁴⁰

a photovoltaic cell based on organic hole transporting materials exhibits very low efficiency ($<1\%$), these systems are very attractive because all the technological issues (sealing, packaging, and maintenance) induced by the use of corrosive electrolytes are limited. However, the major problem associated with all solid-state dye sensitized hybrid solar cells is the filling of the porous TiO_2 film by the hole-transporting organic material.⁵⁴⁷

The literature covering the photovoltaic properties of mesoporous TiO_2 thin films is not extensive but appears to be consistent. Several experiments indicate that the solid–pore architecture of the mesoporous films contributes to the facile electron transfer to the collector electrode, to increase the electron–hole pair density generated at the hybrid interface and to promote hole-transporting organic material impregnation. The mesoporous films thus represent a “host material” for polymer that differs from nanocrystalline films with the same nominal compositions and structure. The first evidence of this behavior was obtained from current–voltage characteristic measurements of hybrid solid-state solar cells (liquid electrolyte) using either TiO_2 mesoporous layer or colloidal anatase TiO_2 films as the n-type electrode. These experiments showed that mesoporous anatase TiO_2 thin films exhibit a light-to-electricity conversion (up to 5.31%) comparable to that of nanocrystalline colloidal anatase TiO_2 films with the same thickness.^{215,540,543} Several authors have also reported the importance of the crystallinity of TiO_2 nanoparticles as well as their interconnection in the inorganic network.^{543,545} Lancelle-Beltran et al.²¹⁵ investigated the photovoltaic performance as a function of the mesostructure and crystallinity of the porous TiO_2 film in all solid state photovoltaic cells. They reported that the best photovoltaic properties are obtained for fully nanocrystalline TiO_2 films with the highest specific surface area, corresponding to the largest polymer– TiO_2 interface (Figure 26). In these studies, an optimum is obtained for films thickness of 1.5 μm .

However, the performance seems to be limited by the thickness of the TiO_2 mesoporous films and by the quality of

the hybrid interpenetrating semiconductor nanostructure.³⁸⁵ Recent experiments indicate that further improvement in solar conversion efficiency is possible. An increase of solar conversion efficiency by 50% is obtained for cells containing TiO₂ mesoporous films with a thickness $\geq 1 \mu\text{m}$.⁵⁴¹ Current–voltage studies demonstrate a high solar conversion efficiency of thick mesoporous TiO₂ films and highlighted the promises raised by mesoporous TiO₂ films for dye sensitized cells.

7.2.3. Electrochemical/Electrochromic. Mesoporous nanocrystalline thin films offer attributes for electrochemical applications: a network of nanoscopic oxides, which serves as an uninterrupted three-dimensional (3-D) pathway for ion and electron conduction, and an interpenetrated through-connected mesoporous network. In addition, this mesoporous network does also serve as “host material” for electroactive species. In this way, fast ionic or electronic carrier transport in the internal surface area of the mesoporous network may occur. Because mesoporous thin films exhibit a very high internal surface area, they can produce efficient electrochemical reactions at the interfaces, which often represents the critical phase of any electrochemical system.

Sallard et al.^{112,548} explored the effect of mesoporous WO₃ thin films in their various crystallinity forms on electrochemical lithiation (capacity and rate). The Li capacity trend for these materials obtained by rapid voltammetric cycling ($5 \text{ mV} \cdot \text{s}^{-1}$) was amorphous mesoporous thin films \sim noncrystalline thin films prepared by other techniques $>$ crystalline mesoporous films \gg polycrystalline dense films. This study shows that the high rate Li capacity for crystalline mesoporous films is higher than for the corresponding polycrystalline materials. This confirms the accessibility of molecular reactants to the nanoscale domains through the organized continuous volume of mesopores. Similarly, Frindell et al.⁵³⁷ have shown that mesoporous Ce–TiO₂ thin films exhibit a different electrochemical behavior compared to sol–gel derived ceria–titania films. It turns out to be correlated to the larger number of interfacial surface states in the mesoscopically ordered thin films. Deepa et al.²⁷⁹ have studied the effect of cycling on the electrochemical activity of these periodically organized mesoporous thin films and have shown superior electrochemical activity. However, the mechanism by which lithium is inserted in these mesoporous thin films is still not reported by the authors.

Reiman et al.⁵⁴⁹ have studied the capacity of mesoporous TiO₂ thin films to store charges for supercapacitor application. They showed that periodically organized mesoporous TiO₂ thin films are reduced under cathodic polarization, due to the facile insertion of lithium in the porous nanostructure, and that the self-discharge is slow. Doping mesoporous TiO₂ thin films with cerium does also imply a modification in their electrochemical behavior.

WO₃ POMTFs present also good electrochromic properties, due to the high crystallinity of the pore wall, the facile accessibility of the pore, and the high specific surface area which increases the number of electrolyte–WO₃ interfaces. Films with small thickness have been tested and exhibited high coloration efficiency compared to typical films. In addition, these mesoporous thin films have a fast electrochromic response time (30 s, for coloration and bleaching).

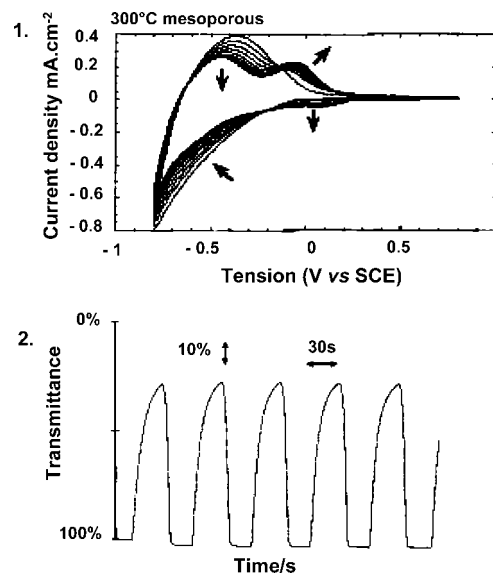


Figure 27. 1. Evolution of the cyclic voltammogram during cycling for a 300 °C mesoporous tungsten oxide thin film calcined at 300 °C. The arrows show the evolution in the position and intensity of the peaks with cycling. 2. Variation in the transmittance at 650 nm as a function of time for the mesoporous tungsten oxide films heated at 300 °C and a voltage step between -0.8 V and $+0.8 \text{ V}$ vs SCE. The voltage changes the polarity each 30 s. Panels 1 and 2 adapted with permission from ref 550. Copyright 2001 The Royal Society of Chemistry.

In addition, this network does also prevent nanoparticles from either coalescence or agglomeration. Finally, cycling studies between different states (between the transparent and the blue colored states) have no effect on the film electrochromic performance. Recently, some studies⁵⁴⁸ have shown that the mesoporous highly crystalline WO₃ films display long-term cycling stability under various conditions including several hundreds of cycles and various temperatures ranging from 20 to 70 °C. These results point out that the 3-D mesoporosity must be combined with a fully crystalline inorganic matrix to achieve the best performance. In this context, highly crystalline WO₃ mesoporous films are very promising for electrochromism applications. However, unchanged electrochemical/electrochromic characteristics over a million cycles need to be demonstrated to confirm, for example, their potential as a cathode in electrochromic windows. In related experiments, cyclic voltammetry has been used to provide some insight on the nature of the site(s) of proton association in electrically conductive WO₃ mesoporous thin films (Figure 27).⁵⁵⁰

The results suggest that the surface chemistry may influence the behavior of proton insertion. WO₃ mesoporous thin films exhibit three potential sites for proton insertion, the corresponding reversible active site, shallow trap site (reversible), and deep trap site (irreversible). The existence of these different sites is mainly correlated to the surface chemistry of these mesoporous films.

With a more original approach, Jheong et al.⁴⁴⁵ have studied the electrochromic property of the viologen-anchored mesoporous TiO₂ films and showed that the electrochromic devices fabricated from the meso-TiO₂ had high coloration efficiency and fast switching response, compared to nanocrystalline films having comparable particle size. They attributed this good performance to the well-organized meso-

pore structures and the high surface area, which offers an efficient electrolyte transport through the porous network and a fast electron transfer.

The unique electrical and electrochemical properties of POMTFs have been showed on the Sn doped In_2O_3 system.¹²⁵ The self-assembly strategy combined with a controlled crystallization step of the inorganic network involves acetylacetonate as precursors and block copolymer as the directing agent. These POMTFs exhibit a well-defined 3D network of mesopores, with ellipsoidal pores of $16 \text{ nm} \times 8 \text{ nm}$ and a specific surface of $45 \text{ cm}^2 \cdot \text{cm}^{-2}$. The most significant feature of the Sn doped In_2O_3 mesoporous thin films is its temperature-resistivity dependence. The non-calcined and amorphous mesoporous films exhibit no measurable electrical conductivity while the crystallized films have a resistance of $3 \times 10^5 \Omega$. Further improvement has been achieved by treating the mesoporous films in reduced atmospheres, nitrogen or hydrogen. This treatment increases the concentration of free charge carriers by creating oxygen vacancies. Despite their high porosity, these mesoporous films exhibit high conductivity with only value of 1–2 orders of magnitude lower than dense films.¹²⁵

An enhancement of proton conduction has also been observed in mesoporous zirconium phosphate films.¹²² These films exhibit higher proton conductivity than the ones with disordered porosity. In these mesostructures, this excellent proton conductivity is correlated to the high concentration of $-\text{OH}$ entities grafted on the pores' inner surface. As the pores are well-connected to each other, efficient proton diffusion pathways are thus created. However, one may consider that in these mesostructured films, the proton conductivity might be anisotropic and readily depends on the orientation of pore channels. Accordingly, the synthesis of orientated films might be a useful tool to design effective proton conductive architectures.

Another feature of periodically organized mesoporous thin films is their capacity to incorporate and anchor optoelectroactive species because of their well-defined, accessible 3D mesoporosity and their high specific surface area.^{125,286,551,552} The architectures of these mesoporous thin films have, thus, been used for the development of organic-inorganic hybrid thin films. The results reported by Fattakhova-Rohlfing et al. provide important insight about the ability of transparent ITO conducting films with 3D mesoporous architecture to serve as "host materials" for active centers.¹²⁵ For example, anion-substituted dye molecules were ionically grafted onto the surface of ITO films modified with alkylammonium cations. The amount of dye incorporated into the mesoporous ITO films significantly exceeded that of dense ITO films used as reference. Fattakhova-Rohlfing et al.¹²⁵ addressed also the ability of the mesoporous Sn-doped In_2O_3 films to act as a support for electrochemically active ferrocene moieties. The ferrocene entities were covalently grafted to the large accessible inner surface of the mesoporous films. The cyclic voltammograms present two symmetrical peaks, indicative of fast electron transport in the 3D mesoporous network. This concept has been developed in dye-sensitized solar cells.

Making the conductive layer porous with a very thin dye-sensitized semiconductor film on the pore wall would overcome

problems with electron collection, which in general results from slow transport through the semiconductor films. This would operate by drastically decreasing the diffusion path length. Furthermore, organic entities can be grafted at the surface of these mesoporous TiO_2 thin films with the objective to develop hybrid architectures for chemically modified electrodes. Martinez-Ferrero et al.²³³ have reported the synthesis of ferrocenylphosphonic acid functionalized mesostructured porous nanocrystalline titanium oxide films. In these films, a pseudo diffusive electron hopping between the redox species and the inorganic TiO_2 network occurs, and it is due to the specific anisotropic order of the mesoporous TiO_2 layer. An electronic diffusion coefficient ($D_{\text{app}} \sim 10^{-14} \text{ m}^2 \cdot \text{s}^{-1}$) has also been determined, and it is comparable to the one measured on mesoporous films of TiO_2 phytate, confirming the accessibility of the pores and the interesting charge transfer properties in these mesostructured films.⁵⁵³ The transport of molecules in these mesoporous architectures can, however, be tuned and depends on the nature of the functional groups attached to the pore surface (the length of organic chains, the functionality size, or the polarity) and on the geometrical constraints including the pore size, the pore orientation, and their interconnection.⁴⁴⁴ This capability is very interesting for the fabrication of robust membranes selective to probes. Finally, these POMTFs have also been used as a support for metal electrodeposition.²³²

7.2.4. Catalysis. Catalysis is another area where the inherent characteristics of mesoporous thin films are generating enormous interest. Sol-gel chemistry and processing allow specific compositions (Tables 2 and 3) to be developed with a highly porous morphology so that the solid network might be tailored to the specific reaction while the mesoporous network serves as the equivalent of an efficient pathway for molecular transport. The continuous mesoporous network of these films facilitates the flux of reactant molecules that access the catalytically active "internal surface" area. Another interesting feature of mesoporous thin film catalysts is the degree of crystallinity in the inorganic pore walls that can be tailored by straightforward annealing conditions. Indeed, heterogeneous catalysts are, in general, nonsmooth, high surface area, nanoscale materials. However, one can wonder if the catalytic activity derives from the disorder structure rather than from crystalline structure. In the literature, only few studies reported catalytic activities on inorganic mesoporous thin films. It is very difficult to draw conclusions on the catalysis mechanisms involved and on the impact of the ordered mesostructure on the catalytic activity. Periodically organized mesoporous thin films of Pt- SnO_2 have been reported to exhibit high sensitivity and selectivity toward CO at 200°C .^{554,555} The structure and the response of the sensor material have been found to be mostly governed by the Pt content.

Furthermore, the flexibility of the sol-gel method coupled with the EISA and the processing used allow the design of "multifunctionnal" catalysts. Sol-gel chemistry and processing help to design catalysts where the solid network and the guest in the mesoporous network are tailored to specific reactions. Cortial et al.⁴⁸ have recently synthesized metallic nanoparticles embedded in mesoporous TiO_2 thin films

exhibiting high selectivity and turnover frequency for allylic nucleophilic substitution with low nanoparticles loading. In these systems, the immobilized Pd nanoparticles are 3 orders of magnitude more active than their homogeneous counterparts. The process is also much more selective as the regioselectivity is in favor of the linear compound. The authors related these features to “confinement effects” which occur in these mesoporous compounds.⁵⁵⁶ This effect is well-known to increase selectivities, activities, and surface acidity. This approach is interesting to develop in the near future mesoporous catalyst thin films where the pores serve as a nanoreactor. For example, a judicious choice of the grafted functions onto the pore walls and the nature of the inorganic metals would allow for catalyzing reactions with several intermediates with only “one catalyst”.^{557–560} Further, mesoporous films can be used to cover the internal surface of a beaker, and “catalytic beaker” can be fabricated.

Even though there are obvious advantages that mesoporous thin films bring to catalysis as either primary catalyst or catalyst support, up to now the transfer of these materials into practical catalytic processes appears to be limited, at least as reported in the open literature.

7.2.5. Optical Properties. Periodically organized mesoporous thin films constitute a very interesting material for optical application, because of their well-ordered cubic array of mesopores and a wall structure composed of 1–5 nm nanocrystallites embedded or not in an amorphous matrix. This interesting two-phase wall structure makes them a particularly attractive host matrix for optically active species such as trivalent rare earth metal (RE) ions. While the glasslike amorphous regions provide an ideal environment for the RE ions, the semiconducting nature of nanocrystallites can be used to sensitize the RE luminescence.^{561,562} Sensitization is an important process for technological applications of RE ions in photonic devices and color displays, since direct excitation of the parity-forbidden intra-f-shell RE metal ion crystal-field transition is inefficient. While the structural properties of mesoporous materials have been extensively studied, the optical properties have been investigated to a lesser degree.

Zhang et al. have reported a mesoporous TiO₂ film exhibiting correct good optical transparency with 85% or more transmittance in the visible region. A blue shift in UV–vis absorption onset was shown for the mesoporous TiO₂ films, indicating a size quantization effect of nanocrystalline titania.³²⁴ Recently, Castro et al.¹¹⁶ have shown the interest of using nanocrystalline rare earth oxide (Eu₂O₃) mesoporous thin films for optical applications. The fluorescence spectra and the fluorescence decay curves exhibit a forbidden $^5D_0 \rightarrow ^7F_0$ electric dipole transition band and an intense band at 615 nm, due to the “hypersensitive” $^5D_0 \rightarrow ^7F_2$ electric dipole transition. The optical features and the nonexponential response of the decay profiles were attributed to Eu³⁺ ions located in highly asymmetric environments, corresponding to the distorted coordination sphere of the grain boundaries. Furthermore, meso-structured rare earth (Eu³⁺, Sm³⁺, and Er³⁺)-doped Y₂O₃ thin films have been synthesized, and their luminescence properties have been measured.⁵⁶³ They exhibit the characteristic $^5D_0 \rightarrow ^7F_J$

transition band. More interestingly, these authors showed a lifetime (τ) value of 2 ms for films heated at 880 °C. This value is longer than the one reported for bulk cubic Y₂O₃:Eu crystals (0.86) or for lamellar Eu³⁺ doped Y₂O₃ nano-hybrids (0.36–0.66).

POMTFS with nanocrystalline walls act as the sensitizing host matrix for luminescent rare-earth ions. In particular, visible and near IR luminescence from Eu(III), Sm(III), Nd(III), Yb(III), and Er(III) has been observed by exciting the band gap of the mesoporous thin films, suggesting energy transfers between nanocrystallites in titania matrix and rare earth ions.⁵⁶⁴ Furthermore, Frindell et al.⁵⁶⁴ have reported a new luminescent material that combines a three-dimensional mesoscopically ordered array of nanocrystalline semiconductor particles with the nearly monochromatic emission of rare earth ions. The excitation of a cubic mesoporous titania thin film within its semiconductor band gap leads to bright narrow bandwidth emission from the europium activator ions by energy transfer from the semiconducting titania nanoparticles array. This array acts as an effective antenna for the excitation light. In addition, the unique two-phase composition of the mesopore walls allows high loading of Eu³⁺ ions (8 mol %) without quenching their photoluminescence. However, the lifetime observed of ~500 μ s is still low compared to reported values for better optimized materials.

8. Outlook

This outlook describes some relevant research directions that must be developed or investigated in depth to produce new insights in the field of porous templated materials. A large part of the future perspectives concerns, of course, mesoporous films and membranes. However, some recent examples also concern more general aspects of nanostructure and self-organization, performed with mesoporous materials shaped as powders. These examples are, in our opinion, important to have in mind, for a broader view of the templated construction of nanomaterials. To shed more light on these possible new advances, this outlook is split in two subtopics: “Chemistry and Processing” and “Hierarchical Complex Porous Architectures” even if obvious overlap does exist between these topics.

Chemistry and Processing. Many mesoporous films and membranes are deposited by spin-coating, dip-coating or mold casting using in general acidic or neutral sol–gel reaction media. Less attention has been given to the construction mesoporous materials and POMTFs using spray-coating, plasma driven sol–gel deposition, electrodeposition, electrospray, and electrospinning.^{565,566} In the future, the development of these processes is important in allowing deposition of mesoporous films on large substrates, in the design finely carved nanopatterns and in obtaining new textures and new shapes.

Additionally, the elaboration of mesoporous thin films in sol–gel derived basic media will allow better stability of the inorganic walls during surfactant removal, thermal treatment, and crystallization. Moreover, surfactant templated growth in basic conditions will give access to some new multicationic oxides, in particular, compositions with trivalent

rare earth, transition metals, and divalent cations that are difficult to produce in acidic or neutral conditions. The basic route will also likely result in the production of mesoporous films having walls composed with new nanocrystalline phases or compounds that have not yet been accessible in their crystalline form. However, such basic conditions require precise tuning of the processing conditions and control over the kinetics of sol–gel polymerization to be amenable to thin film deposition by EISA. Future developments of POMTFs will probably also occur in the field of magnetic based devices and memories. Indeed, innovative POMTFs with nanocrystalline walls having new multicationic oxide compositions exhibiting giant magnetoresistance or composites layers built from interpenetrated magnetic and dielectric components will impact the field of spintronic and multiferroic materials.

Major recent advances in the field concern the synthesis of functional porous mono- and multilayer devices having different chemical compositions. Recently, the creation of porous nanoporous membranes allowing full access to their substrate (dielectric, insulator, conductors, semiconductors, or metallic) through the non-interconnected nanoporations have been reported.^{104,360,362,363} The difference in the chemical affinities between the accessible substrate area (bottom of the perforations) and the inorganic continuous network (surrounding the perforations) give the possibility for selective local functionalization of both phases. These heterogeneous nanostructured surfaces can be seen as tailor-made nanopatterned hybrids and composites on top of which local chemical growth of functional objects is possible. Moreover, this allows, in a second step, to address and selectively locate organic or bio-functionalities, nanoparticles, or nanocrystals. This area is still in its infancy, but there is no doubt that major developments, involving such novel surfaces as nanostructured substrates, will appear in the near future. Multilayer devices built from alternating silica and titania POMTFs have been developed recently by Soler-Illia et al.^{193,444} These devices, made of mesoporous layers of different thickness, refractive index, and pore size, are very promising because they exhibit photonic band gap related properties that can be tuned by the selective adsorption of different molecules. Indeed, depending on their chemical affinity for the pore wall and the nature of the porous layer, its pore size, molecules, or oligomers can selectively adsorb on the different layers and modify their optical properties, thus opening new avenues for the design of smart sensors and optical devices.

Another future direction of research concerns the morphological control of self-assembled POMTFs. The directed assembly of hybrid inorganic–organic mesophases is a very powerful pathway for the organization of mesoporous layers. For many applications, tunable orientation of the porous network is needed. Consequently, many attempts to orient the porous framework orthogonal or quasi orthogonal to the substrate surface have been performed as already discussed in section 5. Among them, the most reported strategy concerns the use of anodic alumina as an exotemplate.^{343,344,567,568} In addition, other orientation strategies already discussed in part 5, including the stimulated self-assembly of amphiphilic

BCP–silica hybrid 2D hexagonal mesophase by using two functionalized glass slide surfaces,³⁵² the combination of hybrid mesophase assembly with electric, magnetic, and mechanical external fields, or convecting flow, have produced promising signs but no convincing results.^{345,348,569} Quasi orthogonal pore orientation was obtained through a controlled diffuse sintering of matter via a tuned thermal treatment to give grid-like mesoporous titania films,¹¹³ while direct access to the substrate is achieved through nanoporous membranes.^{360,362,363} The best achievement of perpendicular pores, which is certainly one of the best route to follow in the future, is the postalignment of PS-PEO micelles by adjusting both film interface's interfacial tensions. Indeed, Freer et al.³⁵⁹ present nice TEM pictures of 200 nm thick SiO₂ films exhibiting channel nanopores running perpendicularly from one interface to the other. Some of these strategies should be also transferred to POMTFs.

Today, the world of organic polymers, sol–gel chemistry, and soft matter have been successfully married, with these scientific communities collaborating more and more in the field of materials science. The use of POMMs can yield better structural definition for resulting composite materials allowing a better understanding of the basic science occurring during such a complex elaboration process. Indeed, the organized confined structure provided by POMMs is currently used to study the growth of polymers by ATRP using grafting from or grafting to strategies.^{570–576} The impetus behind such research is the design of new mesoporous hosts having polymeric nanovalves that can be thermally or chemically (pH, solvent) controlled for use as smart carriers for controlled delivery systems. Much interesting work has been developed with POMMs in the area of biomaterials.^{395,577–579} Biocarriers for the controlled release of drugs, new materials for implants, multifunctional carriers associating hyperthermia treatments, controlled release of active components, and targeting and imaging, via NMR, of tumors, represent just some of the relevant aspects of POMM based research for biomedical applications.^{85,572,576} POMTFs in principle can also be interesting as medical or cosmetic patches. However, for many of these applications a more complete knowledge of the biocompatibility and the chemical and structural evolution of the mesoporous inorganic or hybrid materials is strongly needed. In tune with this perspective is the use of POMTFs as excellent model systems to study the stability of mesoporous oxide and mixed-metal oxide materials in biological media. Recently, the dynamic behavior (stability toward dissolution of the film in the medium), including the pore size distribution, mechanical properties, and composition of nanoscale mesoporous oxide and mixed-metal oxide films exposed to biologically relevant environments has been studied using environmental ellipsometry porosimetry and XPS.²⁵⁸ The dynamic properties of the films can be tuned by varying the composition, porosity, and calcination temperature.

Another important area of research concerns the synthesis and processing of POMTFs using renewable and/or abundant raw materials sources via environmentally friendly, green chemistry processes. The raw materials can come from the abundant inorganic materials (silica, calcium carbonate,

phosphates, etc.) which are found in nature as components in many vegetal or living organisms (diatoms, shells, sand, rice husks, etc.).^{580,581} Biosurfactants or amphiphilic biopolymer templates can be extracted from natural products or can be synthesized from the transformation of biomass via catalyzed cascading reactions. The construction of mesoporous materials under environmentally friendly conditions starting from the initial precursors and templates and using organic solvent-free media is an important future challenge. Today nanostructuring of coatings using the self-organization properties of monodisperse functional nanosized particles, NBBs, is a field which has not yet been extensively studied.⁵⁸² The collective optical and magnetic properties of the resulting nanostructured assemblies are particularly interesting because they can be tuned by varying the nanocrystal spacing and arrangement.⁵⁸³ In situ study of nanostructured 2D monolayer assembly can be a useful model to better understand the mechanisms occurring during the “oriented attachment” of NBBs.^{584,585} In recent studies, it appears that the oriented attachment of NBBs, combined or not with partial dissolution–precipitation steps, is responsible for the production of textured anisotropic crystalline particles and mesocrystals.^{585,586} The design and synthesis of new dis-symmetric or Janus type NBBs is also a very important research topic⁵⁸⁷ because these bifunctional nanobricks can impart novel characteristics relevant to the design and construction of new nanomaterials. Indeed, if these Janus type NBBs are carrying strongly different hydrophilic and hydrophobic components they will likely behave as “new surfactants” that can self-assemble to generate innovative 2D or 3D nanostructured hybrid assemblies. In particular, these chemically polarized NBBs will probably modify the effects of internal forces (Van der Waals, H-bonding, and capillary forces), the substrate (wetting/nonwetting) and external forces (magnetic or optical fields, temperature gradients, pressure, and mechanical strength) during the self-assembly process.

Indeed, construction routes to POMMs and POMTFs using NBBs had not been sufficiently developed. The combination of self-organized systems with template directed sol–gel chemistry will provide better mechanical stability for the nanostructured layers. The sol–gel component can not only add new functionalities but also connect or cement the nanostructured assembly providing robustness, thus opening a door for new material and devices development. Some interesting results have been obtained recently by Brinker’s group^{81,84} who have produced ordered nanogold–silica superlattices via sol–gel assembly using bilayers of capped nanoparticles and polymerizing silica as a cement.

Following this concept, further developments might involve new functional layers utilizing nanoparticles or nanocrystals composed of metals, metallic oxides, chalcogenides, or mesoporous submicronic spheres prepared via aerosol or precipitation processes. In the latter case, the mesoporous NBB spheres could act as functional reservoirs for controlled release applications or as high surface area supports to trap probes for sensing applications. The use of preformed dense or mesoporous NBBs in the presence of templated inorganic or polymeric binders can also improve processing techniques such as ink jet printing or micropen lithography. Controlling

the chemistry during the previous step (synthesis of the NBB) should provide routes for the construction of arrays of mesoporous microdots or micropillars having different shapes and tunable height and volume and with different addressable functionalities that are less sensitive to processing parameters.

Pore size is obviously an important parameter that impacts not only the physicochemical properties of porous material but also the properties of chemical species inside their pores. These modifications of the behavior of a phase within pores are usually called confinement effects and were intensively studied for zeolitic materials. Interfacial interactions, symmetry breaking, and curvature as well as structural frustration and confinement induced entropy losses are known to play important roles in determining molecular organization within physically confined environments.⁵⁵⁶ These so-called confinement effects in porous materials are also known to strongly affect diffusion, phase transformations, catalytic properties, and so forth. However, to date, understanding how the chemical nature of the pore wall and its degree of crystallinity and how the pore size, shape, and connectivity affect the physicochemical properties of the porous materials remains an important challenge, in particular for mesoporous solids and microporous hybrid MOFs.^{588–591} Confinement studies on periodically organized mesoporous materials must be developed because they are potentially ideal candidates to provide clarity to arguments and understanding on confinement.⁵⁵⁶ Mesoporous materials and films can be used as exotemplates to produce nanotubes (metallic nanowires, CNT, etc.) via the nucleation and growth of confined metal–organic precursors or inorganic metallic salts.^{382,552} They can also be utilized as hosts for conducting organic polymers, nanoparticles, clusters, organic dyes, and organometallic precursors to not only design new nano- or molecular composites but also to study and model the catalytic, optical, and magnetic properties of confined species.

Chiral surfactants or chiral organogelator templates can induce the formation of “chiral” porous networks with particularly original architectures. Following these approaches, early results have demonstrated that helicoidal porous nanotubes can be synthesized.^{592–596} Recently, it has been demonstrated that helicoidal mesostructures can be developed in the presence of achiral surfactants. It has been suggested that a simple and purely interfacial mechanism can explain the spontaneous formation of helical mesostructure.⁵⁹⁷ However, to the best of our knowledge, a direct proof demonstrating a real chiral effect coming from confined species in such helicoidal porous materials based on a physical or chemical response (an enantiomeric excess of a catalytic reaction, a nonlinear optical response, or polarization of a propagating light within the nanotube) has not yet been reported. Such “chiral materials” coupled with confined catalytic centers designed via molecular imprinting approaches might yield important breakthroughs in the field of catalysis.

Novel synthesis routes of POMMs without the use of surfactant molecules or polymers as template are emerging.^{277,598} Some of these self-templating based strategies involve very slow hydrolysis of metallic alkoxides that likely provide anisotropic growth of linear metal-oxo polymers^{599,600}

that self-template the reaction media. Indeed, it is well documented that when nonaggregating anisotropic objects (tubes, ribbons, platelets, etc.) reach a certain form factor and volume fraction they fulfill the conditions for lyotropic liquid crystals formation.⁶⁰¹

Is periodic organization of the mesoporous network always needed to achieve optimized function? Ordered porosity allows a kind of facile quality control over the final porous materials and can improve the diffusion process, as shown for some catalytic reactions on hybrid catalysts.^{557,558,602} However, for applications in micro-optics and microelectronics where diffusion of reactants are not key factors, porous organization is not required to obtain smart properties. This has been recently demonstrated in the synthesis of ultralow-refractive-index, ultralow-dielectric-constant optical thin films built from magnesium oxyfluoride vesicle-like hollow nanoparticles. These mesoporous coatings, which are not periodically organized, were prepared via a robust and simple procedure using a controlled thermal treatment to trigger the decomposition of fluoro organic acids into gaseous species and the concomitant nucleation and growth of MgF_2 based nanoparticles. The simultaneous nature of these two processes results in the formation of gaseous nanobubbles that act as porogens during the growing MgF_2 nanoparticle vesicle-like networks. The result is a rigid and highly porous inorganic network composed of coalesced hollow particles and vesicles. These films are highly porous, hydrolytically stable, and mechanically resistant, while exhibiting high optical quality, ultralow refractive index ($n_{700\text{ nm}} = 1.09$), and ultralow dielectric constant ($k_{100\text{ kHz}} = 1.6$).⁶⁰³

Hierarchical and Complex Porous Architectures. Nature has been producing inorganic materials and hybrid composites of remarkable efficiency for millions of years by making use of highly selective structures. Natural materials are highly integrated systems that balance a multitude of properties and functions such as resistance, mechanics, density, permeability, color, hydrophobicity, durability, and recycling.^{604–606} Biomaterials are highly elaborated systems assimilating high level miniaturization, integrated inorganic and organic components, and hierarchical control. Indeed, hierarchical constructions on a scale ranging from nanometers, to micrometers, to millimeters are characteristic of biological structures and serve to address the physical and chemical demands occurring at these different length scales.

The construction of porous materials exhibiting complex hierarchical structures is a particularly interesting challenge for materials chemists. Materials expressing multimodal or multiscale porosity are of major interest, particularly in catalysis, membranes, and separation based processes where optimization of the diffusion and confinement regimes is required. While micro- and mesopores provide the size and shape selectivity for the guest molecules, governing the host–guest interactions, the presence of macroporous channels can facilitate access to these active site regions, avoiding pore blocking by reagents or products, improving transport, and reducing residence times which can lead to coking or other deleterious secondary reactions.

As such, the design of porous materials having multimodal porosity will allow the development of innovative advanced materials with promising applications in many fields: chromatography, membranes and smart coatings, catalysis, photovoltaic and fuel cells, sensors and biosensors, and so forth.

The physicochemical processes described in the present review, mainly based on the coupling of precursors with surfactant templating (or with swelled micelles), allow control over the design and assembly of POMMs in the 1 nm to 500 nm range. Mastering these strategies necessitates (1) control over the complexation, H-bonding, or electrostatic bonding that couple the organic and the mineral components and (2) the tuning of the mineral network formation that governs the curvature and the interface matching. These two physicochemical processes determine the dynamic hybrid interface, the key feature in the marriage between self-assembly and sol–gel processes that lead organized structure on these length scales. Keeping this in mind, porous hierarchical structures can be obtained following several approaches. Recently, micromolding methods have been developed in which macrotemplates (with size ranging from 1000 Å to several micrometers) are coupled directly with the sol–gel–micellar reaction media. The most commonly used submicronic or micronic templates are latex beads or silica nanoparticles, large polymers, microemulsion droplets, organogelators, and bacterial threads.^{10,16,607–609} Moreover, combined with top-down-designed substrates (such as micropatterned PDMS), “sol–gel chemistry and mesoscale template directed self-assembly” (micromolding and POMM based processing) open an easy route for the construction of periodically organized porous devices having multiscale organization.⁶⁰⁷

Finally, in the past few years new strategies to construct multimodal porous materials by associating controlled phase separation phenomena and (if needed) mesoscale templated cooperative self-assembly have appeared. These developments are of paramount importance because they will permit selective functionalization at different length scales. These strategies include utilizing nonporogenic hydrophobic polymeric matrixes as growth media, self-formation of hierarchy based on the synergy between the polymerization kinetics of metal alkoxides and the hydrodynamic flow of produced solvent, controlled foaming processes, and the use of breath figures combined with sol–gel precursors or NBBs.⁶¹⁰

The growth of surfactant templated sol–gel materials in nonporogenic polymers or in molten polymers also allows the design of novel functional hierarchical inorganic and hybrid architectures. Recently, an approach to forming transparent hierarchical hybrid functionalized membranes using in situ generation of mesostructured hybrid phases inside a nonporogenic hydrophobic polymeric host matrix such as PVDF or PVBu was reported. Controlling the affinities between organic and inorganic components allowed the designed length-scale partitioning of organized hybrid nanomaterials with tuned functionalities from the angstrom to centimeter (figure) size scales. After functionalization of the mesoporous hybrid silica component, the resulting membranes exhibited good ionic conductivity, offering

interesting opportunities for the design of solid electrolytes, fuel cells, and other ion-transport microdevices.⁶¹¹

Self-formation of hierarchy with multiscale porosity via hydrolysis of transition metal alkoxides was recently reported by Su et al.^{612–614} The proposed mechanism is based on the synergy between the polymerization kinetics of highly reactive transition metal alkoxides and the hydrodynamic flow of the solvent produced by the leaving groups upon hydrolysis and condensation. First, a transition metal alkoxide drop introduced in aqueous medium yields instantaneously the production of a zirconium–oxo polymer based shell. The progressing inorganic polymerization generates zirconium oxide based nanoparticles and pressurized domains inside the droplet due to the evolved alcohol and water molecules. The expulsion of the solvent creates funnel-like macropores orthogonally oriented with respect to the smooth particle surface, while the micro- or meso-porosity results from self-aggregation of the zirconium oxide based nanoparticles.

New strategies following integrative chemistry routes which combine soft matter and soft chemistry have been developed for the synthesis of hierarchically porous materials.⁶¹⁵ The processing used involves sol–gel chemistry coupled with air–liquid foams or with direct or reverse biliquid process foams. The use of gas–porogen or micro-emulsions based methods in combination with surfactants and inorganic or hybrid precursors results in processes that can be easily scaled up. The precursors for the construction of the mineral scaffold can be molecular, such as metal alkoxides, metallic salts, and organosilanes, or nanoparticle based by using NBBs of titania, zirconia, or silica.^{615–619} Moreover these advanced materials with multiscale porosity can be organically functionalized and/or loaded with metallic particles, allowing new developments in the field of adsorption, sensing, and catalysis.⁶²⁰

The strategy for the construction of honeycomb-like macroporous films induced by breath figures (Marangoni–Besnard effects) in the presence of NBBs is general, simple, and versatile because it allows the directional assembly of a large variety of structurally well defined nanoparticles with very different chemical compositions into complex porous architectures. This strategy was first demonstrated for the elaboration of CeO₂ based honeycomb-like micro-/macroporous membranes prepared by assembling phenyl-functionalized CeO₂ nanoparticles using biopolymers (the poly(*g*-benzyl-L-glutamate)) as a template.^{621,622} SiO₂, TiO₂, CeO₂, Co, CdS, and zeolites nanoparticles have all recently been used as NBBs to produce such porous films or membranes with hierarchically porous structures (Figure 28). This strategy can likely be extended to carbides, nitrides, inorganic–organic (or bio-) hybrid nanoparticles. It is also a very promising approach to produce polymodal porous films and membranes, because the resulting materials could inherit the interesting functional properties of the nanoparticle precursors.^{622–624} Moreover, the adjustable size of the nanobuilding units permits facile tuning of mesoporosity from a mean size of 2–50 nm. This simple method will also be of great interest for industrial applications in terms of commercial powder products.

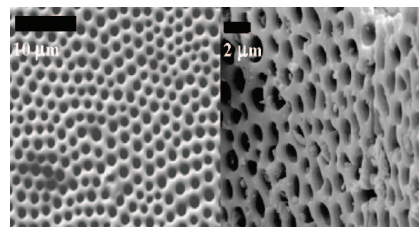


Figure 28. Films made of micro–macro-textured CeO₂ based nanomaterials obtained via the combination of NBBs and breath figures. Reprinted with permission from refs 621 and 622. Copyright 2002 and 2004 The Royal Society of Chemistry.

The final aim of all these approaches will be to tailor-make complex hierarchical structures possessing multiple functionalities in registry, enabling responses to external stimuli and even developing a certain degree of autonomy and intelligence. The integrative synthesis of new functional porous materials possessing hierarchical structures opens up lands of opportunity in numerous areas. However, today, one major challenge that remains is the ability to selectively localize different functionalities across the different length scales. The recently coined “Integrative Chemistry”⁶¹⁵ is indeed a multidisciplinary domain where soft matter, soft chemistry, and smart processing meet.^{604,605}

9. Conclusion

Periodically organized mesoporous films and membranes constitute a challenging domain in materials chemistry that is experiencing explosive growth. Indeed, the chemical strategies made accessible by combining the sol–gel based growth of inorganic or hybrid networks with self-assembled surfactant mesophases allow the development of innovative mesoporous materials having complex and diverse architectures. In the next couple of years, a more important development of nanoporous films having new compositions (multicationic oxides, ceramic–ceramic composites, non-oxides, carbon, metals, MOF, etc.), tunable orientation, and accessibility can be expected.

The potential utility of these nanostructured porous materials is currently recognized in advanced domains including optical devices, photocatalysis, catalysts, photovoltaic cells, adsorption, and sensors. The further optimization of the properties of these mesoporous materials requires a sound knowledge of their structure–property relationships, as well as a deeper understanding of the governing formation mechanisms. A better understanding of the nanoscale structure, composition, and morphology is critical in establishing such structure–property relationships in POMTFs. Among the relevant characterization techniques, the high potential of 2D GISAXS for the mesostructure determination of POMTFs has clearly been demonstrated. Additionally, X-ray reflectometry and EEP are very useful tools for determining pores size, pore accessibility, surface area, and mechanical properties of POMTFs. The chemical nature and the morphology of the porous network can be accessed by XRD for crystalline phases, vibrational spectroscopies (IR–Raman), and HRTEM. This latter technique will likely become even more useful through the recent development of 3D HRTEM tomography. The successes realized in the last years in the

field of POMTFs and membranes are also clearly related to the ability of materials chemists to control hybrid interfaces and to tune the kinetics of sol–gel polymer growth with the thermodynamics of the micellar organization.

For membranes, where the quantity of porous matter is sufficient, high-speed solid-state MAS NMR appears to be a very powerful tool to analyze the composition and the structure of hybrid interfaces.^{305,436} However, in our opinion techniques that can give accurate information (either ex situ and in situ) on the chemical speciation of periodically organized mesoporous films are still lacking, though optically polarized ¹²⁹Xe NMR might fulfill part of this challenge. The development of techniques accessible for routine use at the laboratory level to study the thermal evolution of the POMTFs during surfactant removal, network consolidation, and crystallization of the walls will also be very important for the future developments of PMOTFs. Recent experiments using thermo-ellipsoporosimetry demonstrate that this technique might be very useful for this purpose.⁶²⁵

Today, one major challenge in the area of porous materials with hierarchical structures remains the ability to selectively localize different functionalities across the different length scales. Future emphasis in POMMs and POMTFs research will be dedicated to the construction by design of new, responsive porous materials with multimodal porosity. These advanced materials will exploit the synergies between ceramics and hybrids, between bottom-up and top-down approaches to tailor-make new films, membranes, and devices exhibiting coupled properties (smart membranes that combine sensing–separation–catalysis functions, new hybrid actuators, smart electrochemical or photoelectrochemical cells, etc.) and that can adapt their response to an external stimulus (pH, solvent, light, external fields, temperature).

Glossary

AFM	atomic force microscopy
ATRP	atom radical polymerization
BdB	Broekhoff and De Boer model
CSD	chemical solution deposition
CTAB	cetyltrimethylammonium bromide
CTAC	cetyltrimethylammonium chloride
DA	diacetylene
DFT	density functional theory
DM	dodecylmethacrylate
DSSC	dye-sensitized solar cells
EDX	energy dispersive X-ray
EEP	environmental ellipsometric porosimetry (atmospheric)
EISA	evaporation induced self-assembly
EP	ellipsoporosimetry
EXSY	exchange ¹²⁹ Xe NMR spectroscopy
FAM SE	5,6-carboxyfluorescein succinimidyl ester
FDM	ferrocene dimethanol
FDMDG	ferrocene dimethanol diethylene glycol
FTIR	Fourier transform infrared
GI-SAXS	grazing incidence X-ray scattering
HMDS	hexadimethylsilazane
ITO	indium tin oxide
LCT	liquid crystal templating
MOFs	metaloxide frameworks
MTES	methyltriethoxysilane
NBBs	nanobuilding blocks
NEA	nanoelectrode array
NI	nano-indentation
NIPAM	N-isopropylacrylamide
NMR	nuclear magnetic resonance

NPC	neutral point charge
OHPXe NMR	optically hyperpolarized ¹²⁹ Xe NMR
PALS	positron annihilation lifetime spectroscopy
PB	polybutadiene
PDA	polydiacetylene
PDM	polydodecylmethacrylate
PEO	polyethyleneoxide
PLD	pulsed laser deposition
PNIPAM	poly(N-isopropylacrylamide)
POMMs	periodically organized mesoporous materials
POMTFs	periodically organized mesoporous thin films
PPO	polypropyleneoxide
PS	polystyrene
PSD	pore size distribution
PVBu	polyvinyl butyral
PVDF	poly(vinylidene fluoride)
PZC	point of zero charge
QCM	quartz crystal microbalance
RBS	Rutherford back scattering
RE	rare earth (lanthanide)
RS	Raman spectroscopy
SAM	self-assembled monolayer
SANS	small angle neutron scattering
SAW	surface acoustic waves
SAXS	small angle X-ray scattering
SDBM	triethoxysilyldibenzoylmethane
SEM	scanning electron microscopy
SSQ	silsesquioxane
TEM	transmission electron microscopy
TIPB	1,3,5-triisopropylbenzene
TEOS	tetraethylorthosilicate
TM	transition metal
TMB	trimethyl benzene
TMO	transition metal oxide
TMOs	transition metal oxides
TMOS	tetramethylorthosilicate
TSS	tunable steady state
VTES	vinyltriethoxysilane
WAXS	wide angle X-ray scattering
XANES	X-ray absorption near edge structure
XPS	X-ray dispersive electron spectroscopy
XRD	X-ray diffraction
XRR	X-ray reflectometry

References

- (1) Evans, D. F.; Wennerström, H. *The Colloidal Domain, Where Physics, Chemistry, Biology and Technology Meet*; VCH Publishers: New York, 1994.
- (2) Israëlachvili, J. *Intramolecular and Surface Forces*, 2nd ed.; Academic Press: New York, 1992.
- (3) Sanchez, C.; Soler-Illia, G. J. A. A.; Ribot, F.; Lalot, T.; Mayer, C. R.; Cabuil, V. *Chem. Mater.* **2001**, *13*, 3061.
- (4) Sanchez, C.; Ribot, F. *New J. Chem.* **1994**, *18*, 1007.
- (5) Livage, J.; Henry, M.; Sanchez, C. *Prog. Solid State Chem.* **1988**, *18*, 259.
- (6) Brinker, C. J.; Scherer, G. W. *Sol-Gel Science*; Academic Press: San Diego, 1990.
- (7) Chiola, V.; Ritsko, J. E.; Vanderpool, C. D. U.S. Patent 3,556,725, 1971.
- (8) Di Renzo, F.; Cambon, H.; Dutartre, R. *Microporous Mater.* **1997**, *10*, 283.
- (9) Kresge, C. T.; Leonowicz, M. E.; Roth, W. J.; Vartuli, J. C.; Beck, J. S. *Nature* **1992**, *359*, 710.
- (10) Mann, S.; Burkett, S. L.; Davis, S. A.; Fowler, C. E.; Mendelson, N. H.; Sims, S. D.; Walsh, D.; Whilton, N. T. *Chem. Mater.* **1997**, *9*, 2300.
- (11) Ozin, G. A. *Chem. Commun.* **2000**, *6*, 419.
- (12) Antonietti, M.; Ozin, G. A. *Chem. Eur. J.* **2004**, *10*, 28.
- (13) Antonietti, M.; Berton, B.; Göltner, C.; Hentze, H.-P. *Adv. Mater.* **1998**, *10*, 154.
- (14) Bagshaw, S. A.; Prouzet, E.; Pinnavaia, T. *Science* **1995**, *269*, 1242.
- (15) Attard, G. S.; Bartlett, P. N.; Coleman, N. R. B.; Elliott, J. M.; Owen, J. R.; Wang, J. H. *Science* **1997**, *278*, 838.
- (16) Soler-Illia, G. J. A. A.; Sanchez, C.; Lebeau, B.; Patarin, J. *Chem. Rev.* **2002**, *102*, 4093.
- (17) Beck, J. S.; Vartuli, J. C.; Roth, W. J.; Leonowicz, M. E.; Kresge, C. T.; Schmitt, K. D.; Chu, C. T. W.; Olson, D. H.; Sheppard, E. W. *J. Am. Chem. Soc.* **1992**, *114*, 10834.
- (18) Tanev, P. T.; Pinnavaia, T. J. *Chem. Mater.* **1996**, *8*, 2068.
- (19) Tanev, P. T.; Pinnavaia, T. J. *Science* **1995**, *267*, 865.

- (20) Zhao, D.; Feng, J.; Huo, Q.; Melosh, N.; Fredrickson, G. H.; Chmelka, B. F.; Stucky, G. D. *Science* **1998**, 279, 548.
- (21) Galarneau, A.; Cambon, H.; Renzo, F. D.; Fajula, F. *Langmuir* **2001**, 17, 8328.
- (22) Yang, P.; Zhao, D.; Margolese, D. I.; Chmelka, B. F.; Stucky, G. D. *Nature* **1998**, 396, 152.
- (23) Yang, P.; Zhao, D.; Margolese, D. I.; Chmelka, B. F.; Stucky, G. D. *Chem. Mater.* **1999**, 11, 2813.
- (24) Antonelli, D. M.; Ying, J. Y. *Angew. Chem., Int. Ed. Engl.* **1995**, 34, 2014.
- (25) Antonelli, D. M.; Ying, J. Y. *Angew. Chem., Int. Ed. Engl.* **1996**, 35, 426.
- (26) Attard, G. S.; Glyde, J. C.; Göltner, C. G. *Nature* **1995**, 378, 366.
- (27) Brinker, C. J.; Lu, Y.; Sellinger, A.; Fan, H. *Adv. Mater.* **1999**, 11, 579.
- (28) Lu, Y. F.; Fan, H. Y.; Doke, N.; Loy, D. A.; Assink, R. A.; LaVan, D. A.; Brinker, C. J. *J. Am. Chem. Soc.* **2000**, 122, 5258.
- (29) Lu, Y.; Ganguli, R.; Drewien, C. A.; Anderson, M. T.; Brinker, C. J.; Gong, W.; Guo, Y.; Soye, H.; Dunn, B.; Huang, M. H.; Zink, J. I. *Nature* **1997**, 389, 364.
- (30) Schuth, F. *Chem. Mater.* **2001**, 13, 3184.
- (31) Stein, A. *Microporous Mesoporous Mater.* **2001**, 44–45, 227.
- (32) Polzar, S.; Antonietti, M. *Chem. Commun.* **2002**, 10, 02.
- (33) Ryoo, R.; Joo, S. H.; Jun, S. J. *Phys. Chem. B* **1999**, 103, 7743.
- (34) Ryoo, R.; Joo, S. H.; Kruk, M.; Jaroniec, M. *Adv. Mater.* **2001**, 13, 677.
- (35) Goltner, C. G.; Antonietti, M. *Adv. Mater.* **1997**, 9, 431.
- (36) Ying, J. Y.; Mehnert, C. P.; Wong, M. S. *Angew. Chem., Int. Ed.* **1999**, 38, 56.
- (37) Sayari, A.; Liu, P. *Microporous Mater.* **1997**, 12, 149.
- (38) Patarin, J.; Lebeau, B.; Zana, R. *Curr. Opin. Colloid Interface Sci.* **2002**, 7, 107.
- (39) Soler-Illia, G. J. A. A.; Crepaldi, E. L.; Grosso, D.; Sanchez, C. *Curr. Opin. Colloid Interface Sci.* **2003**, 8, 109.
- (40) Palmqvist, A. E. C. *Curr. Opin. Colloid Interface Sci.* **2003**, 8, 145.
- (41) Moller, K.; Bein, T. *Chem. Mater.* **1998**, 10, 2950.
- (42) Sanchez, C.; Soler-Illia, G. J. A. A.; Ribot, F.; Grosso, D. C. R. *Chim.* **2003**, 6, 1131.
- (43) Stein, A.; Melde, B. J.; Schroden, R. C. *Adv. Mater.* **2000**, 12, 1403.
- (44) Hoffmann, F.; Corneli, M.; Morell, J.; Fröba, M. *Angew. Chem., Int. Ed.* **2006**, 45, 3216.
- (45) Firouzi, A.; Kumar, D.; Bull, L. M.; Besier, T.; Sieger, P.; Huo, Q.; Walker, S. A.; Zasadzinski, J. A.; Glinka, C.; Nicol, J.; Margolese, D.; Stucky, G. D.; Chmelka, B. F. *Science* **1995**, 267, 1138.
- (46) Monnier, A.; Schuth, F.; Huo, Q.; Kumar, D.; Margolese, D.; Maxwell, R. S.; Stucky, G. D.; Krishnamurti, M.; Petroff, P.; Firouzi, A.; Janicke, M.; Chmelka, B. F. *Science* **1993**, 261, 1299.
- (47) Boissière, C.; Larbot, A.; van der Lee, A.; Kooyman, P. J.; Prouzet, E. *Chem. Mater.* **2000**, 12, 2902.
- (48) Cortial, G.; Siutkowski, M.; Goettmann, F.; Moores, A.; Boissière, C.; Grosso, D.; Le Floch, P.; Sanchez, C. *Small* **2006**, 2, 1042.
- (49) Gacoin, T.; Besson, S.; Boilot, J. P. *J. Phys.: Condens. Matter* **2006**, 18, S85.
- (50) Goettmann, F.; Fischer, A.; Antonietti, M.; Thomas, A. *Angew. Chem., Int. Ed.* **2006**, 45, 4467.
- (51) Groenewolt, M.; Antonietti, M. *Adv. Mater.* **2005**, 17, 1789.
- (52) Macquarrie, D. J. *Chem. Commun.* **1996**, 1961.
- (53) Burkett, S. L.; Sims, S. D.; Mann, S. *Chem. Commun.* **1996**, 1367.
- (54) Lim, M. H.; Stein, A. *Chem. Mater.* **1999**, 11, 3285.
- (55) Nicole, L.; Boissière, C.; Grosso, D.; Quach, A.; Sanchez, C. *J. Mater. Chem.* **2005**, 15, 3598.
- (56) Crepaldi, E. L.; Soler-Illia, G. J. A. A.; Grosso, D.; Albouy, P. A.; Sanchez, C. *Chem. Commun.* **2001**, 1582.
- (57) Angelome, P. C.; Soler-Illia, G. J. A. A. *Chem. Mater.* **2005**, 17, 322.
- (58) Angelome, P. C.; Aldabe-Bilmes, S.; Calvo, M. E.; Crepaldi, E. L.; Grosso, D.; Sanchez, C.; Soler-Illia, G. J. A. A. *New J. Chem.* **2005**, 29, 59.
- (59) Park, S. S.; Ha, C. S. *Chem. Rec.* **2006**, 6, 32.
- (60) Soler-Illia, G. J. A. A.; Innocenzi, P. *Chem. Eur. J.* **2006**, 12, 4478.
- (61) Judeinstein, P.; Sanchez, C. *J. Mater. Chem.* **1996**, 6, 511.
- (62) Inagaki, S.; Guan, S.; Ohsuna, T.; Terasaki, O. *Nature* **2002**, 416, 304.
- (63) Kapoor, M. P.; Yang, Q.; Inagaki, S. *J. Am. Chem. Soc.* **2002**, 124, 15176.
- (64) Dag, O.; Yoshina, I. C.; Asefa, T.; MacLachlan, M. J.; Grondy, H.; Coombs, N.; Ozin, G. A. *Adv. Funct. Mater.* **2001**, 11, 213.
- (65) Kuroki, M.; Asefa, T.; Whitnal, W.; Kruk, M.; Yoshina-Ishii, C.; Jaroniec, M.; Ozin, G. A. *J. Am. Chem. Soc.* **2002**, 124, 13886.
- (66) Rebbin, V.; Jakubowski, M.; Potz, S.; Froba, M. *Microporous Mesoporous Mater.* **2004**, 72, 99.
- (67) Morell, J.; Wolter, G.; Froba, M. *Chem. Mater.* **2005**, 17, 804.
- (68) Asefa, T.; MacLachlan, M. J.; Coombs, N.; Ozin, G. A. *Nature* **1999**, 402, 867.
- (69) Corriu, R. J. P.; Mehdi, A.; Reye, C.; Thieuleux, C. *New J. Chem.* **2003**, 27, 905.
- (70) Elhamzaoui, H.; Toupance, T.; Maugey, M.; Zakri, C.; Jousseau, B. *Langmuir* **2007**, 23, 785.
- (71) Elhamzaoui, H.; Jousseau, B.; Riague, H.; Toupance, T.; Dieudonne, P.; Zakri, C.; Maugey, M.; Allouchi, H. *J. Am. Chem. Soc.* **2004**, 126, 8130.
- (72) Steunou, N.; Förster, S.; Florian, P.; Antonietti, M.; Sanchez, C. *J. Mater. Chem.* **2002**, 12, 3426.
- (73) Ba, J. H.; Polleux, J.; Antonietti, M.; Niederberger, M. *Adv. Mater.* **2005**, 17, 2509.
- (74) Deshpande, A. S.; Pinna, N.; Smarsly, B.; Antonietti, M.; Niederberger, M. *Small* **2005**, 1, 313.
- (75) Riley, A. E.; Korlann, S. D.; Richman, E. K.; Tolbert, S. H. *Angew. Chem., Int. Ed.* **2006**, 45, 235.
- (76) Sun, D.; Riley, A. E.; Cadby, A. J.; Richman, E. K.; Korlann, S. D.; Tolbert, S. H. *Nature* **2006**, 441, 1126.
- (77) Fan, J.; Boettcher, S. W.; Stucky, G. D. *Chem. Mater.* **2006**, 18, 6391.
- (78) Lee, U. H.; Lee, H.; Wen, S.; Mho, S. I.; Kwon, Y. U. *Microporous Mesoporous Mater.* **2006**, 88, 48.
- (79) Hwang, Y. K.; Lee, K. C.; Kwon, Y. U. *Chem. Commun.* **2001**, 1738.
- (80) Bosc, F.; Ayral, A.; Albouy, P.-A.; Datas, L.; Guizard, C. *Chem. Mater.* **2004**, 16, 2208.
- (81) Fan, H. Y.; Yang, K.; Boye, D. M.; Sigmon, T.; Malloy, K. J.; Xu, H. F.; Lopez, G. P.; Brinker, C. J. *Science* **2004**, 304, 567.
- (82) Fan, H. Y.; Leve, E. W.; Scullin, C.; Gabaldon, J.; Tallant, D.; Bunge, S.; Boyle, T.; Wilson, M. C.; Brinker, C. J. *Nano Lett.* **2005**, 5, 645.
- (83) Fan, H. Y.; Chen, Z.; Brinker, C. J.; Clawson, J.; Alam, T. *J. Am. Chem. Soc.* **2005**, 127, 13746.
- (84) Fan, H. Y.; Wright, A.; Gabaldon, J.; Rodriguez, A.; Brinker, C. J.; Jiang, Y. B. *Adv. Funct. Mater.* **2006**, 16, 891.
- (85) Julian Lopez, B.; Boissière, C.; Chaneac, C.; Grosso, D.; Vasseur, S.; Miraux, S.; Duguet, E.; Sanchez, C. *J. Mater. Chem.* **2007**, 17, 1563.
- (86) Schuth, F.; Schmidt, W. *Adv. Mater.* **2002**, 14, 629.
- (87) Taguchi, A.; Schuth, F. *Microporous Mesoporous Mater.* **2005**, 77, 1.
- (88) Corma, A. *Chem. Rev.* **1997**, 97, 2373.
- (89) Anderson, M. T.; Martin, J. E.; Odinek, J.; Newcomer, P. In *Microporous & Macroporous Materials*; Lobo, R. F., Beck, J. S., Suib, S. L., Corbin, D. R., Davi, M. E., Iton, L. E., Zones, S. I., Eds.; Materials Research Society: Pittsburgh, 1996; Vol. 431, p 217.
- (90) Ogawa, G. *Chem. Commun.* **1996**, 1149.
- (91) Ogawa, M. *J. Am. Chem. Soc.* **1994**, 116, 7941.
- (92) Yang, H.; Kuperman, A.; Coombs, N.; Mamiche-Afara, S.; Ozin, G. A. *Nature* **1996**, 379, 703.
- (93) Yang, H.; Coombs, N.; Ozin, G. A. *J. Mater. Chem.* **1998**, 8, 1205.
- (94) Brinker, C. J. *MRS Bull.* **2004**, 29, 631.
- (95) Boissière, C.; Grosso, D.; Amenitsch, H.; Gibaud, A.; Coupe, A.; Baccile, N.; Sanchez, C. *Chem. Commun.* **2003**, 2798.
- (96) Grosso, D.; Soler-Illia, G. J. A. A.; Babonneau, F.; Sanchez, C.; Albouy, P. A.; Brunet Bruneau, A.; Balkenende, A. R. *Adv. Mater.* **2001**, 13, 1085.
- (97) Crepaldi, E. L.; Soler-Illia, G. J. A. A.; Bouchara, A.; Grosso, D.; Durand, D.; Sanchez, C. *Angew. Chem., Int. Ed.* **2003**, 42, 347.
- (98) Crepaldi, E. L.; Soler-Illia, G. J. A. A.; Grosso, D.; Cagnol, F.; Ribot, F.; Sanchez, C. *J. Am. Chem. Soc.* **2003**, 125, 9770.
- (99) Crepaldi, E. L.; Grosso, D.; Soler-Illia, G. J. A. A.; Albouy, P. A.; Amenitsch, H.; Sanchez, C. *Chem. Mater.* **2002**, 14, 3316.
- (100) Crepaldi, E. L.; Soler-Illia, G. J. A. A.; Grosso, D.; Sanchez, M. *New J. Chem.* **2003**, 27, 9.
- (101) Alberius, P. C. A.; Frindell, K. L.; Hayward, R. C.; Kramer, E. J.; Stucky, G. D.; Chmelka, B. F. *Chem. Mater.* **2002**, 14, 3284.
- (102) Kirsch, B. L.; Richman, E. K.; Riley, A. E.; Tolbert, S. H. *J. Phys. Chem. B* **2004**, 108, 12698.
- (103) Pido, L.; Grosso, D.; Soler-Illia, G. J. A. A.; Crepaldi, E. L.; Sanchez, C.; Albouy, P. A.; Amenitsch, H.; Euzen, P. *J. Mater. Chem.* **2002**, 12, 557.
- (104) Grosso, D.; Boissière, C.; Smarsly, B.; Brezesinski, T.; Pinna, N.; Albouy, P. A.; Amenitsch, H.; Antonietti, M.; Sanchez, C. *Nat. Mater.* **2004**, 3, 787.
- (105) de Zarate, D. O.; Boissière, C.; Grosso, D.; Albouy, P. A.; Amenitsch, H.; Amoros, P.; Sanchez, C. *New J. Chem.* **2005**, 29, 141.
- (106) Soler-Illia, G. J. A. A.; Crepaldi, E. L.; Grosso, D.; Sanchez, C. *J. Mater. Chem.* **2004**, 14, 1879.
- (107) Smarsly, B.; Grosso, D.; Brezesinski, T.; Pinna, N.; Boissière, C.; Antonietti, M.; Sanchez, C. *Chem. Mater.* **2004**, 16, 2948.
- (108) Brezesinski, T.; Fischer, A.; Iimura, K.; Sanchez, C.; Grosso, D.; Antonietti, M.; Smarsly, B. M. *Adv. Funct. Mater.* **2006**, 16, 1433.
- (109) Kuemmel, M.; Grosso, D.; Boissière, U.; Smarsly, B.; Brezesinski, T.; Albouy, P. A.; Amenitsch, H.; Sanchez, C. *Angew. Chem., Int. Ed.* **2005**, 44, 4589.
- (110) Idrissi, K. N.; Ayral, A.; Klotz, M.; Albouy, P. A.; El, M. A.; Van, d. L. A.; Guizard, C. *Mater. Lett.* **2001**, 50, 57.
- (111) Brezesinski, T.; Antonietti, M.; Groenewolt, M.; Pinna, N.; Smarsly, B. *New J. Chem.* **2005**, 29, 237.
- (112) Brezesinski, T.; Fattakhova-Rohlfing, D.; Sallard, S.; Antonietti, M.; Smarsly, B. M. *Small* **2006**, 2, 1203.
- (113) Grosso, D.; Soler-Illia, G. J. A. A.; Crepaldi, E. L.; Cagnol, F.; Sinturel, C.; Bourgeois, A.; Brunet Bruneau, A.; Amenitsch, H.; Albouy, P. A.; Sanchez, C. *Chem. Mater.* **2003**, 15, 4562.
- (114) Brezesinski, T.; Groenewolt, M.; Antonietti, M.; Smarsly, B. *Angew. Chem., Int. Ed.* **2006**, 45, 781.
- (115) Cabot, A.; Arbiol, J.; Cornet, A.; Morante, J. R.; Chen, F. L.; Liu, M. L. *Thin Solid Films* **2003**, 436, 64.
- (116) Castro, Y.; Julian, B.; Boissière, C.; Viana, B.; Amenitsch, H.; Grosso, D.; Sanchez, C. *Nanotechnology* **2007**, 18, 055705/1–055705/7.
- (117) Dros, A. B.; Grosso, D.; Boissière, C.; Soler-Illia, G. J. A. A.; Albouy, P.-A.; Amenitsch, H.; Sanchez, C. *Microporous Mesoporous Mater.* **2006**, 94, 208.
- (118) Perez, M. D.; Otal, E.; Bilmes, S. A.; Soler-Illia, G. J. A. A.; Crepaldi, E. L.; Grosso, D.; Sanchez, C. *Langmuir* **2004**, 20, 6879.

- (119) Brezesinski, T.; Smarsly, B.; Iimura, K.; Grosso, D.; Boissière, C.; Amenitsch, H.; Antonietti, M.; Sanchez, C. *Small* **2005**, *1*, 889.
- (120) Pan, J. H.; Lee, W. I. *Chem. Mater.* **2006**, *18*, 847.
- (121) Xu, X.; Tian, B. Z.; Kong, J. L.; Zhang, S.; Liu, B. H.; Zhao, D. Y. *Adv. Mater.* **2003**, *15*, 1932.
- (122) Nishiyama, Y.; Tanaka, S.; Hillhouse, H. W.; Nishiyama, N.; Egashira, Y.; Ueyama, K. *Langmuir* **2006**, *22*, 9469.
- (123) Malfatti, L.; Kidchob, T.; Costacurta, S.; Falcaro, P.; Schiavuta, P.; Amenitsch, H.; Innocenzi, P. *Chem. Mater.* **2006**, *18*, 4553.
- (124) Baeck, S. H.; Choi, K. S.; Jaramillo, T. F.; Stucky, G. D.; McFarland, E. W. *Adv. Mater.* **2003**, *15*, 1269.
- (125) Fattakhova-Rohlfing, D.; Brezesinski, T.; Rathousky, J.; Feldhoff, A.; Oekermann, T.; Wark, M.; Smarsly, B. *Adv. Mater.* **2006**, *18*, 2980.
- (126) Brezesinski, T.; Smarsly, B.; Groenewolt, M.; Antonietti, M.; Grosso, D.; Boissière, C.; Sanchez, C. *Nanoporous Materials IV*; Elsevier: Amsterdam, 2005; Vol. 156, p 243.
- (127) Brezesinski, T.; Groenewolt, M.; Pinna, N.; Amenitsch, H.; Antonietti, M.; Smarsly, B. M. *Adv. Mater.* **2006**, *18*, 1827.
- (128) Grosso, D.; Boissière, C.; Nicole, L.; Sanchez, C. *J. Sol-Gel Sci. Technol.* **2006**, *40*, 141.
- (129) Grosso, D.; Cagnol, F.; Soler-Illia, G. J. A. A.; Crepaldi, E. L.; Amenitsch, H.; Brunet-Bruneau, A.; Bourgeois, A.; Sanchez, C. *Adv. Funct. Mater.* **2004**, *14*, 309.
- (130) Choi, K. S.; Lichtenegger, H. C.; Stucky, G. D.; McFarland, E. W. *J. Am. Chem. Soc.* **2002**, *124*, 12402.
- (131) Luo, H. M.; Sun, L.; Lu, Y. F.; Yan, Y. S. *Langmuir* **2004**, *20*, 10218.
- (132) Xue, T.; Xu, C. L.; Zhao, D. D.; Li, X. H.; Li, H. L. *J. Power Sources* **2007**, *164*, 953.
- (133) Edler, K. J. *Soft Matter* **2006**, *2*, 284.
- (134) Edler, K. J.; Roser, S. J. *Int. Rev. Phys. Chem.* **2001**, *20*, 387.
- (135) Edler, K. J. In *Handbook of Sol-Gel Science & Technology - Processing characterization & applications*; Sakka, S., Ed.; Kluwer Academic Publishers: Norwell, MA, 2005; Vol. 1, p 541.
- (136) Nishiyama, N.; Tanaka, S.; Egashira, Y.; Oku, Y.; Ueyama, K. *Chem. Mater.* **2003**, *15*, 1006.
- (137) Tanaka, S.; Nishiyama, N.; Oku, Y.; Egashira, Y.; Ueyama, K. *J. Am. Chem. Soc.* **2004**, *126*, 4854.
- (138) Balkus, K. J.; Scott, A. S.; Gimon-Kinsel, M. E.; Blanco, J. H. *Microporous Mesoporous Mater.* **2000**, *38*, 97.
- (139) Grosso, D.; Babonneau, F.; Albouy, P. A.; Amenitsch, H.; Balkenende, A. R.; Brunet Bruneau, A.; Rivory, J. *Chem. Mater.* **2002**, *14*, 931.
- (140) Grosso, D.; Babonneau, F.; Sanchez, C.; Soler-Illia, G. J. A. A.; Crepaldi, E. L.; Albouy, P. A.; Amenitsch, H.; Balkenende, A. R.; Brunet Bruneau, A. *J. Sol-Gel Sci. Technol.* **2003**, *26*, 561.
- (141) Gibaud, A.; Grosso, D.; Smarsly, B.; Baptiste, A.; Bardeau, J. F.; Babonneau, F.; Doshi, D. A.; Chen, Z.; Brinker, C. J.; Sanchez, C. *J. Phys. Chem. B* **2003**, *107*, 6114.
- (142) Dourdain, S.; Bardeau, J. F.; Colas, M.; Smarsly, B.; Mehdi, A.; Ocko, B. M.; Gibaud, A. *Appl. Phys. Lett.* **2005**, *86*.
- (143) Bardeau, J. F.; Goubil, A.; Dutreilh-Colas, M.; Dourdain, S.; Mehdi, A.; Gibaud, A. *Thin Solid Films* **2006**, *495*, 191.
- (144) Henderson, M. J.; Gibaud, A.; Bardeau, J. F.; White, J. W. *J. Mater. Chem.* **2006**, *16*, 2478.
- (145) Gibaud, A.; Dourdain, S.; Vignaud, G. *Appl. Surf. Sci.* **2006**, *253*, 3.
- (146) Dourdain, S.; Mehdi, A.; Bardeau, J. F.; Gibaud, A. *Thin Solid Films* **2006**, *495*, 205.
- (147) Brunet-Bruneau, A.; Bourgeois, A.; Cagnol, F.; Grosso, D.; Sanchez, C.; Rivory, J. *Thin Solid Films* **2004**, *455–56*, 656.
- (148) Boissière, C.; Grosso, D.; Lepoutre, S.; Nicole, L.; Brunet-Bruneau, A.; Sanchez, C. *Langmuir* **2005**, *21*, 12362.
- (149) Bourgeois, A.; Bruneau, A. B.; Fisson, S.; Demarets, B.; Grosso, D.; Cagnol, F.; Sanchez, C.; Rivory, J. *Thin Solid Films* **2004**, *447*, 46.
- (150) Sakatani, Y.; Grosso, D.; Nicole, L.; Boissière, C.; Soler-Illia, G. J. A. A.; Sanchez, C. *J. Mater. Chem.* **2006**, *16*, 77.
- (151) Nossov, A.; Haddad, E.; Guenneau, F.; Mignon, C.; Gédéon, A.; Grosso, D.; Babonneau, F.; Bonhomme, C.; Sanchez, C. *Chem. Commun.* **2002**, *21*, 2476.
- (152) Haddad, E.; Nossov, A.; Guenneau, F.; Nader, M.; Grosso, D.; Sanchez, C.; Gedeon, A. *Stud. Surf. Sci. Catal.* **2004**, *154*, 1464.
- (153) Nader, M.; Guenneau, F.; Boissière, C.; Grosso, D.; Sanchez, C. In *IMMS*; Tang, Y.; Zhao, D., Eds.; Elsevier Science Ltd.: Shanghai, 2007.
- (154) Brinker, C. J.; Dunphy, D. R. *Curr. Opin. Colloid Interface Sci.* **2006**, *11*, 126.
- (155) Melosh, N. A.; Davidson, P.; Chmelka, B. F. *J. Am. Chem. Soc.* **2000**, *122*, 823.
- (156) Tanaka, S.; Tate, M. P.; Nishiyama, N.; Ueyama, K.; Hillhouse, H. W. *Chem. Mater.* **2006**, *18*, 5461.
- (157) Pai, R. A.; Watkins, J. J. *Adv. Mater.* **2006**, *18*, 241.
- (158) Hayward, R. C.; Chmelka, B. F.; Kramer, E. J. *Adv. Mater.* **2005**, *17*, 2591.
- (159) Hayward, R. C.; Chmelka, B. F.; Kramer, E. J. *Macromolecules* **2005**, *38*, 7768.
- (160) Aksay, I.; Trau, M.; Manne, S.; Honma, I.; Yao, N.; Zhou, L.; Fenter, P.; Eisenberger, P.; Gruner, S. *Science* **1996**, *273*, 892.
- (161) Yang, H.; Coombs, N.; Sokolov, I.; Ozin, G. *Nature* **1996**, *381*, 589.
- (162) Yang, H.; Coombs, N.; Dag, 951 > O.; Sokolov, I.; Ozin, G. A. *J. Mater. Chem.* **1997**, *7*, 1755.
- (163) Roser, S. J.; Patel, H. M.; Lovell, M. R.; Muir, J. E.; Mann, S. *Chem. Commun.* **1998**, 829.
- (164) Ruggles, J. L.; Holt, S. A.; Reynolds, P. A.; Brown, A. S.; Creagh, D. C.; White, J. W. *Phys. Chem. Chem. Phys.* **1999**, *1*, 323.
- (165) Faget, L.; Berman, A.; Regev, O. *Thin Solid Films* **2001**, *386*, 6.
- (166) Edler, K. J.; Brennan, T.; Roser, S. J. *Thin Solid Films* **2006**, *495*, 2.
- (167) Yuan, Z.; Burckel, D. B.; Atanassov, P.; Fan, H. Y. *J. Mater. Chem.* **2006**, *16*, 4637.
- (168) Hozumi, A.; Kojima, S.; Nagano, S.; Seki, T.; Shirahata, N.; Kameyama, T. *Langmuir* **2007**, *23*, 3265.
- (169) Attard, G. S.; Coleman, N. R. B.; Elliott, J. M. *Stud. Surf. Sci. Catal.* **1998**, *117*, 89.
- (170) Nandhakumar, I. S.; Gabriel, T.; Li, X.; Attard, G. S.; Markham, M.; Smith, D. C.; Baumberg, J. J. *Chem. Commun.* **2004**, 1374.
- (171) Urade, V. N.; Wei, T. C.; Tate, M. P.; Kowalski, J. D.; Hillhouse, H. W. *Chem. Mater.* **2007**, *19*, 768.
- (172) Huang, L. C.; Richman, E. K.; Kirsch, B. L.; Tolbert, S. H. *Microporous Mesoporous Mater.* **2006**, *96*, 341.
- (173) Brinker, C. J.; Hurd, A. J. *J. Phys. III* **1994**, *4*, 1231.
- (174) He, C. Q.; Muramatsu, M.; Ohdaira, T.; Oshima, N.; Kinomura, A.; Suzuki, R.; Kobayashi, Y. *Radiat. Phys. Chem.* **2007**, *76*, 204.
- (175) He, C. Q.; Muramatsu, M.; Oshima, N.; Ohdaira, T.; Kinomura, A.; Suzuki, R. *Phys. Lett. A* **2006**, *355*, 73.
- (176) Grosso, D.; Balkenende, A. R.; Albouy, P.-A.; Laverne, M.; Mazerolles, L.; Babonneau, F. *J. Mater. Chem.* **2000**, *10*, 2085.
- (177) Klotz, M.; Albouy, P.-A.; Ayrat, A.; Ménager, C.; Grosso, D.; van der Lee, A.; Cabuil, V.; Babonneau, F.; Guizard, C. *Chem. Mater.* **2000**, *12*, 1721.
- (178) Soler-Illia, G. J. A. A.; Crepaldi, E. L.; Grosso, D.; Durand, D.; Sanchez, C. *Chem. Commun.* **2002**, *20*, 2298.
- (179) Yu, K.; Wu, X.; Brinker, C. J.; Rimeester, J. *Langmuir* **2003**, *19*, 7282.
- (180) Renard, C.; Ricolleau, C.; Fort, E.; Besson, S.; Gacoin, T.; Boilot, J. P. *Appl. Phys. Lett.* **2002**, *80*, 300.
- (181) Besson, S.; Gacoin, T.; Jacquiod, C.; Ricolleau, C.; Babonneau, D.; Boilot, J. P. *J. Mater. Chem.* **2000**, *10*, 1331.
- (182) Besson, S.; Ricolleau, C.; Gacoin, T.; Jacquiod, C.; Boilot, J.-P. *J. Phys. Chem. B* **2000**, *104*, 12095.
- (183) Falcaro, P.; Costacurta, S.; Mattei, G.; Amenitsch, H.; Marcelli, A.; Guidi, M. C.; Piccinini, M.; Nucara, A.; Malfatti, L.; Kidchob, T.; Innocenzi, P. *J. Am. Chem. Soc.* **2005**, *127*, 3838.
- (184) Available at <http://www.esrf.fr/computing/expg/subgroups/dataanalysis/FIT2D/index.html> (accessed July 2007).
- (185) <http://www.ncnr.nist.gov/programs/crystallography/software/cmpri/> (accessed July 2007).
- (186) Tate, M. P.; Urade, V. N.; Kowalski, J. D.; Wei, T. C.; Hamilton, B. D.; Eggiman, B. W.; Hillhouse, H. W. *J. Phys. Chem. B* **2006**, *110*, 9882.
- (187) Tate, M. P.; Hillhouse, H. W. *J. Phys. Chem. C* **2007**, *111*, 7645.
- (188) Ruland, W.; Smarsly, B. M. *J. Appl. Crystallogr.* **2007**, *40*, 409.
- (189) Besson, S.; Ricolleau, C.; Gacoin, T.; Jacquiod, C.; Boilot, J. P. *Microporous Mesoporous Mater.* **2003**, *60*, 43.
- (190) Gibaud, A.; Bardeau, J. F.; Dutreilh-Colas, M.; Bellour, M.; Balasubramanian, V. V.; Robert, A.; Mehdi, A.; Reye, C.; Corriu, R. J. J. *J. Mater. Chem.* **2004**, *14*, 1854.
- (191) Doshi, D. A.; Gibaud, A.; Liu, N. G.; Sturmayer, D.; Malanoski, A. P.; Dunphy, D. R.; Chen, H. J.; Narayanan, S.; MacPhee, A.; Wang, J.; Reed, S. T.; Hurd, A. J.; van Swol, F.; Brinker, C. J. *J. Phys. Chem. B* **2003**, *107*, 7683.
- (192) Boettcher, S. W.; Bartl, M. H.; Hu, J. G.; Stucky, G. D. *J. Am. Chem. Soc.* **2005**, *127*, 9721.
- (193) Fuentes, M. C.; López-Alcaraz, F. J.; Marchi, M. C.; Troiani, H. E.; Luca, V.; Míguez, H.; Soler-Illia, G. J. A. A. *Adv. Funct. Mater.* **2007**, *17*, 1247.
- (194) Ruland, W.; Smarsly, B. J. *Appl. Crystallogr.* **2004**, *37*, 575.
- (195) Ruland, W.; Smarsly, B. J. *Appl. Crystallogr.* **2005**, *38*, 78.
- (196) Smarsly, B.; Gibaud, A.; Ruland, W.; Sturmayer, D.; Brinker, C. J. *Langmuir* **2005**, *21*, 3858.
- (197) Gregg, S. J.; Sing, K. S. W. *Adsorption, surface area and porosity*, 2nd ed.; Academic Press: New York, 1982.
- (198) Rouquerol, F.; Rouquerol, J.; Sing, K. *Adsorption by Powders and Porous Solids*; Academic Press: New York, 1999.
- (199) Barrett, E. P.; Joyner, L. G.; Halenda, P. P. *J. Am. Chem. Soc.* **1951**, *73*, 373.
- (200) Broekhoff, J.; De Boer, J. H. *J. Catal.* **1967**, *9*, 8.
- (201) Broekhoff, J.; De Boer, J. H. *J. Catal.* **1969**, *10*, 368.
- (202) Galarneau, A.; Desplandier, D.; Dutartre, R.; Di Renzo, F. *Microporous Mesoporous Mater.* **1999**, *27*, 297.
- (203) Ravikovitch, P. I.; Neimark, A. V. *Adsorption* **2005**, *11*, 265.
- (204) Deshpande, A. S.; Shchukin, D. G.; Ustinovich, E.; Antonietti, M.; Caruso, R. A. *Adv. Funct. Mater.* **2005**, *15*, 239.
- (205) Kowalczyk, P.; Jaroniec, M.; Kaneko, K.; Terzyk, A. P.; Gauden, P. A. *Langmuir* **2005**, *21*, 10530.
- (206) Ustinov, E. A.; Do, D. D. *Colloids Surf., A* **2006**, *272*, 68.
- (207) Klotz, M.; Ayrat, A.; Guizard, C.; Cot, L. J. *J. Mater. Chem.* **2000**, *10*, 663.
- (208) Zukal, A. *Microporous Mesoporous Mater.* **2006**, *92*, 220.
- (209) Chiu, C. Y.; Chiang, A. S. T.; Chao, K. J. *Microporous Mesoporous Mater.* **2006**, *91*, 244.
- (210) Abeles, F. *Opt. Acta* **1957**, *4*, 42.
- (211) Baklanov, M. R.; Mogilnikov, K. P.; Polovinkin, V. G.; Dultsev, F. N. *J. Vac. Sci. Technol., B* **2000**, *18*, 1385.

- (212) Fuertes, M. C.; Colodrero, S.; Lozano, G.; Rodriguez, A.; Grosso, D.; Boissiere, C.; Sanchez, C.; Soller-Ilia, G. A. A.; Miguez, H. *J. Phys. Chem. C* **2008**, Submitted.
- (213) Angelomé, P. C.; Andrini, L.; Calvo, M. E.; Requejo, F. G.; Bilmes, S. A.; Soller-Ilia, G. J. A. *J. Phys. Chem. B* **2007**, *111*, 10886.
- (214) Murray, C.; Flannery, C.; Streiter, I.; Schulz, S. E.; Baklanov, M. R.; Mogilnikov, K. P.; Himcinschi, C.; Friedrich, M.; Zahn, D. R. T.; Gessner, T. *Microelectron. Eng.* **2002**, *60*, 133.
- (215) Lancelle-Beltran, E.; Prene, P.; Boscher, C.; Belleville, P.; Buvat, P.; Lambert, S.; Guillet, F.; Boissière, C.; Grosso, D.; Sanchez, C. *Chem. Mater.* **2006**, *18*, 6152.
- (216) Saxena, R.; Rodriguez, O.; Cho, W.; Gill, W. N.; Plawsky, J. L.; Baklanov, M. R.; Mogilnikov, K. P. *J. Non-Cryst. Solids* **2004**, *349*, 189.
- (217) Dourdain, S.; Gibaud, A. *Appl. Phys. Lett.* **2005**, *87*.
- (218) SOPRA; Optical solutions: Bois-Colombes, France, 2007 (<http://www.sopra-sa.com>).
- (219) Wohltjen, H. *Sens. Actuators* **1984**, *5*, 307.
- (220) Hietala, S. L.; Smith, D. M.; Hietala, V. M.; Frye, G. C.; Martin, S. J. *Langmuir* **1993**, *9*, 249.
- (221) Liu, N. G.; Assink, R. A.; Brinker, C. J. *Chem. Commun.* **2003**, 370.
- (222) Maex, K.; Baklanov, M. R.; Shamiryan, D.; Iacopi, F.; Brongersma, S. H.; Yanovitskaya, Z. S. *J. Appl. Phys.* **2003**, *93*, 8793.
- (223) Ito, T.; Fraissard, J. J. *Chem. Phys.* **1982**, *76*, 5225.
- (224) Bonardet, J. L.; Fraissard, J.; Gedeon, A.; Springuel-Huet, M. A. *Catal. Rev., Sci. Eng.* **1999**, *41*, 115.
- (225) Terskikh, V. V.; Moudrakovski, I. L.; Breeze, S. R.; Lang, S.; Ratcliffe, C. I.; Ripmeester, J. A.; Sayari, A. *Langmuir* **2002**, *18*, 5653.
- (226) Fraissard, T.; Ito, T.; Springuel-Huet, M. A. *J. Chim. Phys. Phys.-Chim. Biol.* **1988**, *85*, 747.
- (227) Nader, M.; Guenneau, F.; Boissière, C.; Grosso, D.; Sanchez, C.; Gedeon, A. *Stud. Surf. Sci. Catal.* **2007**, *165*, 555.
- (228) Nader, M.; Guenneau, F.; Boissiere, C.; Grosso, D.; Sanchez, C.; Gedeon, A. *Chem. Mater.* **2008**, Submitted.
- (229) Audebert, P.; Griesmar, P.; Hapiot, P.; Sanchez, C. *J. Mater. Chem.* **1992**, *2*, 1293.
- (230) Etienne, M.; Cortot, J.; Walcarius, A. *Electroanalysis* **2007**, *19*, 129.
- (231) Etienne, M.; Quach, A.; Grosso, D.; Nicole, L.; Sanchez, C.; Walcarius, A. *Chem. Mater.* **2007**, *19*, 844.
- (232) Etienne, M.; Grosso, D.; Boissière, C.; Sanchez, C.; Walcarius, A. *Chem. Commun.* **2005**, 4566.
- (233) Martinez-Ferrero, E.; Grosso, D.; Boissière, C.; Sanchez, C.; Oms, O.; Leclercq, D.; Vioux, A.; Miomandre, F.; Audebert, P. *J. Mater. Chem.* **2006**, *16*, 3762.
- (234) Etienne, M.; Walcarius, A. *Electrochem. Commun.* **2005**, *7*, 1449.
- (235) Fattakhova-Rohlfing, D.; Rathousky, J.; Rohlfing, Y.; Bartels, O.; Wark, M. *Langmuir* **2005**, *21*, 11320.
- (236) Liu, N. G.; Dunphy, D. R.; Atanassov, P.; Bunge, S. D.; Chen, Z.; Lopez, G. P.; Boyle, T. J.; Brinker, C. J. *Nano Lett.* **2004**, *4*, 551.
- (237) Gerung, H.; Brinker, C. J.; Brueck, S. R. J.; Han, S. M. *J. Vac. Sci. Technol., A* **2005**, *23*, 347.
- (238) Innocenzi, P.; Kidchob, T.; Bertolo, J. M.; Piccinini, M.; Guidi, M. C.; Marcelli, C. *J. Phys. Chem. B* **2006**, *110*, 10837.
- (239) Choi, S. Y.; Lee, B.; Carew, D. B.; Mamak, M.; Peiris, F. C.; Speakman, S.; Chopra, N.; Ozin, G. A. *Adv. Funct. Mater.* **2006**, *16*, 1731.
- (240) Choi, S. Y.; Mamak, M.; vonFreyman, G.; Chopra, N.; Ozin, G. A. *Nano Lett.* **2006**, *6*, 2456.
- (241) Yanagisawa, T.; Shimizu, T.; Kuroda, K.; Kato, C. *Bull. Chem. Soc. Jpn.* **1990**, *63*, 1535.
- (242) Yanagisawa, T.; Shimizu, T.; Kuroda, K.; Kato, C. *Bull. Chem. Soc. Jpn.* **1990**, *63*, 988.
- (243) Martin, J. E.; Anderson, M. T.; Odinek, J.; Newcomer, P. *Langmuir* **1997**, *13*, 4133.
- (244) Ayral, A.; Balzer, C.; Dabadie, T.; Guizard, C.; Julbe, A. *Catal. Today* **1995**, *25*, 219.
- (245) Dabadie, T.; Ayral, A.; Guizard, C.; Cot, L.; Lacan, P. *J. Mater. Chem.* **1996**, *6*, 1789.
- (246) Ogawa, M. *Langmuir* **1995**, *11*, 4639.
- (247) Ferrer, M.; Lianos, P. *Langmuir* **1996**, *12*, 5620.
- (248) Sellinger, A.; Weiss, P. M.; Anh, N.; Lu, Y.; Assink, R. A.; Gong, W.; Brinker, C. J. *Nature Mater.* **2008**, *7*, 256.
- (249) Huang, M. H.; Dunn, B. S.; Soyley, H.; Zink, J. I. *Langmuir* **1998**, *14*, 7331.
- (250) Ogawa, M.; Ishikawa, H.; Kikuchi, T. *J. Mater. Chem.* **1998**, *8*, 1783.
- (251) Ogawa, M.; Kikuchi, T. *Adv. Mater.* **1998**, *10*, 1077.
- (252) Ryoo, R.; Ko, C. H.; Cho, S. J.; Kim, J. M. *J. Phys. Chem. B* **1997**, *101*, 10610.
- (253) Zhao, D.; Yang, P.; Melosh, N.; Feng, J.; Chmelka, B. F.; Stucky, G. D. *Adv. Mater.* **1998**, *10*, 1380.
- (254) Zhao, D.; Yang, P.; Margolese, D. I.; Chmelka, B. F.; Stucky, G. D. *Chem. Commun.* **1998**, *22*, 2499.
- (255) Fan, H.; Hartshorn, C.; Buchheit, T.; Tallant, D.; Assink, R.; Simpson, R.; Kissel, D. J.; Lacks, D. J.; Torquato, S.; Brinker, C. J. *Nat. Mater.* **2007**, *6*, 418.
- (256) Williford, R. E.; Li, X. S.; Addleman, R. S.; Fryxell, G. E.; Baskaran, S.; Birnbaum, J. C.; Coyle, C.; Zemanian, T. S.; Wang, C.; Courtney, A. R. *Microporous Mesoporous Mater.* **2005**, *85*, 260.
- (257) Nishiyama, N.; Tanaka, S.; Egashira, Y.; Oku, Y.; Ueyama, K. *Chem. Mater.* **2002**, *14*, 4229.
- (258) Bass, J. D.; Grosso, D.; Boissière, C.; Belamie, E.; Coradin, T.; Sanchez, C. *Chem. Mater.* **2007**, *19*, 4349.
- (259) Naik, S. P.; Yokoi, T.; Fan, W.; Sasaki, Y.; Wei, T. C.; Hillhouse, H. W.; Okubo, T. *J. Phys. Chem. B* **2006**, *110*, 9751.
- (260) Fang, H.; Zhang, M.; Shi, W. H.; Wan, T. L. *J. Non-Cryst. Solids* **2006**, *352*, 2279.
- (261) Hwang, Y. K.; Patil, K. R.; Jung, S. H.; Chang, J. S.; Ko, Y. J.; Park, S. E. *Microporous Mesoporous Mater.* **2005**, *78*, 245.
- (262) Husing, N.; Launay, B.; Doshi, D.; Kickelbick, G. *Chem. Mater.* **2002**, *14*, 2429.
- (263) Delattre, L.; Babonneau, F. *Chem. Mater.* **1997**, *9*, 2385.
- (264) Grosso, D.; Crepaldi, E. L.; Soller-Ilia, G. J. A. A.; Cagnol, F.; Baccile, N.; Babonneau, F.; Albouy, P. A.; Amenitsch, H.; Sanchez, C. *Nanotechnology in Mesoporous Materials*; In *Studies in surface science and catalysis*; Elsevier: New York, 2003; Vol. 146, p 281.
- (265) Grosso, D.; Illia, G.; Crepaldi, E. L.; Charleux, B.; Sanchez, C. *Adv. Funct. Mater.* **2003**, *13*, 37.
- (266) Crepaldi, E. L.; Soller-Ilia, G. J. A. A.; Grosso, D.; Albouy, P. A.; Amenitsch, H.; Sanchez, C. *Nanoporous Materials III*; Elsevier: Amsterdam, 2002; Vol. 141, p 235.
- (267) Brezesinski, T.; Erpen, C.; Iimura, K.; Smarsly, B. *Chem. Mater.* **2005**, *17*, 1683.
- (268) Brezesinski, T.; Groenewolt, M.; Gibaud, A.; Pinna, N.; Antonietti, M.; Smarsly, B. M. *Adv. Mater.* **2006**, *18*, 2260.
- (269) Smarsly, B.; Xomeritakis, G.; Yu, K.; Liu, N. G.; Fan, H. Y.; Assink, R. A.; Drewien, C. A.; Ruland, W.; Brinker, C. J. *Langmuir* **2003**, *19*, 7295.
- (270) Smarsly, B.; Antonietti, M. *Eur. J. Inorg. Chem.* **2006**, 1111.
- (271) Polarz, S.; Orlov, A. V.; Schuth, F.; Lu, A. H. *Chem. Eur. J.* **2007**, *13*, 592.
- (272) Huang, M. H.; Kartono, F.; Dunn, B.; Zink, J. I. *Chem. Mater.* **2002**, *14*, 5153.
- (273) Choi, S. Y.; Mamak, M.; Coombs, N.; Chopra, N.; Ozin, G. A. *Adv. Funct. Mater.* **2004**, *14*, 335.
- (274) Choi, H.; Stathatos, E.; Dionysiou, D. D. *Appl. Catal., B* **2006**, *63*, 60.
- (275) Cernigoi, U.; Stangar, U. L.; Trebbe, P.; Krasovec, U. O.; Gross, S. *Thin Solid Films* **2006**, *495*, 327.
- (276) Yu, S. Z.; Wong, T. K. S.; Hu, X.; Pita, K. *Thin Solid Films* **2004**, *63*, 311.
- (277) Velasquez, C.; Rojas, F.; Esparza, J. M.; Ortiz, A.; Campero, A. *J. Phys. Chem. B* **2006**, *110*, 11832.
- (278) Lai, W. H.; Shieh, J.; Teoh, L. G.; Hung, I. M.; Liao, C. S.; Hon, M. H. *J. Alloys Compd.* **2005**, *396*, 295.
- (279) Deepa, M.; Srivastava, A. K.; Sood, K. N.; Agnihotry, S. A. *Nanotechnology* **2006**, *17*, 2625.
- (280) Yuan, J. G.; Zhang, Y. Z.; Le, J.; Song, L. X.; Hu, X. F. *Mater. Lett.* **2007**, *61*, 1114.
- (281) Teoh, L. G.; Hon, Y. M.; Shieh, J.; Lai, W. H.; Hon, M. H. *Sens. Actuators, B* **2003**, *96*, 219.
- (282) Wang, T. W.; Liu, L.; Liu, W. P.; Ma, Z. H.; Yang, Z.; Duan, A. H.; Ruan, Q. *Chem. J. Chinese Univ.* **2006**, *27*, 2026.
- (283) Yu, C. Z.; Tian, B. Z.; Zhao, D. Y. *Curr. Opin. Solid State Mater.* **2003**, *7*, 191.
- (284) Tian, B. Z.; Liu, X. Y.; Tu, B.; Yu, C. Z.; Fan, J.; Wang, L. M.; Xie, S. H.; Stucky, G. D.; Zhao, D. Y. *Nat. Mater.* **2003**, *2*, 159.
- (285) Soller Illia, G. J. A. Private communication.
- (286) Martinez-Ferrero, E.; Sakatani, Y.; Boissière, C.; Grosso, D.; Fuertes, A.; Fraxedas, J.; Sanchez, C. *Adv. Funct. Mater.* **2007**, *17*, 3348.
- (287) Choi, K. S.; McFarland, E. W.; Stucky, G. D. *Adv. Mater.* **2003**, *15*, 2018.
- (288) Attard, G. S.; Leclerc, S. A. A.; Maniguet, S.; Russell, A. E.; Nandhakumar, I.; Bartlett, P. N. *Chem. Mater.* **2001**, *13*, 1444.
- (289) Whitehead, A. H.; Elliott, J. M.; Owen, J. R.; Attard, G. S. *Chem. Commun.* **1999**, 331.
- (290) Li, X. H.; Nandhakumar, I. S.; Gabriel, T.; Attard, G. S.; Markham, M. L.; Smith, D. C.; Baumberg, J. J.; Govender, K.; O'Brien, P.; Smyth-Boyle, D. *J. Mater. Chem.* **2006**, *16*, 3207.
- (291) Gabriel, T.; Nandhakumar, I. S.; Attard, G. S. *Electrochem. Commun.* **2002**, *4*, 610.
- (292) Braun, P. V.; Osenar, P.; Tohver, V.; Kennedy, S. B.; Stupp, S. I. *J. Am. Chem. Soc.* **1999**, *121*, 7302.
- (293) Braun, P. V.; Osenar, P.; Twardowski, M.; Tew, G. N.; Stupp, S. I. *Adv. Funct. Mater.* **2005**, *15*, 1745.
- (294) Miao, S. D.; Miao, Z. J.; Liu, Z. M.; Han, B. X.; Zhang, H.; Zhang, J. *Microporous Mesoporous Mater.* **2006**, *95*, 26.
- (295) Williford, R. E.; Fryxell, G. E.; Li, X. S.; Addleman, R. S. *Microporous Mesoporous Mater.* **2005**, *84*, 201.
- (296) Laughlin, R. G. *The aqueous phase behavior of surfactants*; Academic Press Limited: San Diego, 1996.
- (297) Forster, S.; Antonietti, M. *Adv. Mater.* **1998**, *10*, 195.
- (298) Grosso, D.; Babonneau, F.; Soller-Ilia, G. J. A. A.; Albouy, P. A.; Amenitsch, H. *Chem. Commun.* **2002**, *7*, 748.
- (299) Grosso, D.; Balkenende, A. R.; Albouy, P.-A.; Ayral, A.; Amenitsch, H.; Babonneau, F. *Chem. Mater.* **2001**, *13*, 1848.
- (300) Innocenzi, P.; Malfatti, L.; Kidchob, T.; Costacurta, S.; Falcaro, P.; Piccinini, M.; Marcelli, A.; Morini, P.; Sali, D.; Amenitsch, H. *J. Phys. Chem. C* **2007**, *111*, 5345.
- (301) Nishida, F.; McKiernan, J. M.; Dunn, B.; Zink, J. I.; Brinker, C. J.; Hurd, A. J. *J. Am. Ceram. Soc.* **1995**, *78*, 1640.

- (302) Cagnol, F.; Grosso, D.; Soler-Illia, G. J. A. A.; Crepaldi, E. L.; Babonneau, F.; Amenitsch, H.; Sanchez, C. *J. Mater. Chem.* **2003**, *13*, 61.
- (303) Zhou, X. F.; Yu, C. Z.; Tang, J. W.; Yan, X. X.; Zhao, D. Y. *Microporous Mesoporous Mater.* **2005**, *79*, 283.
- (304) Dourdain, S.; Rezaire, A.; Mehdi, A.; Ocko, B. M.; Gibaud, A. *Physica B* **2005**, *357*, 180.
- (305) Baccile, N.; Laurent, G.; Bonhomme, C.; Innocenzi, P.; Babonneau, F. *Chem. Mater.* **2007**, *19*, 1343.
- (306) Jung, S. B.; Ha, T. J.; Park, H. H. *J. Appl. Phys.* **2007**, *101*, 024109.
- (307) Besson, S.; Gacoin, T.; Ricolleau, C.; Jacquiod, C.; Boilot, J. P. *J. Mater. Chem.* **2003**, *13*, 404.
- (308) Ogawa, M.; Masukawa, N. *Microporous Mesoporous Mater.* **2000**, *38*, 35.
- (309) Urade, V. N.; Bollmann, L.; Kowalski, J. D.; Tate, M. P.; Hillhouse, H. W. *Langmuir* **2007**, *23*, 4268.
- (310) Naik, S. P.; Ogura, M.; Okubo, T. *Ind. Eng. Chem. Res.* **2005**, *44*, 4156.
- (311) Jung, S. B.; Park, H. H. *Thin Solid Films* **2006**, *494*, 320.
- (312) He, C. Q.; Suzuki, R.; Ohdaira, T.; Oshima, N.; Kinomura, A.; Muramatsu, M.; Kobayashi, Y. *Chem. Phys.* **2007**, *331*, 213.
- (313) Choungnet, A.; Heitz, C.; Sondergard, E.; Albouy, P. A.; Klotz, M. *Thin Solid Films* **2006**, *495*, 40.
- (314) Miyata, H.; Kuroda, K. *Chem. Mater.* **2000**, *12*, 49.
- (315) Innocenzi, P.; Falcaro, P.; Grosso, D.; Babonneau, F. *J. Phys. Chem. B* **2003**, *107*, 4711.
- (316) Clark, T.; Ruiz, J. D.; Fan, H. Y.; Brinker, C. J.; Swanson, B. I.; Parikh, A. N. *Chem. Mater.* **2000**, *12*, 3879.
- (317) Falcaro, P.; Grosso, D.; Amenitsch, H.; Innocenzi, P. *J. Phys. Chem. B* **2004**, *108*, 10942.
- (318) Kleitz, F.; Schmidt, W.; Schuth, F. *Microporous Mesoporous Mater.* **2003**, *65*, 1.
- (319) Innocenzi, P.; Malfatti, L.; Kidchob, T.; Falcaro, P.; Costacurta, S.; Guglielmi, M.; Mattei, G.; Bello, V.; Amenitsch, H. *J. Synchrotron Radiat.* **2005**, *12*, 734.
- (320) Williford, R. E.; Addleman, R. S.; Li, X. S.; Zemanian, T. S.; Birnbaum, J. C.; Fryxell, G. E. *J. Non-Cryst. Solids* **2005**, *351*, 2217.
- (321) Chemin, N.; Klotz, M.; Rouessac, V.; Ayrat, A.; Barthel, E. *Thin Solid Films* **2006**, *495*, 210.
- (322) Naik, S. P.; Ogura, M.; Sasakura, H.; Yamaguchi, Y.; Sasaki, Y.; Okubo, T. *Thin Solid Films* **2006**, *495*, 11.
- (323) Wu, C.-W.; Ohsuna, T.; Kuwabara, M.; Kuroda, K. *J. Am. Chem. Soc.* **2006**, *128*, 4544.
- (324) Zhang, Y.; Wang, J.; Li, J. *J. Electroceram.* **2006**, *16*, 499.
- (325) Fattakhova Rohlfing, D.; Wark, M.; Brezesinski, T.; Smarsly, B. M.; Rathousky, J. *Adv. Funct. Mater.* **2007**, *17*, 123.
- (326) Huang, L.; Kawi, S.; Hidajat, K.; Ng, S. C. *Microporous Mesoporous Mater.* **2005**, *82*, 87.
- (327) Ghosh, K.; Vyas, S. M.; Lehmiller, H. J.; Rankin, S. E.; Knutson, B. L. *J. Phys. Chem. B* **2007**, *111*, 363.
- (328) Fukumoto, H.; Nagano, S.; Kawatsuki, N.; Seki, T. *Colloids Surf., A* **2006**, *309*.
- (329) Dattelbaum, A. M.; Amweg, M. L.; Ruiz, J. D.; Ecke, L. E.; Shreve, A. P.; Parikh, A. N. *J. Phys. Chem. B* **2005**, *109*, 14551.
- (330) Tanaka, S.; Tada, H.; Maruo, T.; Nishiyama, N.; Egashira, Y.; Ueyama, K. *Thin Solid Films* **2006**, *495*, 186.
- (331) Chernysheva, M. V.; Eliseev, A. A.; Napolskii, K. S.; Lukashin, A. V.; Tretyakov, Y. D.; Grigoryeva, N. A.; Grigoryev, S. V.; Wolff, M. *Thin Solid Films* **2006**, *495*, 73.
- (332) Hozumi, A.; Sugimura, H.; Hiraku, K.; Kameyama, T.; Takai, O. *Nano Lett.* **2001**, *1*, 395.
- (333) Takahashi, M.; Maeda, T.; Uemura, K.; Yao, J.; Tokuda, Y.; Yoko, T.; Kaji, H.; Marcelli, A.; Innocenzi, P. *Adv. Mater.* **2007**, *19*, 4343.
- (334) Wu, C. W.; Aoki, T.; Kuwabara, M. *Nanotechnology* **2004**, *15*, 1886.
- (335) Yang, P. D.; Wirsberger, G.; Huang, H. C.; Cordero, S. R.; McGehee, M. D.; Scott, B.; Deng, T.; Whitesides, G. M.; Chmelka, B. F.; Buratto, S. K.; Stucky, G. D. *Science* **2000**, *287*, 465.
- (336) Gates, B. D.; Xu, Q.; Stewart, M.; Ryan, D.; Willson, C. G.; Whitesides, G. M. *Chem. Rev.* **2005**, *105*, 1171.
- (337) Fan, H. Y.; Lu, Y. F.; Stump, A.; Reed, S. T.; Baer, T.; Schunk, R.; Perez, L. V.; Lopez, G. P.; Brinker, C. J. *Nature* **2000**, *405*, 56.
- (338) Fan, H. Y.; Reed, S.; Baer, T.; Schunk, R.; Lopez, G. P.; Brinker, C. J. *Microporous Mesoporous Mater.* **2001**, *44*, 625.
- (339) Mougenot, M.; Lejeune, M.; Baumard, J. F.; Boissière, C.; Ribot, F.; Grosso, D.; Sanchez, C.; Noguera, R. *J. Am. Ceram. Soc.* **2006**, *89*, 1876.
- (340) Gulians, V. V.; Carreon, M. A.; Lin, Y. S. *J. Membr. Sci.* **2004**, *235*, 53.
- (341) Villacusa, L. A.; Mihi, A.; Rodríguez, I.; Garcia-Bennett, A. E.; Miguez, H. *J. Phys. Chem. B* **2005**, *109*, 19643.
- (342) Trau, M.; Yao, N.; Kim, E.; Xia, Y.; Whitesides, G. M.; Aksay, I. A. *Nature* **1997**, *390*, 674.
- (343) Yamaguchi, A.; Uejo, F.; Yoda, T.; Uchida, T.; Tanamura, Y.; Yamashita, T.; Teramae, N. *Nat. Mater.* **2004**, *3*, 337.
- (344) Wu, Y. Y.; Cheng, G. S.; Katsov, K.; Sides, S. W.; Wang, J. F.; Tang, J.; Fredrickson, G. H.; Moskovits, M.; Stucky, G. D. *Nat. Mater.* **2004**, *3*, 816.
- (345) Wang, D. H.; Ji, X. L.; Pang, J. B.; Hu, Q. Y.; Xu, H. F.; Lu, Y. F. *Phys. Chem. Chem. Phys.* **2003**, *5*, 4070.
- (346) Walcarus, A.; Sibottier, E.; Etienne, M.; Ghanbaja, J. *Nat. Mater.* **2007**, *6*, 602.
- (347) Yamauchi, Y.; Sawada, M.; Sugiyama, A.; Osaka, T.; Sakka, Y.; Kuroda, K. *J. Mater. Chem.* **2006**, *16*, 3693.
- (348) Yamauchi, Y.; Sawada, M.; Noma, T.; Ito, H.; Furumi, S.; Sakka, Y.; Kuroda, K. *J. Mater. Chem.* **2005**, *15*, 1137.
- (349) Boissière, C.; Martinez, M. A. U.; Kooyman, P.; Kruijff, T. R.; Larbot, A.; Prouzet, E. *Chem. Mater.* **2003**, *15*, 460.
- (350) Boissière, C.; Larbot, A.; Prouzet, E. *Stud. Surf. Sci. Catal.* **2001**, *135*, 179.
- (351) Boissière, C.; Larbot, A.; Bourgaux, C.; Prouzet, E.; Bunton, C. A. *Chem. Mater.* **2001**, *13*, 3580.
- (352) Koganti, V. R.; Rankin, S. E. *J. Phys. Chem. B* **2005**, *109*, 3279.
- (353) Koganti, V. R.; Dunphy, D.; Gowrishankar, V.; McGehee, M. D.; Li, X. F.; Wang, J.; Rankin, S. E. *Nano Lett.* **2006**, *6*, 2567.
- (354) Miyata, H.; Kuroda, K. *Chem. Mater.* **1999**, *11*, 1609.
- (355) Miyata, H.; Kawashima, Y.; Itoh, M.; Watanabe, M. *Chem. Mater.* **2005**, *17*, 5323.
- (356) Suzuki, T.; Miyata, H.; Watanabe, M.; Kuroda, K. *Chem. Mater.* **2006**, *18*, 4888.
- (357) Fukumoto, H.; Nagano, S.; Kawatsuki, N.; Seki, T. *Adv. Mater.* **2005**, *17*, 1035.
- (358) Seki, T.; Nagano, S.; Kawashima, Y.; Zettsu, N.; Ubukata, T. *Mol. Cryst. Liq. Cryst.* **2005**, *430*, 107.
- (359) Freer, E. M.; Krupp, L. E.; Hinsberg, W. D.; Rice, P. M.; Hedrick, J. L.; Cha, J. N.; Miller, R. D.; Kim, H. C. *Nano Lett.* **2005**, *5*, 2014.
- (360) Fisher, A.; Kuemmel, M.; Jörn, M.; Linden, M.; Boissière, C.; Nicole, L.; Sanchez, C.; Grosso, D. *Small* **2006**, *2*, 569.
- (361) Cheng, Y.-J.; Gutmann, J. S. *J. Am. Chem. Soc.* **2006**, *128*, 4658.
- (362) Kuemmel, M.; Allouche, J.; Nicole, L.; Boissière, C.; Laberty, C.; Amenitsch, H.; Sanchez, C.; Grosso, D. *Chem. Mater.* **2007**, *19*, 3717.
- (363) Laberty, C.; Kuemmel, L.; Allouche, J.; Boissière, C.; Grosso, D.; Sanchez, C. *J. Mater. Chem.* **2007**, accepted.
- (364) Huang, M. H.; Dunn, B. S.; Zink, J. I. *J. Am. Chem. Soc.* **2000**, *122*, 3739.
- (365) Franville, A. C.; Dunn, B.; Zink, J. I. *J. Phys. Chem. B* **2001**, *105*, 10335.
- (366) Ogawa, M.; Igarashi, T.; Kuroda, K. *Chem. Mater.* **1998**, *10*, 1382.
- (367) Yamaguchi, A.; Amino, Y.; Shima, K.; Suzuki, S.; Yamashita, T.; Teramae, N. *J. Phys. Chem. B* **2006**, *110*, 3910.
- (368) Jung, C.; Hellriegel, C.; Platschek, B.; Wöhrle, D.; Bein, T.; Michaelis, J.; Brauchle, C. *J. Am. Chem. Soc.* **2007**, *129*, 5570.
- (369) Kirstein, J.; Platschek, B.; Jung, C.; Brown, R.; Bein, T.; Brauchle, C. *Nat. Mater.* **2007**, *6*, 303.
- (370) Minoofar, P. N.; Hernandez, R.; Chia, S.; Dunn, B.; Zink, J. I.; Franville, A. C. *J. Am. Chem. Soc.* **2002**, *124*, 14388.
- (371) Scott, B. J.; Bartl, M. H.; Wirsberger, G.; Stucky, G. D. *J. Phys. Chem. A* **2003**, *107*, 5499.
- (372) Stevens, N.; Akins, D. L. *Sens. Actuators, B* **2007**, *123*, 59.
- (373) Minoofar, P. N.; Dunn, B. S.; Zink, J. I. *J. Am. Chem. Soc.* **2005**, *127*, 2656.
- (374) Fu, Y.; Ye, F.; Sanders, W. G.; Collinson, M. M.; Higgins, D. A. *J. Phys. Chem. B* **2006**, *110*, 9164.
- (375) Yui, T.; Tsuchino, T.; Akatsuka, K.; Yamauchi, A.; Kobayashi, Y.; Hattori, T.; Haga, M.; Takagi, K. *Bull. Chem. Soc. Jpn.* **2006**, *79*, 386.
- (376) Wang, X. C.; Yu, J. C. *Macromol. Rapid Commun.* **2004**, *25*, 1414.
- (377) Ahn, K. S.; Kang, M. S.; Lee, J. W.; Kang, Y. S. *J. Appl. Phys.* **2007**, *101*.
- (378) Chen, W.; Sun, X. D.; Cai, Q.; Weng, D.; Li, H. D. *Electrochem. Commun.* **2007**, *9*, 382.
- (379) Ogawa, M.; Kuroda, K.; Mori, J. *Chem. Commun.* **2000**, *24*, 2441.
- (380) Bartl, M. H.; Scott, B. J.; Huang, H. C.; Wirsberger, G.; Popitsch, A.; Chmelka, B. F.; Stucky, G. D. *Chem. Commun.* **2002**, *21*, 2474.
- (381) Tamura, M.; Kemmochi, Y.; Murakami, Y.; Chino, N.; Ogura, M.; Naik, S. P.; Takai, M.; Tsuji, Y.; Maruyama, S.; Okubo, T. *Appl. Phys. A* **2006**, *84*, 247.
- (382) Shi, K. Y.; Chi, Y. J.; Yu, H. T.; Xin, B. F.; Fu, H. G. *J. Phys. Chem. B* **2005**, *109*, 2546.
- (383) Petkov, N.; Mintova, S.; Karaghiosoff, K.; Bein, T. *Mater. Sci. Eng. B* **2003**, *23*, 145.
- (384) Tajima, K.; Ogawa, G.; Aida, T. *J. Polym. Sci., Part B: Polym. Phys.* **2000**, *38*, 4821.
- (385) Coakley, K. M.; Liu, Y. X.; McGehee, M. D.; Frindell, K. L.; Stucky, G. D. *Adv. Funct. Mater.* **2003**, *13*, 301.
- (386) Jang, K. S.; Kim, H. W.; Cho, S. H.; Kim, J. D. *J. Phys. Chem. B* **2006**, *110*, 23678.
- (387) McCaughey, B.; Costello, C.; Wang, D.; Hampsey, J. E.; Yang, Z.; Li, C.; Brinker, C. J.; Lu, Y. *Adv. Mater.* **2003**, *15*, 1266.
- (388) Lu, Y. F.; Yang, Y.; Sellinger, A.; Lu, M. C.; Huang, J. M.; Fan, H. Y.; Haddad, R.; Lopez, G.; Burns, A. R.; Sasaki, D. Y.; Shelnutt, J.; Brinker, C. J. *Nature* **2001**, *410*, 913.
- (389) Yang, Y.; Lu, Y. F.; Lu, M. C.; Huang, J. M.; Haddad, R.; Xomeritakis, G.; Liu, N. G.; Malanoski, A. P.; Sturmayer, D.; Fan, H. Y.; Sasaki, D. Y.; Assink, R. A.; Shelnutt, J. A.; van, S. F.; Lopez, G. P.; Burns, A. R.; Brinker, C. J. *J. Am. Chem. Soc.* **2003**, *125*, 1269.
- (390) Garnweitner, G.; Smarsly, B.; Assink, R.; Ruland, W.; Bond, E.; Brinker, C. J. *J. Am. Chem. Soc.* **2003**, *125*, 5626.
- (391) Garnweitner, G.; Smarsly, B.; Assink, R.; Dunphy, D. R.; Scullin, C.; Brinker, C. J. *Langmuir* **2004**, *20*, 9811.
- (392) Smarsly, B.; Garnweitner, G.; Assink, R.; Brinker, C. J. *Prog. Org. Coat.* **2003**, *47*, 393.
- (393) Zhang, X.; Liu, C. L.; Wu, W. J.; Wang, J. F. *Mater. Lett.* **2006**, *60*, 2086.

- (394) Israelachvili, J.; Mitchell, D. J.; Ninham, B. W. *J. Chem. Soc., Faraday Trans.* **1976**, 72, 1525.
- (395) Baca, H. K.; Ashley, C.; Carnes, E.; Lopez, D.; Flemming, J.; Dunphy, D.; Singh, S.; Chen, Z.; Liu, N. G.; Fan, H. Y.; Lopez, G. P.; Brozik, S. M.; Werner-Washburne, M.; Brinker, C. J. *Science* **2006**, 313, 337.
- (396) Soler-Illia, G. J. A. A.; Angelome, P. C.; Bozzano, P. *Chem. Commun.* **2004**, 2854.
- (397) Angelome, P. C.; Soler-Illia, G. J. A. A. *J. Mater. Chem.* **2005**, 15, 3903.
- (398) Bartl, M. H.; Boettcher, S. W.; Hu, E. L.; Stucky, G. D. *J. Am. Chem. Soc.* **2004**, 126, 10826.
- (399) Alonso, B.; Albouy, P. A.; Durand, D.; Babonneau, F. *New J. Chem.* **2002**, 26, 1270.
- (400) Alonso, B.; Balkenende, A. R.; Albouy, P. A.; Amenitsch, H.; Rager, M. N.; Babonneau, F. *J. Sol-Gel Sci. Technol.* **2003**, 26, 587.
- (401) Yu, K.; Smarsly, B.; Brinker, C. J. *Adv. Funct. Mater.* **2003**, 13, 47.
- (402) Tanaka, S.; Kaihara, Y.; Nishiyama, N.; Oku, Y.; Egashira, Y.; Ueyama, K. *Langmuir* **2004**, 20, 3780.
- (403) Cagnol, F.; Grosso, D.; Sanchez, C. *Chem. Commun.* **2004**, 15, 1742.
- (404) Liu, N. G.; Assink, R. A.; Smarsly, B.; Brinker, C. J. *Chem. Commun.* **2003**, 1146.
- (405) Petkov, N.; Mintova, S.; Jean, B.; Metzger, T.; Bein, T. *Mater. Sci. Eng. B* **2003**, 23, 827.
- (406) Lebeau, B.; Fowler, C. E.; Hall, S. R.; Mann, S. *J. Mater. Chem.* **1999**, 9, 2279.
- (407) Wirsberger, G.; Scott, B. J.; Stucky, G. D. *Chem. Commun.* **2001**, 1, 119.
- (408) Nicole, L.; Boissière, C.; Grosso, D.; Hesemann, P.; Moreau, J.; Sanchez, C. *Chem. Commun.* **2004**, 2312.
- (409) Lei, B. F.; Li, B.; Zhang, H. R.; Lu, S. Z.; Zheng, Z. H.; Li, W. L.; Wang, Y. *Adv. Funct. Mater.* **2006**, 16, 1883.
- (410) Tao, S. Y.; Li, G. T.; Zhu, H. S. *J. Mater. Chem.* **2006**, 16, 4521.
- (411) Liu, N. G.; Chen, Z.; Dunphy, D. R.; Jiang, Y. B.; Assink, R. A.; Brinker, C. J. *Angew. Chem., Int. Ed.* **2003**, 42, 1731.
- (412) Matheron, M.; Bourgeois, A.; Brunet-Bruneau, A.; Albouy, P. A.; Biteau, J.; Gacoin, T.; Boilot, J. P. *J. Mater. Chem.* **2005**, 15, 4741.
- (413) Matheron, M.; Bourgeois, A.; Gacoin, T.; Brunet-Bruneau, A.; Albouy, P. A.; Boilot, J. P.; Biteau, J.; Lacan, P. *Thin Solid Films* **2006**, 495, 175.
- (414) Matheron, M.; Gacoin, T.; Boilot, J. P. *Soft Matter* **2007**, 3, 223.
- (415) Wong, E. M.; Markowitz, M. A.; Qadri, S. B.; Golledge, S.; Castner, D. G.; Gaber, B. P. *J. Phys. Chem. B* **2002**, 106, 6652.
- (416) de Theije, F. K.; Balkenende, A. R.; Verheijen, M. A.; Baklanov, M. R.; Mogilnikov, K. P.; Furukawa, Y. *J. Phys. Chem. B* **2003**, 107, 4280.
- (417) Chen, J. Y.; Pan, F. M.; Chang, L.; Cho, A. T.; Chao, K. J. *J. Vac. Sci. Technol. B* **2005**, 23, 2034.
- (418) Fan, H.; Bentley, H. R.; Kathan, K. R.; Clem, P.; Lu, Y.; Brinker, C. J. *J. Non-Cryst. Solids* **2001**, 285, 79.
- (419) Kohmura, K.; Tanaka, H.; Oike, S.; Murakami, M.; Fujii, N.; Takada, S.; Ono, T.; Seino, Y.; Kikkawa, T. *Thin Solid Films* **2007**, 515, 5019.
- (420) Palaniappan, A.; Li, X.; Tay, F. E. H.; Li, J.; Su, X. D. *Sens. Actuators, B* **2006**, 119, 220.
- (421) Sierocki, P.; Maas, H.; Dragut, P.; Richardt, G.; Vogtle, F.; Cola, L.; Brouwer, F. A. M.; Zink, J. I. *J. Phys. Chem. B* **2006**, 110, 24390.
- (422) Mehdi, A.; Dourdain, S.; Bardeau, J. F.; Reve, C.; Corriu, R. J. P.; Gibaud, A. *J. Nanosci. Nanotechnol.* **2006**, 6, 377.
- (423) Banet, P.; Legagneux, L.; Hesemann, P.; Moreau, J.; Nicole, L.; Quach, A.; Sanchez, C.; Tran-Thi, T.-H. *Sens. Actuators, B* [Online early access]. DOI: 10.1016/j.snb.2007.07.103. Published Online: Aug 2, 2007.
- (424) Hernandez, R.; Franville, A.-C.; Minoofar, P.; Dunn, B.; Zink, J. I. *J. Am. Chem. Soc.* **2001**, 123, 1248.
- (425) Liu, N. G.; Yu, K.; Smarsly, B.; Dunphy, D. R.; Jiang, Y. B.; Brinker, C. J. *J. Am. Chem. Soc.* **2002**, 124, 14540.
- (426) Minoofar, P.; Hernandez, R.; Franville, A. C.; Chia, S. Y.; Dunn, B.; Zink, J. I. *J. Sol-Gel Sci. Technol.* **2003**, 26, 571.
- (427) Li, H. R.; Fu, L. S.; Liu, F. Y.; Wang, S. B.; Zhang, H. J. *New J. Chem.* **2002**, 26, 674.
- (428) Innocenzi, P.; Falcato, P.; Schergna, S.; Maggini, M.; Menna, E.; Amenitsch, H.; Soler-Illia, G. J. A. A.; Grosso, D.; Sanchez, C. *J. Mater. Chem.* **2004**, 14, 1838.
- (429) Quach, A.; Escax, V.; Nicole, L.; Goldner, P.; Guillot-Noël, O.; Aschehoug, P.; Hesemann, P.; Moreau, J.; Gourier, D.; Sanchez, C. *J. Mater. Chem.* **2007**, 17, 2552.
- (430) Tao, S. Y.; Li, G. T. *Colloid Polym. Sci.* **2007**, 285, 721.
- (431) Jung, J. I.; Bae, J. Y.; Bae, B. S. *J. Mater. Chem.* **2004**, 14, 1988.
- (432) Zhang, X.; Wu, W. J.; Wang, J. F.; Liu, C. L. *J. Am. Ceram. Soc.* **2007**, 90, 965.
- (433) Innocenzi, P.; Malfatti, L.; Kidchob, T.; Falcato, P.; Guidi, M. C.; Piccinini, M.; Marcelli, A. *Chem. Commun.* **2005**, 2384.
- (434) Miyata, H.; Suzuki, T.; Fukuoka, A.; Sawada, T.; Watanabe, M.; Noma, T.; Takada, K.; Mukaide, T.; Kuroda, K. *Nat. Mater.* **2004**, 3, 651.
- (435) Sugahara, S.; Kadoya, T.; Usami, K.; Hattori, T.; Matsumura, M. *J. Electrochem. Soc.* **2001**, 148, F120.
- (436) Melosh, N. A.; Lipic, P.; Bates, F. S.; Wudl, F.; Stucky, G. D.; Fredrickson, G. H.; Chmelka, B. F. *Macromolecules* **1999**, 32, 4332.
- (437) Goletto, V.; Dagry, V.; Babonneau, F. *Mater. Res. Soc. Symp. Proc.* **1999**, 576, 229.
- (438) Nagarajan, R. *Curr. Opin. Colloid Interface Sci.* **1997**, 2, 282.
- (439) Nagarajan, R. *Curr. Opin. Colloid Interface Sci.* **1996**, 1, 391.
- (440) Desplandier-Giscard, D.; Galarneau, A.; Di Renzo, F.; Fajula, F. *Stud. Surf. Sci. Catal.* **2001**, 135, 06P27.
- (441) Kumpf, R. A.; Dougherty, D. A. *Science* **1993**, 261, 1708.
- (442) Kim, K. S.; Lee, J. Y.; Lee, S. J.; Ha, T.-K.; Kim, D. H. *J. Am. Chem. Soc.* **1994**, 116, 7399.
- (443) Huo, Q.; Margolese, D. I.; Ciesla, U.; Demuth, D. G.; Feng, P.; Gier, T. E.; Sieger, P.; Firouzi, A.; Chmelka, B. F.; Schuth, F.; Stucky, G. D. *Chem. Mater.* **1994**, 6, 1176.
- (444) Ota, E. H.; Angelome, P. C.; Bilmes, S. A.; Soler-Illia, G. J. A. A. *Adv. Mater.* **2006**, 18, 934.
- (445) Jheong, H. K.; Kim, Y. J.; Pan, J. H.; Won, T. Y.; Lee, W. I. *J. Electroceram.* **2006**, 17, 929.
- (446) Angelome, P. C.; Fuertes, M. C.; Soler-Illia, G. J. A. A. *Adv. Mater.* **2006**, 18, 2397.
- (447) Cho, A. T.; Pan, F. M.; Chao, K. J.; Liu, P. H.; Chen, J. Y. *Thin Solid Films* **2005**, 483, 283.
- (448) Yantasee, W.; Lin, Y. H.; Li, X. H.; Fryxell, G. E.; Zemanian, T. S.; Viswanathan, V. V. *Analyst* **2003**, 128, 899.
- (449) Gu, J. L.; Shi, J. L.; Hua, Z.; Xiong, L. M.; Zhang, L. X.; Li, L. *Chem. Lett.* **2005**, 34, 114.
- (450) Domansky, K.; Liu, J.; Wang, L. Q.; Engelhard, M. H.; Baskaran, S. *J. Mater. Res.* **2001**, 16, 2810.
- (451) Baskaran, S.; Liu, J.; Domansky, K.; Kohler, N.; Li, X. H.; Coyle, C.; Fryxell, G. E.; Thevuthasan, S.; Williford, R. E. *Adv. Mater.* **2000**, 12, 291.
- (452) Coakley, K. M.; Liu, Y. X.; Goh, C.; McGehee, M. D. *MRS Bull.* **2005**, 30, 37.
- (453) Akdogan, Y.; Uzun, C.; Dag, O.; Coombs, N. *J. Mater. Chem.* **2006**, 16, 2048.
- (454) Wark, M.; Wellmann, H.; Rathousky, J. *Thin Solid Films* **2004**, 458, 20.
- (455) Andersson, M.; Birkedal, H.; Franklin, N. R.; Ostomel, T.; Boettcher, S.; Palmqvist, A. E. C.; Stucky, G. D. *Chem. Mater.* **2005**, 17, 1409.
- (456) Buso, D.; Falcato, P.; Costacurta, S.; Guglielmi, M.; Martucci, A.; Innocenzi, P.; Malfatti, L.; Bello, V.; Mattei, G.; Sada, C.; Amenitsch, H.; Gerdova, I.; Hache, A. *Chem. Mater.* **2005**, 17, 4965.
- (457) Chen, L.; Klar, P. J.; Heimbrodt, W.; Kurz, T.; von Nidda, H. A. K.; Loidl, A.; Kouzema, A. V.; Froba, M. *Phys. Status Solidi B* **2006**, 243, 831.
- (458) Kouzema, A. V.; Froba, M.; Chen, L. M.; Klar, P. J.; Heimbrodt, W. *Adv. Funct. Mater.* **2005**, 15, 168.
- (459) Besson, S.; Gacoin, T.; Ricolleau, C.; Boilot, J. P. *Chem. Commun.* **2003**.
- (460) Besson, S.; Gacoin, T.; Ricolleau, C.; Jacquiod, C.; Boilot, J.-P. *Nano Lett.* **2002**, 2, 409.
- (461) Soler-Illia, G. J. A. A.; Sanchez, C. *New J. Chem.* **2000**, 7, 493.
- (462) Hussen, G. N. A.; Shirakawa, H.; Nix, W. D.; Clemens, B. M. *J. Appl. Phys.* **2006**, 100.
- (463) Yang, K.; Fan, H. Y.; Malloy, K. J.; Brinker, C. J.; Sigmon, T. W. *Thin Solid Films* **2005**, 491, 38.
- (464) Adams, W. A.; Bakker, M. G.; Macias, T.; Jefcoat, I. A. *J. Hazard. Mater.* **2004**, 112, 253.
- (465) Adams, W. A.; Bakker, M. G.; Quickenden, T. I. *J. Photochem. Photobiol., A* **2006**, 181, 166.
- (466) Allain, E.; Besson, S.; Durand, C.; Moreau, M.; Gacoin, T.; Boilot, J. P. *Adv. Funct. Mater.* **2007**, 17, 549.
- (467) Shibata, H.; Ohkubo, T.; Kohno, H.; Rangsunvigit, P.; Sakai, H.; Abe, M. *J. Photochem. Photobiol., A* **2006**, 181, 357.
- (468) Goettmann, F.; Moores, A.; Boissière, C.; Le Floch, P.; Sanchez, C. *Small* **2005**, 1, 636.
- (469) Goettmann, F.; Moores, A.; Boissière, C.; Le Floch, P.; Sanchez, C. *Thin Solid Films* **2006**, 495, 280.
- (470) Wang, X. C.; Yu, J. C.; Yip, H. Y.; Wu, L.; Wong, P. K.; Lai, S. Y. *Chem. Eur. J.* **2005**, 11, 2997.
- (471) Petkov, N.; Holzl, M.; Metzger, T. H.; Mintova, S.; Bein, T. *J. Phys. Chem. B* **2005**, 109, 4485.
- (472) Wong, E. M.; Markowitz, M. A.; Qadri, S. B.; Golledge, S. L.; Castner, D. G.; Gaber, B. P. *Langmuir* **2002**, 18, 972.
- (473) Bearzotti, A.; Bertolo, J. M.; Innocenzi, P.; Falcato, P.; Traversa, E. *Sens. Actuators, B* **2003**, 95, 107.
- (474) Bearzotti, A.; Bertolo, J. M.; Innocenzi, P.; Falcato, P.; Traversa, E. *J. Eur. Ceram. Soc.* **2004**, 24, 1969.
- (475) Falcato, P.; Bertolo, J. M.; Innocenzi, P. *J. Sol-Gel Sci. Technol.* **2004**, 32, 107.
- (476) Innocenzi, P.; Falcato, P.; Bertolo, J. M.; Bearzotti, A.; Amenitsch, H. *J. Non-Cryst. Solids* **2005**, 351, 1980.
- (477) Bertolo, J. M.; Bearzotti, A.; Generosi, A.; Palummo, L.; Albertini, V. R. *Sens. Actuators, B* **2005**, 145.
- (478) Innocenzi, P.; Martucci, A.; Guglielmi, M.; Bearzotti, A.; Traversa, E. *Sens. Actuators, B* **2001**, 76, 299.
- (479) Innocenzi, P.; Martucci, A.; Guglielmi, M.; Bearzotti, A.; Traversa, E.; Pivin, J. C. *J. Eur. Ceram. Soc.* **2001**, 21, 1985.
- (480) Wang, Y. D.; Ma, C. L.; Wu, X. H.; Sun, X. D.; Li, H. D. *Talanta* **2002**, 57, 875.
- (481) Wang, Y.; Wu, X. H.; Li, Y. F.; Zhou, Z. L. *Solid-State Electron.* **2004**, 48, 627.
- (482) Yamada, T.; Zhou, H. S.; Uchida, H.; Tomita, M.; Ueno, Y.; Honma, I.; Asai, K.; Katsube, T. *Microporous Mesoporous Mater.* **2002**, 54, 269.
- (483) Yamada, T.; Zhou, H.; Uchida, H.; Honma, I.; Katsube, T. *J. Phys. Chem. B* **2004**, 108, 13341.
- (484) Yulianto, B.; Zhou, H. S.; Yamada, T.; Honma, I.; Asai, K. *ChemPhysChem* **2004**, 5, 261.

- (485) Yulianto, B.; Zhou, H. S.; Yamada, T.; Honma, I.; Katsumura, Y.; Ichihara, M. *Anal. Chem.* **2004**, *76*, 6719.
- (486) Agmon, N. *Chem. Phys. Lett.* **1995**, *244*, 456.
- (487) Yamada, T.; Zhou, H. S.; Honma, I.; Ueno, Y.; Horiuchi, T.; Niwa, O. *Chem. Lett.* **2005**, *34*, 328.
- (488) Gurlo, A.; Riedel, R. *Angew. Chem., Int. Ed.* **2007**, *46*, 3826.
- (489) Eranna, G.; Joshi, B. C.; Runthala, D. P.; Gupta, R. P. *Crit. Rev. Solid State Mater. Sci.* **2004**, *29*, 111.
- (490) Rottman, C.; Ottolenghi, M.; Zusman, R.; Lev, O.; Smith, M.; Gong, G.; Kagan, M. L.; Avnir, D. *Mater. Lett.* **1992**, *13*, 293.
- (491) Lobnik, A.; Oehme, I.; Murkovic, I.; Wolfbeis, O. S. *Anal. Chim. Acta* **1998**, *367*, 159.
- (492) Yang, L.; Saavedra, S. S. *Anal. Chem.* **1995**, *67*, 1307.
- (493) Miled, O. B.; Boissière, C.; Sanchez, C.; Livage, J. *J. Phys. Chem. Solids* **2006**, *67*, 1775.
- (494) Miled, O. B.; Sanchez, C.; Livage, J. *J. Mater. Sci.* **2005**, *40*, 4523.
- (495) Miled, O. B.; Grosso, D.; Sanchez, C.; Livage, J. *J. Phys. Chem. Solids* **2004**, *65*, 1751.
- (496) Qi, Z. M.; Wei, M. D.; Honma, I.; Zhou, H. S. *J. Appl. Phys.* **2006**, *100*.
- (497) Qi, Z. M.; Honma, I.; Zhou, H. *J. Phys. Chem. B* **2006**, *110*, 10590.
- (498) Qi, Z. M.; Zhou, H. S.; Watanabe, T.; Honma, I. *J. Mater. Chem.* **2004**, *14*, 3540.
- (499) Qi, Z. M.; Honma, I.; Zhou, H. S. *Anal. Chem.* **2006**, *78*, 1034.
- (500) Qi, Z. M.; Honma, I.; Zhou, H. *Appl. Phys. Lett.* **2006**, *88*.
- (501) Palaniappan, A.; Su, X. D.; Tay, F. E. H. *IEEE Sens. J.* **2006**, *6*, 1676.
- (502) Miller, R. D. *Science* **1999**, *286*, 421.
- (503) Yang, C. M.; Cho, A. T.; Pan, F. M.; Tsai, T. G.; Chao, K. J. *Adv. Mater.* **2001**, *13*, 1099.
- (504) He, Z. W.; Liu, X.-Q.; Xu, D.-Y.; Wang, Y.-Y. *Phys. Scr.* **2006**, *73*, 384.
- (505) Pan, F. M.; Wu, B. W.; Cho, A. T.; Tsai, K. C.; Tsai, T. G.; Chao, K. J.; Chen, J. Y.; Chang, L. *J. Vac. Sci. Technol. B* **2004**, *22*, 1067.
- (506) Jiang, Y. B.; Liu, N. G.; Gerung, H.; Cecchi, J. L.; Brinker, C. J. *J. Am. Chem. Soc.* **2006**, *128*, 11018.
- (507) Wirsberger, G.; Stucky, G. D. *Chem. Mater.* **2000**, *12*, 2525.
- (508) Wirsberger, G.; Yang, P. D.; Huang, H. C.; Scott, B.; Deng, T.; Whitesides, G. M.; Chmelka, B. F.; Stucky, G. D. *J. Phys. Chem. B* **2001**, *105*, 6307.
- (509) Vogel, R.; Meredith, P.; Kartini, I.; Harvey, M.; Riches, J. D.; Bishop, A.; Heckenberg, N.; Trau, M.; Rubinsztajn Dunlop, H. *ChemPhysChem* **2003**, *4*, 595.
- (510) Vogel, R.; Meredith, P.; Harvey, M. D.; Rubinsztajn Dunlop, H. *Spectrochim. Acta A* **2004**, *60*, 245.
- (511) Scott, B. J.; Wirsberger, G.; McGehee, M. D.; Chmelka, B. F.; Stucky, G. D. *Adv. Mater.* **2001**, *13*, 1231.
- (512) Wirsberger, G.; Scott, B. J.; Chmelka, B. F.; Stucky, G. D. *Adv. Mater.* **2000**, *12*, 1450.
- (513) Hata, H.; Kimura, T.; Ogawa, M.; Sugahara, Y.; Kuroda, K. *J. Sol-Gel Sci. Technol.* **2000**, *19*, 543.
- (514) Furukawa, H.; Inoue, N.; Watanabe, T.; Kuroda, K. *Langmuir* **2005**, *21*, 3992.
- (515) Garcia, J.; Valverde, G.; Cruz, D.; Franco, A.; Zink, J. I.; Minoofar, P. *J. Phys. Chem. B* **2003**, *107*, 2249.
- (516) Wang, J.; Stucky, G. D. *Adv. Funct. Mater.* **2004**, *14*, 409.
- (517) Bartl, M. H.; Scott, B. J.; Wirsberger, G.; Popitsch, A.; Stucky, G. D. *ChemPhysChem* **2003**, *4*, 392.
- (518) Burgraaf, A.; Cot, L. *Fundamentals of inorganic membrane science*; Elsevier science: New York, 1996; Vol. 4.
- (519) Nishiyama, N.; Koide, A.; Egashira, Y.; Ueyama, K. *Chem. Commun.* **1998**, *2147*.
- (520) Nishiyama, N.; Park, D. H.; Koide, A.; Egashira, Y.; Ueyama, K. *J. Membr. Sci.* **2001**, *182*, 235.
- (521) Tsai, C. Y.; Tam, S. Y.; Lu, Y. F.; Brinker, C. J. *J. Membr. Sci.* **2000**, *169*, 255.
- (522) Klotz, M.; Ayril, A.; Guizard, C.; Cot, L. *Sep. Purif. Technol.* **2001**, *25*, 71.
- (523) Xomeritakis, G.; Liu, N. G.; Chen, Z.; Jiang, Y. B.; Kohn, R.; Johnson, P. E.; Tsai, C. Y.; Shah, P. B.; Khalil, S.; Singh, S.; Brinker, C. J. *J. Membr. Sci.* **2007**, *287*, 157.
- (524) Xomeritakis, G.; Naik, S.; Braunbarth, C. M.; Cornelius, C. J.; Pardey, R.; Brinker, C. J. *J. Membr. Sci.* **2003**, *215*, 225.
- (525) Boissière, C.; Martinez, M. U.; Larbot, A.; Prouzet, E. *J. Membr. Sci.* **2005**, *251*, 17.
- (526) Bosc, F.; Lacroix-Desmazes, P.; Ayril, A. *J. Colloid Interface Sci.* **2006**, *304*, 545.
- (527) Bosc, F.; Ayril, A.; Guizard, C. *J. Membr. Sci.* **2005**, *265*, 13.
- (528) Zhao, L.; Yu, Y.; Song, L. X.; Hu, X. F.; Larbot, A. *Appl. Surf. Sci.* **2005**, *239*, 285.
- (529) Tang, J.; Wu, Y. Y.; McFarland, E. W.; Stucky, G. D. *Chem. Commun.* **2004**, *1670*.
- (530) Romeas, V.; Pichat, P.; Guillard, C.; Chopin, T.; Lehaut, C. *New J. Chem.* **1999**, *23*, 365.
- (531) Mills, A.; Wang, J. S. *J. Photochem. Photobiol., A* **2006**, *182*, 181.
- (532) Nakajima, A.; Koizumi, S.; Watanabe, T.; Hashimoto, K. *Langmuir* **2000**, *16*, 7048.
- (533) Fretwell, R.; Douglas, P. *J. Photochem. Photobiol., A* **2001**, *143*, 229.
- (534) Wark, M.; Tschirch, J.; Bartels, O.; Bahnmann, D.; Rathousky, J. *Microporous Mesoporous Mater.* **2005**, *84*, 247.
- (535) Yu, J. C.; Yu, J. G.; Ho, W. K.; Zhao, J. C. *J. Photochem. Photobiol., A* **2002**, *148*, 331.
- (536) Kitamura, T.; Ikeda, M.; Shigaki, K.; Inoue, T.; Anderson, N. A.; Ai, X.; Lian, T. Q.; Yanagida, S. *Chem. Mater.* **2004**, *16*, 1806.
- (537) Frindell, K. L.; Tang, J.; Harrell, J. H.; Stucky, G. D. *Chem. Mater.* **2004**, *16*, 3524.
- (538) Bartl, M. H.; Boettcher, S. W.; Frindell, K. L.; Stucky, G. D. *Acc. Chem. Res.* **2005**, *38*, 263.
- (539) Bosc, F.; Edwards, D.; Keller, N.; Keller, V.; Ayril, A. *Thin Solid Films* **2006**, *495*, 272.
- (540) Lancelle-Beltran, E.; Prene, P.; Boscher, C.; Belleville, P.; Buvat, P.; Sanchez, C. *Adv. Mater.* **2006**, *18*, 2579.
- (541) Zukalova, M.; Zukal, A.; Kavan, L.; Nazeeruddin, M. K.; Liska, P.; Gratzel, M. *Nano Lett.* **2005**, *5*, 1789.
- (542) Huisman, C. L.; Schoonman, J.; Goossens, A. *Sol. Energy Mater. Sol. Cells* **2005**, *85*, 115.
- (543) Hou, K.; Tian, B. Z.; Li, F. Y.; Bian, Z. Q.; Zhao, D. Y.; Huang, C. H. *J. Mater. Chem.* **2005**, *15*, 2414.
- (544) Jiu, J. T.; Isoda, S.; Adachi, M.; Wang, H. *J. Mater. Sci.: Mater. Electron.* **2007**, *18*, 593.
- (545) Oey, C. C.; Djurisic, A. B.; Wang, H.; Man, K. K. Y.; Chan, W. K.; Xie, M. H.; Leung, Y. H.; Pandey, A.; Nunzi, J. M.; Chui, P. C. *Nanotechnology* **2006**, *17*, 706.
- (546) Nunzi, J. M. *C. R. Phys.* **2002**, *3*, 523.
- (547) Spiekermann, S.; Smestad, G.; Kowalik, J.; Tolbert, L.; Gratzel, M. *Synth. Met.* **2001**, *121*, 1603.
- (548) Sallard, S.; Brezesinski, T.; Smarsly, B. M. *J. Phys. Chem. C* **2007**, *111*, 7200.
- (549) Reiman, K. H.; Brace, K. M.; Gordon-Smith, T. J.; Nandhakumar, I.; Attard, G. S.; Owen, J. R. *Electrochem. Commun.* **2006**, *8*, 517.
- (550) Cheng, W.; Baudrin, E.; Dunn, B.; Zink, J. I. *J. Mater. Chem.* **2001**, *11*, 92.
- (551) Vioux, A.; Le Bideau, J.; Mutin, P. H.; Leclercq, D. *Top. Curr. Chem.* **2004**, *232*, 145.
- (552) Tang, J. W. M.; Stucky, G. D. *Electrochem. Commun.* **2003**, *5*, 497.
- (553) McKenzie, K. J.; Marken, F. *Langmuir* **2003**, *19*, 4327.
- (554) Ramgir, N. S.; Hwang, Y. K.; Jung, S. H.; Kim, H. K.; Hwang, J. S.; Mulla, I. S.; Chang, J. S. *Appl. Surf. Sci.* **2006**, *252*, 4298.
- (555) Ramgir, N. S.; Hwang, Y. K.; Jung, S. H.; Mulla, I. S.; Chang, J. S. *Sens. Actuators, B* **2006**, *114*, 275.
- (556) Goettmann, F.; Sanchez, C. *J. Mater. Chem.* **2007**, *17*, 24.
- (557) Goettmann, F.; Boissière, C.; Grosso, D.; Mercier, F.; Le Floch, P.; Sanchez, C. *Chem. Eur. J.* **2005**, *11*, 7416.
- (558) Goettmann, F.; Grosso, D.; Mercier, F.; Mathey, F.; Sanchez, C. *Chem. Commun.* **2004**, *1240*.
- (559) Gelman, F.; Blum, J.; Avnir, D. *J. Am. Chem. Soc.* **2002**, *124*, 14460.
- (560) Martinez-Ortiz, M. D.; Tichit, D.; Gonzalez, P.; Coq, B. *J. Mol. Catal. A: Chem.* **2003**, *201*, 199.
- (561) Conde-Gallardo, A.; Garcia-Rocha, M.; Hernandez-Calderon, I.; Palomino-Merino, R. *Appl. Phys. Lett.* **2001**, *78*, 3436.
- (562) Palomino-Merino, R.; Conde-Gallardo, A.; Garcia-Rocha, M.; Hernandez-Calderon, I.; Castano, V.; Rodriguez, R. *Thin Solid Films* **2001**, *401*, 118.
- (563) Castro, Y.; Julian-Lopez, B.; Boissière, C.; Viana, B.; Grosso, D.; Sanchez, C. *Microporous Mesoporous Mater.* **2007**, *103*, 273.
- (564) Frindell, K. L.; Bartl, M. H.; Popitsch, A.; Stucky, G. D. *Angew. Chem., Int. Ed.* **2002**, *41*, 959.
- (565) Madhugiri, S.; Dalton, A.; Gutierrez, J.; Ferraris, J. P.; Balkus, K. J. *J. Am. Chem. Soc.* **2003**, *125*, 14531.
- (566) Madhugiri, S.; Sun, B.; Smirniotis, P. G.; Ferraris, J. P.; Balkus, K. J. *Microporous Mesoporous Mater.* **2004**, *69*, 77.
- (567) Lu, Q.; Gao, F.; Komarneni, S.; Mallouk, T. E. *J. Am. Chem. Soc.* **2004**, *126*, 8650.
- (568) Wu, Y.; Livneh, T.; Zhang, Y.; Cheng, G.; Wang, J.; Tang, J. *Nano Lett.* **2004**, *4*, 2337.
- (569) Wang, H.; Wang, Z.; Huang, L.; Mitra, A.; Yan, Y. *Langmuir* **2001**, *17*, 2572.
- (570) Zhou, Z.; Zhu, S.; Zhang, D. *J. Mater. Chem.* **2007**, *17*, 2428.
- (571) Save, M.; Granvorka, G.; Bernard, J.; Charleux, B.; Boissière, C.; Grosso, D.; Sanchez, C. *Macromol. Rapid Commun.* **2006**, *27*, 393.
- (572) Fu, Q.; Rao, G. V. R.; Ista, L. K.; Wu, Y.; Andrzejewski, B. P.; Sklar, L. A.; Ward, T. L.; Lopez, G. P. *Adv. Mater.* **2003**, *15*, 1262.
- (573) Lai, C. Y.; Trewyn, B. G.; Jęftinija, D. M.; Jęftinija, K.; Xu, S.; Jęftinija, S.; Lin, V. S. Y. *J. Am. Chem. Soc.* **2003**, *125*, 4451.
- (574) Slowing, I. I.; Trewyn, B. G.; Giri, S.; Lin, V. S. Y. *Adv. Funct. Mater.* **2007**, *17*, 1225.
- (575) Torney, F.; Trewyn, B. G.; Lin, V. S. Y.; Wang, K. *Nat. Nanotechnol.* **2007**, *2*, 295.
- (576) Giri, S.; Trewyn, B. G.; Stellmaker, M. P.; Lin, V. S. Y. *Angew. Chem., Int. Ed.* **2005**, *44*, 5038.
- (577) Vallet-Regi, M. *Dalton Trans.* **2006**, 5211.
- (578) Vallet-Regi, M. *Chem. Eur. J.* **2006**, *12*, 1.
- (579) Vallet-Regi, M. *Materialwiss. Werkstofftech.* **2006**, *37*, 6.
- (580) Johansson, I.; Svensson, M. *Curr. Opin. Colloid Interface Sci.* **2001**, *6*, 178.
- (581) Stangar, U. L.; Husing, N. *Silicon Chem.* **2003**, *2*, 157.
- (582) Pileni, M. P. *J. Phys.: Condens. Matter* **2006**, *18*, S67.
- (583) Pileni, M. P., Ed. *Nanocrystals Forming Mesoscopic Structures*; Wiley-VCH Verlag GmbH & Co.: Weinheim, 2005.
- (584) Ribeiro, C.; Lee, E. J. H.; Longo, E.; Leite, E. R. *ChemPhysChem* **2006**, *7*, 664.
- (585) Colfen, H.; Antonietti, M. *Angew. Chem., Int. Ed.* **2005**, *44*, 5576.

- (586) Bisson, L.; Boissière, C.; Sanchez, C.; Thomazeau, C.; Uzio, D. *MRS Spring Meeting 2007 Proceedings*; MRS: San Francisco, 2007.
- (587) Vilain, C.; Goettmann, F.; Moores, A.; Le Floch, P.; Sanchez, C. *J. Mater. Chem.* **2007**, *33*, 3509.
- (588) Ferey, G. *Chem. Mater.* **2001**, *13*, 3084.
- (589) Li, H.; Eddaoudi, M.; O'Keeffe, M.; Yaghi, O. M. *Nature* **1999**, *402*, 276.
- (590) Serre, C.; Mellot-Draznieks, C.; Surble, S.; Audebrand, N.; Filinchuk, Y.; Ferey, G. *Science* **2007**, *315*, 1828.
- (591) Ferey, G.; Mellot-Draznieks, C.; Serre, C.; Millange, F.; Dutour, J.; Surble, S.; Margiolaki, I. *Science* **2005**, *309*, 2040.
- (592) Ohsuna, T.; Liu, Z.; Che, S. N.; Terasaki, O. *Small* **2005**, *1*, 233.
- (593) van Bommel, K. J. C.; Friggeri, A.; Shinkai, S. *Angew. Chem., Int. Ed.* **2003**, *42*, 980.
- (594) Jung, J. H.; Ono, Y.; Hanabusa, K.; Shinkai, S. *J. Am. Chem. Soc.* **2000**, *122*, 5008.
- (595) Moreau, J. E.; Vellutini, L.; Wong Chi Man, M.; Bied, C. *J. Am. Chem. Soc.* **2001**, *123*, 1509.
- (596) Roy, G.; Miravet, J. F.; Escuder, B.; Sanchez, C.; Llusar, M. *J. Mater. Chem.* **2006**, *16*, 1817.
- (597) Yang, S.; Zhao, L.; Yu, C.; Zhou, X.; Tang, J.; Yuan, P.; Chen, D.; Zhao, D. *J. Am. Chem. Soc.* **2006**, *128*, 10460.
- (598) Shimojima, A.; Kuroda, K. *Angew. Chem., Int. Ed.* **2003**, *42*, 4057.
- (599) Bradley, D. C.; Mehrotra, R. C.; Gaur, D. P. *Metal Alkoxides*; Academic Press: London, 1978.
- (600) Boyd, T. J. *J. Polym. Sci.* **1951**, *1*, 591.
- (601) Onsager, L. *Ann. N.Y. Acad. Sci.* **1949**, *51*, 627.
- (602) Corma, A.; Garcia, H. *Chem. Rev.* **2003**, *103*, 4307.
- (603) Grosso, D.; Boissière, C.; Sanchez, C. *Nat. Mater.* **2007**, *6*, 572.
- (604) Sanchez, C.; Arribart, H.; Giraud Guille, M. M. *Nat. Mater.* **2005**, *4*, 277.
- (605) Mann, S. *Biomimetic Materials Chemistry*; John Wiley & Sons: Weinheim, 1997.
- (606) Bauerlein, E. *Angew. Chem., Int. Ed.* **2003**, *42*, 614.
- (607) Yang, P. D.; Deng, T.; Zhao, D. Y.; Feng, P. Y.; Pine, D.; Chmelka, B. F.; Whitesides, G. M.; Stucky, G. D. *Science* **1998**, *282*, 2244.
- (608) Holland, B. T.; Blanford, C. F.; Stein, A. *Science* **1998**, *281*, 538.
- (609) Llusar, M.; Monros, G.; Roux, C.; Pozzo, J. L.; Sanchez, C. *J. Mater. Chem.* **2003**, *13*, 2505.
- (610) Matsushita, S. I.; Kurono, N.; Sawadaishi, T.; Shimomura, M. *Synth. Met.* **2004**, *147*, 237.
- (611) Valle, K.; Belleville, P.; Pereira, F.; Sanchez, C. *Nat. Mater.* **2006**, *5*, 107.
- (612) Leonard, A.; Su, B.-L. *Colloids Surf., A* **2007**, *300*, 129.
- (613) Vantomme, A.; Leonard, A.; Yuan, Z.-Y.; Su, B.-L. *Colloids Surf., A* **2007**, *300*, 70.
- (614) Su, B.-L.; Vantomme, A.; Surahy, L.; Pirard, R.; Pirard, J.-P. *Chem. Mater.* **2007**, *19*, 3325.
- (615) Backov, R. *Soft Matter* **2006**, *2*, 452.
- (616) Carn, F.; Achard, M. F.; Babot, O.; Deleuze, H.; Reculosa, S.; Backov, R. *J. Mater. Chem.* **2005**, *15*, 3887.
- (617) Carn, F.; Saadaoui, H.; Masse, P.; Ravaine, S.; Julian-Lopez, B.; Sanchez, C.; Deleuze, H.; Talham, D. R.; Backov, R. *Langmuir* **2006**, *22*, 5469.
- (618) Carn, F.; Steunou, N.; Livage, J.; Colin, A.; Backov, R. *Chem. Mater.* **2005**, *17*, 644.
- (619) Carn, F.; Colin, A.; Achard, M. F.; Deleuze, H.; Sanchez, C.; Backov, R. *Adv. Mater.* **2005**, *17*, 62.
- (620) Ungureanu, F.; Birot, M.; Laurent, G.; Deleuze, H.; Babot, O.; Julian Lopez, B.; Achard, M. F.; Popa, M.; Sanchez, C.; Backov, R. *Chem. Mater.* **2007**, *19*, 5786.
- (621) Bouchara, A.; Soler-Illia, G. J. A. A.; Chane-Ching, J. Y.; Sanchez, C. *Chem. Commun.* **2002**, 1234.
- (622) Bouchara, A.; Mosser, G.; Soler-Illia, G. J. A. A.; Chane-Ching, J. Y.; Sanchez, C. *J. Mater. Chem.* **2004**, *14*, 2347.
- (623) Bunz, U. H. F. *Adv. Mater.* **2006**, *18*, 973.
- (624) Sakatani, Y.; Boissière, C.; Grosso, D.; Nicole, L.; Soler-Illia, G. J. A. A.; Sanchez, C. *Chem. Mater.* **2008**, DOI: 10.1021/cm701986b.
- (625) Bass, J. D.; Grosso, D.; Boissière, C.; Sanchez, C. *J. Am. Chem. Soc.* **2008**, submitted.

CM702100T